Medicines for All Institute

Summary of Process Development Work on Synthesis of Lenacapavir

Report Prepared by:

Dr. Limei Jin
Dr. Justina M. Burns
Dr. John M. Saathoff
Dr. Anand Shinde
Dr. Daryl Guthrie
Dr. Aline Nunes de Souza
Dr. Rama Sayini
Dr. Ramesh Vediyappan
Sam R. Hochstetler

Contact: m4all@vcu.edu

August 2025





Executive Summary

This process development report (PDR)^a describes the results of route scouting, process development, scale-up and process documentation of a novel lenacapavir sodium synthesis at Medicines for All Institute (M4ALL). A new, cost-efficient and potentially scalable synthetic approach toward the synthesis of lenacapavir is disclosed.

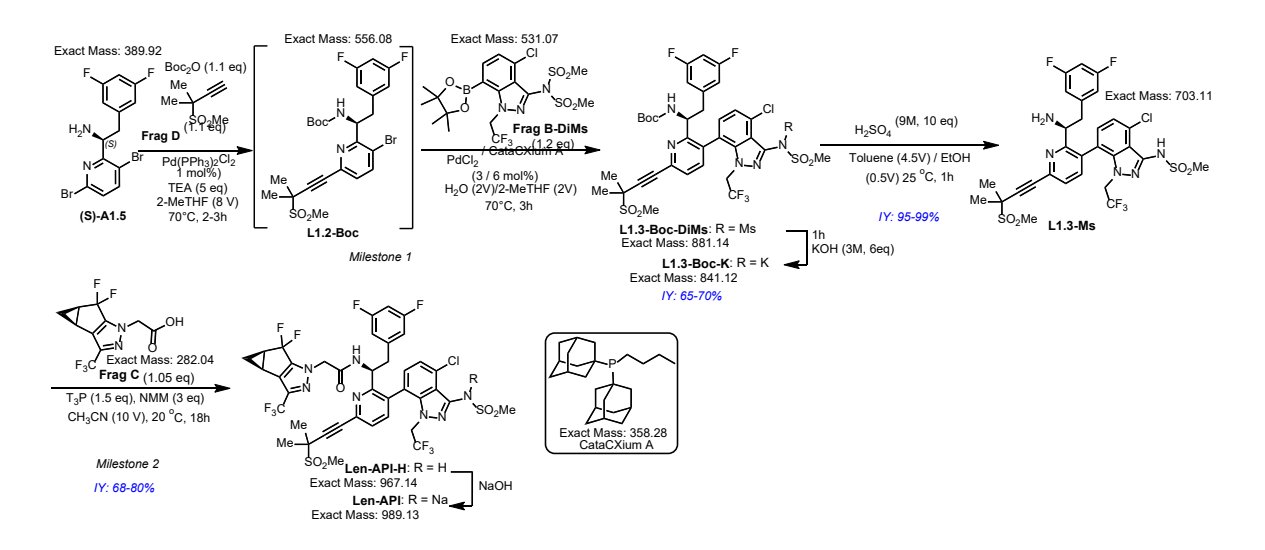
Lenacapavir is a first-in-class drug that targets the HIV capsid protein, developed by Gilead Sciences Inc. It has been approved by the FDA twice; first, in 2022 for the treatment of multi-drug resistant HIV under the brand name Sunlenca®, and again in 2025 for HIV pre-exposure prophylaxis (PrEP) under the brand name Yeztugo®. In 2020, Gilead Sciences disclosed the medicinal chemistry route to the lenacapavir free base. This route involved multiple Pd-catalyzed coupling reactions and required careful management of intermediates exhibiting atropisomerism. To decrease the analytical and processing complexity associated with atropisomeric compounds and enhance synthetic efficiency, Gilead developed a scale-up process for lenacapavir sodium (disclosed in 2024; probable manufacturing route). This four-step process commenced from a 2,5dibromopyridine core. The dibromopyridine was sequentially submitted to alkynylation, amide coupling with a chiral pyrazole carboxylic acid, Suzuki cross-coupling with an indazole boronic ester, telescoped bis-methanesulfonylation and hydrolysis to yield the API. Expensive starting materials – for example, the chiral pyrazole carboxylic acid (Frag C) and its early-stage incorporation - contribute to high overall costs for lenacapavir API. Space-time-yield inefficiencies intrinsic to the stepwise Pd-catalyzed couplings, together with iterative Pd removal steps, further contribute to high process costs for synthesis of lenacapavir sodium API.

Herein, we report a new approach to make lenacapavir sodium (see synthetic scheme below). It is a three-step process starting from a chiral bromopyridine core – (S)-1-(3,6-dibromopyridin-2-yl)-2-(3,5-difluorophenyl)ethan-1-amine (**Frag A**). The process includes a telescoped sequential Pd-catalyzed coupling (Milestone 1), Boc-deprotection and a late-stage amidation with **Frag C** (Milestone 2). The sequential one-pot Pd-catalyzed couplings comprise four transformations – Boc-protection, Pd-catalyzed Heck coupling with **Frag D**, Suzuki coupling

^a An analytical development report (**GFN-002-LEN-ADR**) is provide in a separate document, detailing the analytical methods used for all intermediates, impurities and the final API.

^b Wagner, A. M. et. al. Org. Process Res. Dev. **2024**, 28, 3382–3395.

with N-(4-chloro-7-(4,4,5,5-tetramethyl-1,3,2-dioxaborolan-2-yl)-1-(2,2,2-trifluoroethyl)-1H-indazol-3-yl)-N-(methylsulfonyl)methanesulfonamide (**Frag B-DiMs**), and selective monodemesylation. After Boc deprotection, amidation with **Frag C** is carried out at the last step to complete the synthesis of lenacapavir sodium API. This process affords lenacapavir API in 50-55% overall yield with a purity > 99.9 wt% (HPLC), ~ 99 A% (235 nm), and Pd content < 10 ppm. Compared to Gilead scaling up process, M4ALL's new process poses several advantages: 1) The one-pot Heck-Suzuki sequence lowers Pd consumption from 5 mol% to 4 mol% and reduces intermediate purification steps; 2) Streamlined Pd removal and fewer isolations enhance spacetime yield and reduce effluent; 3) The process simplifies handling of atropisomereric intermediates; and 4) Late-stage amidation with **Frag C** lowers overall raw material costs. As a result, technoeconomic (TE) cost analysis suggests that, M4ALL's new process offers an overall raw material cost (RMC) reduction of 20-30%.^c



^c Technoeconomic analyses of the API process for M4All and Gilead are based on the respective raw material costs of fragments reported in the literature. Detailed data from these technoeconomic analyses is not included in this PDR. For further information, please contact M4ALL directly.

Medicines for All – Contributors to the Research and Report

Contributor	Title/Role
Dr. Ryan Littich	Chief Technology Officer
Dr. Limei Jin	Assoc Dir., Process Development (Project Lead)
Jason Kelly	Assoc Dir., Manufacturing Science & Technology
Dr. John M. Saathoff	Research Scientist
Dr. Anand Shinde	Research Scientist
Dr. Daryl Guthrie	Research Scientist
Dr. Aline Nunes de Souza	Postdoctoral Researcher
Dr. Rama Sayini	Postdoctoral Researcher
Dr. Ramesh Vediyappan	Postdoctoral Researcher
Sam Hochstetler	Analytical Chemist
Dr. Justina M. Burns	Assoc Dir of Analytical Chemistry
Janie Wierzbicki	Assoc Dir of Project Management Office

Contents

1	Introduc	tion	6
2	Results	and Discussion	10
2.1	One-pot	sequential Pd-catalyzed coupling reactions (Milestone 1)	10
	2.1.1	Condition screening and optimization	11
	2.1.2	Practical workup and purification for scalability	22
	2.1.3	Process safety assessment for Milestone 1	31
	2.1.4	Impurities identification and RT marker	33
2.2	H ₂ SO ₄ -b	pased deBoc reaction and process development (Milestone 2)	34
	2.2.1	Condition screening and optimization	35
	2.2.2	Practical workup and purification for scalability	37
	2.2.3	Safety assessment of the process	41
	2.2.4	Impurities identification and RT marker	42
2.3	T3P-pro	omoted amidation and process development (Milestone 2)	43
	2.3.1	Condition screening and optimization	44
	2.3.2	Practical workup and purification Len-API	47
	2.3.3	Safety assessment of the process	50
	2.3.4	Impurities identification and RT marker	52
2.4	Conclus	ions	52
3	Append	ix	53
3.1	Process	documentation (PDFs embedded)	53
3.2	Experim	nental details	54
3.3	NMR S ₁	pectra	76
4	Acknow	rledgements	103
5	Referen	ces	104





1 Introduction

The Human Immunodeficiency Virus (HIV) continues to pose one of the most urgent and enduring challenges to global public health. It is estimated that more than 600,000 people die from HIV-related illnesses each year, with over 40 million deaths recorded since the beginning of the epidemic. Currently, approximately 40 million individuals are living with HIV worldwide, including 1.5 million children; more than 1 million new infections occur annually. Among the most promising therapies for HIV treatment is lenacapavir, a first-in-class antiviral that targets the HIV capsid protein. In 2021 protein approach disrupts multiple stages of the viral life cycle. Lenacapavir's long-acting nature and availability in both oral and injectable forms have positioned it as a first-line treatment for HIV infection. In 2022, the U.S. Food and Drug Administration (FDA) approved lenacapavir for the treatment of multi-drug-resistant HIV. Notably, the drug also demonstrated strong efficacy in preventing HIV. Marketed under the tradename *Yeztugo*®, lenacapavir was approved by the FDA in 2025 for use as a pre-exposure prophylaxis (PrEP) against HIV.

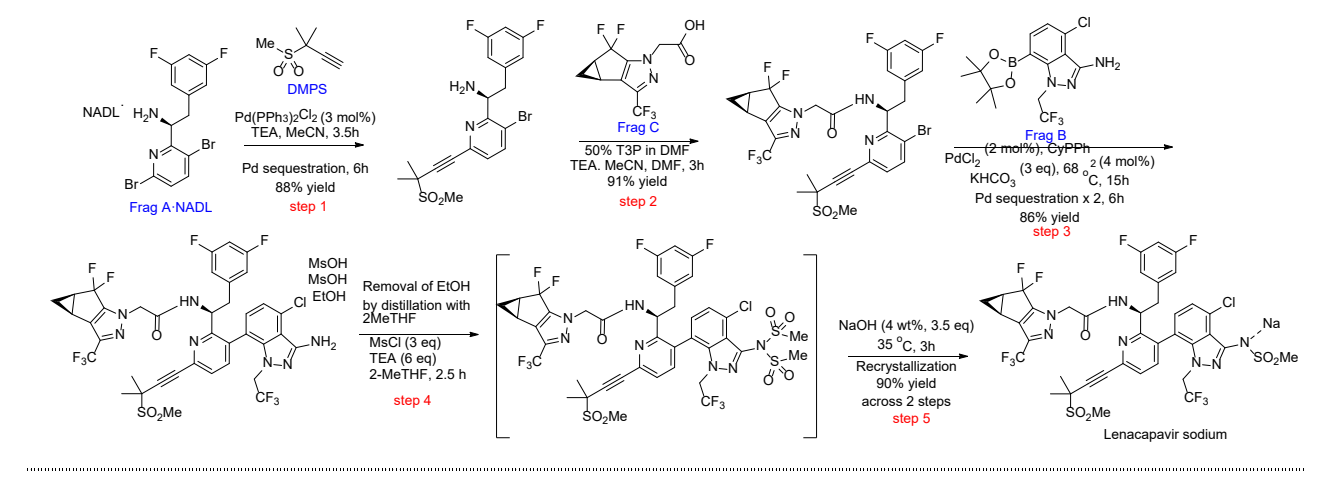
Despite its clinical success, lenacapavir has faced criticism over its cost. ^{10–12} According to 2024 data, Gilead Sciences priced the drug between \$30,625 and \$44,819 per person per year (pppy), an unaffordable range for many individuals, especially those in middle- and low-income countries. The current cost of goods (COG) for the active pharmaceutical ingredient (API) stands at \$64,480 per kilogram, with imports sourced from India. ¹¹ To make lenacapavir more accessible, the target pppy price is set below \$100. Achieving this goal requires reducing the generic manufacturing cost of the API to \$10,000 per kilogram or less. ¹³ The recent voluntary licensing agreement between Gilead and six pharmaceutical companies represents a major step toward expanding access to lenacapavir for both prevention and treatment in low- and middle-income countries. ¹⁴

Lenacapavir was first reported by Gilead Sciences in a family of patents and publications in 2018-2023.^{15–19} In 2020, Gilead Sciences disclosed the medicinal chemistry route to the lenacapavir free base.^{17,19} The synthesis commenced from the N-Boc-protected chiral bis-bromopyridine core and proceeded through a series of transformations, including Sonogashira coupling, Suzuki cross-coupling, and bis-methanesulfonylation. This was followed by selective

mono-demesylation, Boc-deprotection and final amidation to yield the API. This route involved multiple Pd-catalyzed coupling reactions and required careful management of intermediates exhibiting atropisomerism. To decrease the analytical and processing complexity associated with atropisomeric compounds and enhance synthetic efficiency, Gilead Sciences revealed a scale-up process for lenacapavir sodium in 2024,²⁰ which is characterized by the convergence of three advanced intermediates (or **Frag A**, **B**, **C**) and a propargyl sulfone (DMPS or **Frag D**, in Figure 1.1). The central fragment of lenacapavir is **Frag A** (chiral amine), which is joined to **Frag D** through Heck alkynylation,²¹ to **Frag C** (chiral carboxylic acid) using a T3P-promoted amide coupling, and then to **Frag B** (indazole boronic ester) using the Suzuki-Miyaura reaction (Scheme 1.1 (a)).

Figure 1.1 Retrosynthetic disconnections for lenacapavir and its constituents for chemical synthesis.

a) Gilead scale-up process (2024)



b) M4ALL new streamlined process (2025)

Scheme 1.1 a) Gilead's scale-up process for the synthesis of lenacapavir revealed on 2024 OPRD paper.²⁰ b) M4All new process for the synthesis of lenacapavir.

>75% vield after recrystallization

The current groundbreaking synthetic approach enabled the successful construction of the complex lenacapavir API molecule, representing a significant advancement in HIV drug development. However, this approach faces three major issues that challenge its cost-effectiveness. First, the early-stage introduction of **Frag C**, itself a key cost driver, increases raw material (RM) costs. Second, the process utilizes two distinct palladium-catalyzed couplings (Heck; Suzuki-Miyaura), which add to RM and operational costs (e.g., late-stage palladium sequestration to meet pharmaceutical purity standards). Third, the workflow is hindered by demanding purification

processes, reducing throughput and increasing production complexity. To address opportunities for complexity and cost reduction, the development of a new synthesis pathway is essential.

With ongoing support from the Gates Foundation, M4ALL has been entrusted with reducing the overall cost of this complex API molecule. With the aim to lower the RMC for synthesis of lenacapavir API (**Len-API**), a one-pot synthesis was identified, optimized, scaled up to decagram scale, and documented the process (Scheme 1.1 (b)). M4ALL's process research and development efforts pursued two key milestones.

- Milestone 1 (MS1): One-pot, sequential Pd-catalyzed Heck and Suzuki coupling to link Frag A²² with Frag D and Frag B²³. This sequence includes 4 transformations: Boc-protection, Heck coupling, Suzuki coupling, and mono de-mesylation, affording L1.3-K-Boc in 60-70% isolated yield with 85 90% weight assay of the potassium salt form after liquid-liquid extraction (LLE) workup. The solvent MIBK provides excellent LLE results in MS1 purification. SiliaMetS SH was identified as a suitable scavenger for reducing Pd residue to less than 10 ppm.
- Milestone 2 (MS2): H₂SO₄-mediated Boc deprotection, followed by a late-stage amidation with **Frag** C²⁴ to furnish lenacapavir sodium API. Undesired amidation on the free methylsulfonamide (–HNMs) moiety has been minimized during the reaction and via purification. LLE then recrystallization delivered high purity and good isolated yield.

As illustrated in Scheme 1.1 (b), M4ALL's new process featured a streamlined one-pot Heck-Suzuki sequence and late-stage **Frag** C incorporation.^d The synthesis begins with the coupling of **Frag** A and **Frag** D in the presence of Boc₂O and a catalytic amount of PdCl₂(PPh₃)₂. The resulting Heck product undergoes a telescoped Suzuki coupling with **Frag** B-DiMs (derivatized from **Frag** B with one step), followed by KOH treatment to yield the key intermediate **L1.3-K-Boc**. Subsequent Boc deprotection and T3P-mediated amidation with **Frag** C produce chemically pure lenacapavir API, finalized through recrystallization. Importantly, the process was

-

^d With support from the Gates Foundation during Year 1 (2023-2024), M4ALL successfully developed new chemistry and process that significantly reduced the overall cost of Fragments A, B, and C.

designed to minimize alterations to the incumbent advanced intermediates, facilitating uptake by generic pharmaceutical manufacturers, which is another core tenet of the M4ALL's mission.

Compared to Gilead scaling up process, M4ALL's new process poses several advantages as summarized below:

- The one-pot Heck-Suzuki sequence lowers Pd consumption from 5 mol% to 4 mol% and reduces intermediate purification steps.
- Streamlined Pd removal and fewer isolations enhance space-time yield and reduce effluent.
- o The process simplifies handling of atropisomereric intermediates.
- o Late-stage amidation with Frag C lowers overall synthesis costs.

In the following sections, we present a detailed R&D process development of lenacapavir.

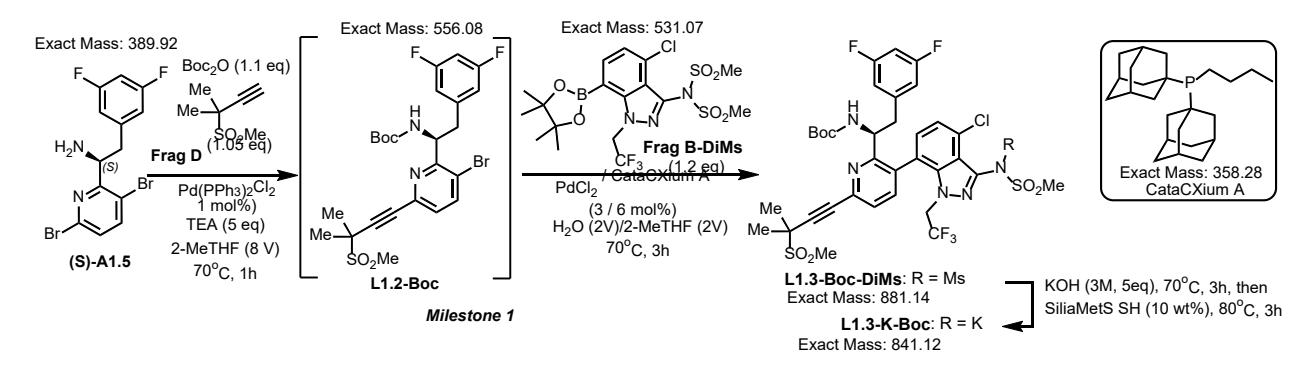
2 Results and Discussion

2.1 One-pot sequential Pd-catalyzed coupling reactions (Milestone 1)

With the aim to lower the RMC for synthesis of lenavapavir API (Len-API), numerous routes were scouted at M4ALL during the year of 2024-2025. Among these endeavors, a one-pot double-dosed synthesis of L1.3-K-Boc was identified, optimized, scaled up to decagram scale, and documented the process.

The one-pot sequential synthesis of potassium (*S*)-(7-(2-(1-((tert-butoxycarbonyl)amino)-2-(3,5-difluorophenyl)ethyl)-6-(3-methyl-3-(methylsulfonyl)but-1-yn-1-yl)pyridin-3-yl)-4-chloro-1-(2,2,2-trifluoroethyl)-1H-indazol-3-yl)(methylsulfonyl)amide (**L1.3-K-Boc**) involves four key transformations, starting from (*S*)-1-(3,6-dibromopyridin-2-yl)-2-(3,5-difluorophenyl)ethan-1-amine (**Frag A**, (*S*)-A1.5).^{22,25} The sequence begins with in-situ Boc protection of the amine, followed by a Heck alkynylation.²¹ A subsequent Suzuki reaction with N-(4-chloro-7-(4,4,5,5-tetramethyl-1,3,2-dioxaborolan-2-yl)-1-(2,2,2-trifluoroethyl)-1H-indazol-3-yl)-N-(methylsulfonyl)methanesulfonamide (**Frag B-DiMs**)^{23,26} introduces the indazole fragment. Demesylation using KOH selectively removed one mesyl group, yielding the potassium

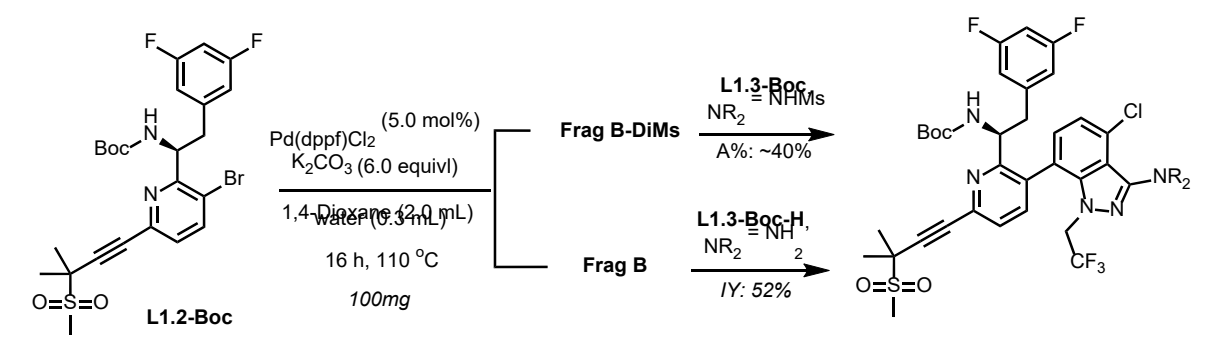
sulfonamide salt **L1.3-K-Boc**. The crude product is then treated with the metal sequestrant SiliaMetS SH, reducing residual Pd content to below 10 ppm (Scheme 2.1.1).



Scheme 2.1.1 M4All one-pot double-dose sequential Pd couplings for L1.3-K-Boc synthesis.

2.1.1 Condition screening and optimization

Our initial efforts toward Milestone 1, which focused on developing Pd-free couplings and approaches that avoided amine protection, ^{27–29} proved instrumental to developing the topical process. Attempts to install the alkyne moiety via nucleophilic aromatic substitution (S_NAr) of **Frag D-Na** (generated from **Frag D** and NaH) with **Frag A** were unsuccessful. Similarly, CuI-catalyzed alkynylation trials resulted in recovery of the starting materials. While the unprotected amine in **Frag A** was well tolerated in the Heck alkynylation, the subsequent Suzuki coupling with either **Frag B-DiMs** or **Frag B** failed to incorporate the indazole fragment. Neither Cu(I) catalysis nor S_NAr substitution proved effective. One key takeaway from our study is that the protected amine in **Frag A** is necessary for the Pd-catalyzed Suzuki reaction. As shown in Scheme 2.1.2, both Suzuki coupling between the Boc-protected amine **L1.2-Boc** and either **Frag B** or **Frag B-DiMs** proceeded smoothly, yielding the desired coupling products. Notably, the reaction with **Frag B-DiMs** resulted in in-situ demesylation, eliminating the need for a separate demesylation step. Although the overall yield was moderate, these early findings informed our development of a more process-friendly, one-pot Pd-catalyzed coupling strategy.



Scheme 2.1.2 Evaluation of L1.2-Boc (Boc-protected amine) in Suzuki coupling with Frag B and Frag B-DiMs.

An initial demonstration of the in-situ Boc protection combined with Heck reaction was conducted to assess the feasibility of the one-pot approach and to generate retention time (RT) reference standards. The reaction of **Frag A** with **Frag D** and Boc₂O, in the presence of 0.6 mol% of PdCl₂(PPh₃)₂, yielded the desired Boc-protected Heck coupling product **L1.2-Boc** with approximately 95 A% (275 nm); approximately 5 A% (275 nm) of bisalkynylated products were also detected (Scheme 2.1.3). Notably, the Heck reaction proceeded more slowly in the absence of Boc₂O, highlighting the beneficial role of in-situ Boc protection in promoting reaction efficiency.

Scheme 2.1.3 Evaluation of one-pot *in-situ* Boc protection and Heck reaction with Frag A.

An extensive catalyst screen was conducted for the Heck reaction to identify the most suitable systems and to establish a catalyst pool for the subsequent Suzuki coupling.^{30,31} While many catalysts were effective, a number of highly active systems promoted the formation of a bisalkynylated byproduct, **L1.2-Boc-DiFd** (Scheme 2.13). XPhos-Pd-G2, XPhos-Pd-G3, and PdCl₂/XPhos were among them (Table 2.1.1). However, precatalysts such as Pd(PPh₃)₂Cl₂, Pd(PPh₃)₄ and Pd(dppf)Cl₂ proved effective in the Heck reaction between **Frag A** and **Frag D** in the presence of Boc₂O, affording **L1.2-Boc** within 1h, without significant amount of bisalkynylation byproducts.

To enable a well-designed one-pot Pd-catalyzed sequence, catalyst screening for the Suzuki reaction was subsequently performed. The first parameter evaluated was the Pd/L catalyst system. The reaction of L1.2-Boc with Frag B-DiMs was investigated using various Pd catalysts. Preformed catalysts such as Pd(PPh₃)₂Cl₂, Pd(PPh₃)₄ and Pd(dppf)Cl₂ – which provided favorable alkynylation outcomes – showed moderate Suzuki-Miyaura activity. Conversely, more sterically hindered and electronically rich systems like XPhos-Pd-G2, XPhos-Pd-G3, and PdCl₂/XPhos demonstrated strong performance in the Suzuki coupling, supporting the feasibility of a one-pot, double-dosed approach (vide infra).³² Notably, under Suzuki conditions, one of the methylsulfonamide groups was cleaved, yielding the desired product without the need for an additional hydrolysis step. These findings supported M4ALL's hypothesis that a one-pot Heck-Suzuki sequence could be achieved.

Table 2.1.1 Single dose Pd/L catalyst screen for one-pot Heck/Suzuki reaction.

				In-process analysis (A%, 275 nm) ^b						
# ^a	ELN	Pd/L (5 mol%)	Ste	p 1 (alky	nylation)	Step 2	(Suzuki)			
			L1.1- Boc	L1.2- Boc	L1.2-Boc- DiFd	L1.3- Boc ^c	L1.2-Boc			
1	AHS186-X20-1	Pd(PPh ₃) ₂ Cl ₂	4	90	1	30	14			
2	AHS186-X20-2	Pd(PPh ₃) ₄	8	79	-	20	25			
3	AHS186-X20-3	Pd(dppf)Cl ₂	11	87	2	15	49			
4	AHS186-X21-1	PdCl ₂ / PPh ₃	3.2	81	0.6	34	15			
5	AHS186-X21-2	PdCl ₂ / TFP	2	91	3	30	24			
6	AHS186-X22-1	Pd ₂ (dba) ₃ / PPh ₃	0.1	72	5	50	15			
7	AHS186-X22-2	Pd ₂ (dba) ₃ / TFP	ND	77	3	39	19			

^aAll reactions were performed on 100 mg scale of (rac)-L1.1-Boc; ^bA% measured at 275 nm by LC-MS; ^cTwo atropisomers (minor/major (A%) ~ 1/5) were observed.

To assess the feasibility and practicality of a telescoped one-pot Heck–Suzuki sequence from Frag A to L1.3-Boc, an initial reaction was conducted using Pd(PPh₃)₂Cl₂ (5 mol%) as a single catalyst (Table 2.1.1). This sequential transformation afforded L1.3-Boc in approximately 30 A%, with 14 A% (275 nm) of the intermediate L1.2-Boc remaining. Given the modest conversion to L1.3-Boc, a comprehensive condition screen was undertaken to enhance the efficiency of both coupling steps. The following parameters were systematically evaluated: 1) Pd/ligand combinations; 2) base selection; 3) solvent system, and 4) reaction temperature (data not shown). As summarized in Table 2.1.1, the choice of catalyst and ligand had a significant impact on the outcome of the Heck-Suzuki sequence. Among screened catalysts and precatalyst systems (Pd/L), Pd₂dba₃ / PPh₃ delivered the highest yield of L1.3-Boc, albeit with quantities of L1.2-Boc remaining unconverted. Variations in base and solvent did not improve yields of L1.3-Boc and adjusting the reaction temperature from room temperature (rt) to 100 °C failed to enhance performance. While this study demonstrated that a single-dose Pd catalyst strategy could, in principle, affect the telescoped Heck-Suzuki sequence, it was ultimately limited by its Suzuki coupling performance.°

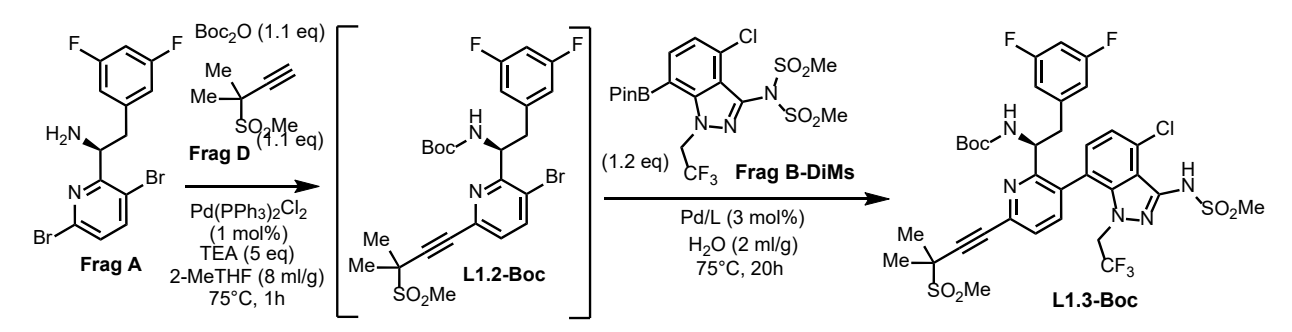
Modest conversion to **L1.3-Boc** and the persistent presence of intermediate **L1.2-Boc** highlighted the need of improvement of activity of catalyst in Suzuki reaction. Building on the benefits observed from the alkynylation-co-Boc-protection step using Pd(PPh₃)₂Cl₂ (1 mol%) as a

14

^e Notably, two atropisomers of **L1.3-Boc** were observed following the Suzuki coupling with **Frag B-DiMs**. The ratio of minor to major isomers was approximately 1:5, based on A% (275 nm).

catalyst, f a double-dose catalyst approach strategy was pursued. This involved introducing a second Pd catalyst dose specifically to enhance the Suzuki coupling efficiency.

Table 2.1.2 Double-dosed Pd/L catalyst screen for one-pot Heck/Suzuki reaction.



# ^a	ELN	Pd/L	In-process analy	$vsis (A\%, 275 nm)^b$
#	ELN	Pd/L	L1.3-Boc ^c	L1.2-Boc
1	DAG173-X26-1	PdCl ₂ / CyPPh ₂	59	7
2	DAG173-X26-2	PdCl ₂ / XPhos	56	15
3	DAG173-X26-3	PdCl ₂ / SPhos	55	13
4	DAG173-X26-6	PdCl ₂ / RuPhos	55	15
5	DAG173-X27-2	PdCl ₂ / tBuBrettPhos	53	17
6	AHS186-X25-6	PdCl ₂ / dppf	60	ND
7	DAG173-X27-5	PdCl ₂ / CataCXium A	73	<5
8	DAG173-X27-6	PdCl ₂ / BIDIME	62	<5
9	DAG173-X28-1	$Pd(PPh_3)_2Cl_2$	52	<5 ^d
10	DAG173-X28-2	Pd(PPh ₃) ₄	54	<8 ^d
11	DAG173-X28-3	Pd(dppf)Cl ₂	54	<4 ^d
12	DAG173-X28-4	XPhos Pd G2	50	<14 ^d
13	DAG173-X28-5	XPhos Pd G3	51	<16 ^d
14	DAG173-X28-6	PdCl ₂ / TFP	49	<13 ^d

^aAll reactions were performed on 100 mg scale of rac-A1.5; In-situ Boc-protection and Heck coupling afforded **L1.2-Boc** in >90A% in all screens with 1 mol% of Pd(PPh₃)₂Cl₂ as catalyst; ^bA% measured at 275 nm by LCMS; ^cTwo atropisomers (minor/major (A%) ~ 1/5) were observed; ^d**L1.2-Boc** co-eluted with **L1.3-Boc-DiMs** isomer.

A variety of preformed Pd-catalysts and Pd/L combinations were investigated as a second dose of catalyst in the Suzuki reaction. As summarized in Table 2.1.2, this dual-catalyst strategy addressed the limitations of the single-dose system, offering a more robust and higher-yielding approach for the telescoped Heck–Suzuki sequence. Catalysts well-suited for sterically hindered Suzuki reactions, such as PdCl₂/CataCXium A³³ and PdCl₂/BIDIME,³⁴ performed well in this

15

^f Catalyst loading screens (data not shown) indicated that 5 mol% Pd(PPh₃)₂Cl₂ was unnecessary, as 1 mol% delivered comparable yields.

sequence. Notably, PdCl₂/CataCXium A delivered 73 A% (275 nm) of L1.3-Boc. Based on these results, various Pd sources were evaluated within the double-dosed catalytical system (Table 2.1.3). In addition to PdCl₂, Pd(OAc)₂ yielded 52 A% (275 nm) of L1.3-Boc, though a significant amount of intermediate L1.2-Boc remained unreacted. Homogenous catalyst Pd₂(dba)₃ achieved full conversion of L1.2-Boc, resulting in 64 A% (275 nm) of L1.3-Boc. Preformed catalysts such as Pd(allyl)Cl and Pd(dppf)Cl₂ also achieved good conversion of L1.2-Boc, with Pd(dppf)Cl₂ yielding 72 A% (275 nm) of L1.3-Boc. The choice of solvent in the Heck-Suzuki sequence proved critical; when CH₃CN was used, less than 5 A% (275 nm) of L1.3-Boc was detected. Across all catalytic systems tested, a notable amount of L1.3-Boc-DiMs was observed, indicating the need for an optimized base to enable efficient demesylation. Notably, across all double-dosed sequence, 1 mol% of Pd(PPh₃)₂Cl₂ was used as the catalyst in the Heck reaction, consistently yielding L1.2-Boc in 85-95 A% (275 nm).

Table 2.1.3 Evaluation of Pd source with CataCXium A ligand in one-pot Heck-Suzuki reactions.

			Step 2 (Suzuki)					
#	ELN^a	Pd	In-process analysis (A%, 275 nm) ^b					
		(3 mol%)	L1.3-Boc ^c	L1.2-Boc ^e				
1	AHS186-X25-1	PdCl ₂	67	≥11	≤6			
2	AHS186-X26-2 ^d	PdCl ₂	5	13	20			
3	AHS186-X25-2	$Pd(OAc)_2$	52	>7	<16			
4	AHS186-X25-3	Pd ₂ (dba) ₃	63	16	ND			
5	AHS186-X25-7	Pd(allyl)Cl	51	14	ND			
6	AHS186-X25-4	Pd(dppf)Cl ₂	71	≥12	≤3			

^aAll reactions were performed on 100 mg scale of racemic Frag A; ^bA% measured at 275 nm by LCMS; ^cTwo atropisomers (minor/major (A%) $\sim 1/5$) were observed; ^dMeCN was used as solvent; ^eL1.2-Boc co-eluted with L1.3-Boc-DiMs isomer. ND = non-detect.

To facilitate easier purging of Pd species during workup, PdCl₂ was selected as the Pd resource as the second dose of catalyst in Suzuki reaction. Before evaluating bases for demesylation, a base screening was conducted for both Heck and Suzuki reactions. As summarized in Table 2.1.4, triethylamine (TEA) emerged as the optimal base for the Heck reaction. In contrast,

switching to inorganic bases commonly used in the Suzuki reactions (e.g., NaOH, K₂CO₃ or K₃PO₄) resulted in low yields of **L1.2-Boc**. With TEA as the base for the Heck step, the effect of adding an inorganic base to the Suzuki reaction was further explored. Among those tested, K₂CO₃ performed best, delivering 80 A% (275 nm) of **L1.3-Boc** along with 2.6 A% (275 nm) of **L1.3-Boc-DiMs**, and a full conversion of **L1.2-Boc**. These results further underscored the importance of base optimization in enhancing the efficiency of the demesylation process.

Table 2.1.4 Evaluation of base in one-pot Heck-Suzuki reactions.

		Step 1 (Heck)			Step 2 (Suzuki)			
#	ELN^a		A ^c	% ^b			$A\%^b$	
		Base	L1.1-	L1.2-	Base	L1.3-	L1.3-Boc-	L1.2-
			Boc	Boc		\mathbf{Boc}^c	DiMs	Boc
1	DAG173-X30-1	NaOH (3M)	30	66	-	24^d	ND	ND
2	DAG173-X31-1	$K_2CO_3(3M)$	91	4	-	15 ^e	30	ND
3	DAG173-X32-1	$K_3PO_4(3M)$	79	14	-	ſ	ſ	ſ
4	DAG173-X30-2	Et ₃ N	ND	91	NaOH (3M)	63^d	12	ND
5	DAG173-X31-2	Et ₃ N	ND	94	$K_2CO_3(3M)$	80^e	2	ND
6	DAG173-X32-2	Et ₃ N	0.3	92	$K_3PO_4(3M)$	56 ^f	ND	19

"All reactions were performed on 100 mg scale of racemic Frag A; ^bA% measured at 275 nm by LCMS; ^cTwo atropisomers (minor/major (A%) ~ 1/5) were observed.; ^d21h; ^e4h; ^fNot proceeded for Suzuki due to lower conversion of Heck step; ND= non-detect.

Base screening for demesylation was conducted, observing the current double-dosed conditions (i.e., using Pd(PPh₃)₂Cl₂ as the catalyst and TEA as the base in the Heck reaction, then PdCl₂/CataCXium A as the second catalytic dose in the Suzuki reaction). As shown in Table 2.1.5, all tested inorganic bases, including NaOH, K₂CO₃, K₃PO₄, and KOH, achieved excellent conversion in the demesylation step, with residual **L1.3-Boc-DiMs** remaining below 1 A%. As concomitant formation of potassium salts aided precipitation during workup, KOH was selected as the preferred base for demesylation following completion of the Suzuki transformation.

Table 2.1.5 Base screening for demesylation for synthesis of L1.3-Boc.

# ^a	ELN	Page (5 ag)	Time (h)	In-process as	nalysis (A%) ^b
#	ELN	Base (5 eq)	Time (h)	L1.3-Boc ^c	L1.3-Boc-DiMs
1	AHS186-X28-1	NaOH (3M)	2	82	ND
2	DAG173-X31-3	$K_2CO_3(3M)$	4	80	0.3
3	DAG173-X32-3	$K_3PO_4(3M)$	4	82	ND
4	RVE196-X16	KOH (3M)	2	81	0.6

^aAll reactions were performed with racemic A1.5 on 100 mg scale, after completion, the reaction mixture was acidified with HOAc to afford L1.3-Boc; b A% measured at 275 nm by LCMS; c Two atropisomers (minor/major (A%) \sim 1/5) were observed.

Thus, unoptimized conditions for the one-pot, double-dosed Heck-Suzuki sequence were as follows:

• Boc protection & Heck reaction

- o A one-pot Boc protection and Heck alkynylation was performed using **Frag A** (1 equiv), **Frag D** (1.1 equiv), Boc₂O (1.1 equiv), Et₃N (5 equiv) and Pd(PPh₃)₂Cl₂ (1 mol%) in 2-MeTHF (8 V) at 75 °C for 2-3 h. This afforded **L1.2-Boc** in 90-95 A% (275 nm).
- o 5-10 A% of L1.2-Boc-DiFd was observed as a side product during the Heck step.^g

• Suzuki reaction & Demesylation

O The crude Heck reaction mixture was submitted to a Suzuki coupling with **Frag B-DiMs** (1.2 equiv), PdCl₂ (3 mol%)/CataCXium A (6 mol%), and water (2 V) at 75 °C for 3 h. This was followed by demesylation using KOH (3M, 5 equiv) at 75 °C for an additional 3 h, yielded **L1.3-Boc** in 80-85 A% (275 nm).

g The purity and the stoichiometry of **Frag D** are critical to minimizing formation of the side product **L1.2-Boc-DiFd**. Employing 1.03 eq of **Frag D** (> 97 wt% purity) successfully limited the side product to NMT 5 A% of the side product. See Table 2.1.5 for details.

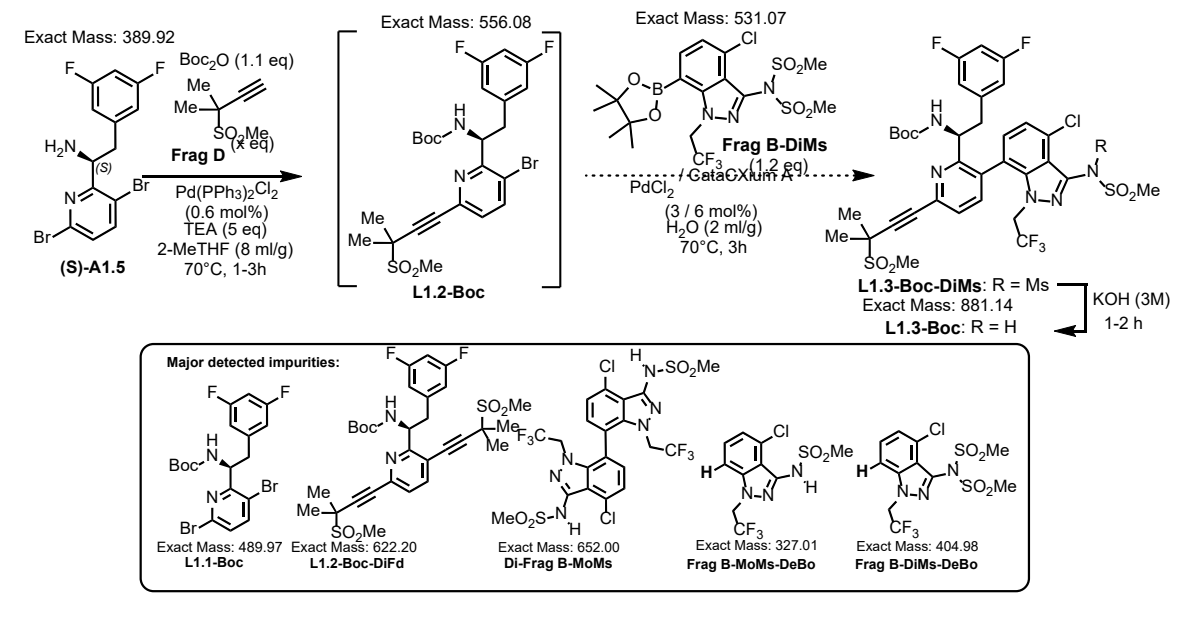
 5-10 A% de-boronated species derived from Frag B-DiMs was observed during the Suzuki step.

To identify the optimal reagent equivalents for maximizing yield, improving reaction purity profile, and achieving the best RMC economics, a Design of Experiments (DOE) analysis was performed for each Pd-catalyzed coupling step. For the Heck reaction, a central composition design (CCD) was employed, evaluating 4 factors (equivalent of Frag D, catalyst loading, reaction temperature, and solvent volume) with 5 levels of each factor. Similarly, the Suzuki reaction was optimized using a 5-factor, 5-level CCD approach, examining equivalents of **Frag B-DiMs**, PdCl₂ loading, CataCXium A amount, reaction temperature, and water volume. However, the individually optimized conditions for each step could not be directly applied to the one-pot telescoped sequence, likely due to the complexity and interdependence of the system. As a result, a one-factor-at-a-time (OFAT) strategy was adopted for fine-tuning and process development.

DOE examination of **Frag D** equivalents revealed that the Heck reaction occurred at both bromide positions in **Frag A**. The initial coupling preferentially targeted the ortho-bromo site, however, excess **Frag D** also reacted with the meta-bromo position, leading to undesired bisalkynylation. This side reaction not only consumed the desired product **L1.2-Boc**, but also increased impurity levels, complicating downstream purification. Conversely, insufficient **Frag D** resulted in incomplete conversion of **L1.1-Boc**, which would subsequently react with **Frag B-DiMs** during the Suzuki step. This led to the formation of bis-Suzuki side products, further complicating purification during the final API isolation. To determine the optimal equivalent of **Frag D** for the Heck reaction, an equivalency screen was performed while keeping all other reaction conditions constant. As summarized in Table 2.1.6, using 1.06 equivalents of **Frag D** achieved full conversion of **L1.1-Boc**, yielding approximately 95 A% (275 nm) **L1.2-Boc** along with a manageable amount of side product **L1.2-Boc-DiFd**.

Table 2.1.6 Optimization of equivalents of **Frag D** to minimize the undesired bisalkynylation.

^h DOE design was carried out by Design-Expert® software, version 23.1.8 (64-bit), Stat-Ease, Inc., Minneapolis, MN, USA, www.statease.com.



ua	EVV	Frag D	Time/ In-process (A%) ^c				
# ^a	ELN	(eq)	h	L1.1-Boc	L1.2-Boc	L1.2-Boc- DiFd	Frag \mathbf{D}^d
1	DAG173-X40-1	1.01	4	1.0	94.7	4.2	ND
2	DAG173-X41-1	1.02	3	0.8	94.7	4.4	ND
3	AHS186-X34-1	1.03	2	0.4	94.8	4.7	ND
4	AHS186-X33-2	1.06	2	0	94.6	5.4	ND
5^b	AHS186-X35	1.03	3	1.0	95	3.2	0.3

^a1g of **(S)-A1.5**; ^b5 g of **(S)-A1.5**; ^cHPLC was measured at 275 nm; ^dGC-MS TIC Area%. ND: not determined.

In parallel, efforts were made to lower RMC of the telescoped process by reducing the amount of **Frag B-DiMs** and/or catalyst loading in the Suzuki reaction. As shown in Table 2.1.7, a range of **Frag B-DiMs** equivalents (1.0 - 1.2) and PdCl₂/CataCXium A loadings (2/4 to 3/6 mol%) were evaluated. These conditions delivered comparable conversions to **L1.3-Boc** (74-82 A%), with varied and noteworthy quantities of residual **L1.2-Boc** (5-14 A%). Based on these findings, the condition employing 1.2 equivalents of **Frag B-DiMs**, 3 mol% of PdCl₂ and 6 mol% of CataCXium A was selected for scale-up.

Table 2.1.7 Optimization of equivalents of **Frag B-DiMs** and catalyst loading for Suzuki reaction.

					In-process	analysis (A%	o, 275 nm) ^a	
#	ELN	Frag B- DiMs (eq)	Pd/L (mol%)	L1.2- Boc	L1.2-Boc- DiFd	L1.2- MoMs- DeBo	Di-Frag B-MoMs	L1.3- Boc ^b
1	DAG173-X40-1	1.0	2/4	14	2.6	5.6	0.9	74
2	DAG173-X40-2	1.1	2/4	8	2.4	5.9	0.6	80
3	DAG173-X42	1.2	2/4	5	2.8	6.7	0.7	80
4	AHS186-X34-1	1.1	3/6	7.4	2.8	4	0	82

 a A% (Area%) was measured by HPLC (or LC-MS) at 275 nm; b Two atropisomers (minor/major (A%) ~ 1/5) were observed.

Thus, the optimized reaction conditions for the one-pot, double-dosed Heck-Suzuki sequence are as follows. Critical process parameters identified to date are also summarized.

• Boc protection & Heck reaction

- o A one-pot Boc protection and Heck reaction was performed using **Frag A** (1 equiv), **Frag D** (1.06 equiv), Boc₂O (1.1 equiv), Et₃N (5 equiv) and Pd(PPh₃)₂Cl₂ (1 mol%) in 2-MeTHF (8 V) at 75 °C for 2-3 h. This afforded **L1.2-Boc** in 90-95 A% (275 nm).
- Less than 5 A% of L1.2-Boc-DiFd was observed as a side product during the Heck step.

• Suzuki reaction & Demesylation

- The crude Heck reaction mixture was subjected to Suzuki coupling with Frag B-DiMs (1.2 equiv), PdCl₂ (3 mol%)/CataCXium A (6 mol%), and water (2 V) at 75 °C for 3 h. This was followed by demesylation using KOH (3M, 5 equiv) at 75 °C for an additional 3 h, yielded L1.3-Boc in 80-90 A% (275 nm).
- 5-10 A% de-boronated species derived from Frag B-DiMs were observed during the Suzuki step.

• Critical process parameters (CPPs)

- o **Inert atmosphere**: Failure to achieve complete deoxygenation of the reaction system will result in low conversion of **L1.2-Boc**. See section 2.1.2 for details.
- L1.1-Boc Consumption: Residual L1.1-Boc must be below 0.2 A% (275 nm). Bis-Suzuki side product from L1.1-Boc introduces challenges during API purification.
- o **Boc2O** Addition: Boc2O should be added at a temperature no higher than room temperature due to the exothermic nature of the Boc-protection.
- Potassium salt of L1.3-Boc formation: Forming L1.3-K-Boc enabled efficient liquidliquid extraction (LLE) workup and precipitation during purification.

2.1.2 Practical workup and purification for scalability

With optimized reaction conditions established, efforts shifted toward developing an LLE method for efficient workup, removal of impurities and Pd residues, and product precipitation. To evaluate the solubility and partitioning behavior of **L1.3-Boc**, its p*K*a was measured in MTBE via acid-base titration,³⁵ and determined to be approximately 10.5 (Figure 2.1.1). Partitioning between MTBE and water across varying pH levels was assessed by HPLC. As shown in Figure 2.1.1, **L1.3-Boc** exhibited high solubility in MTBE at pH values below 10 (0.5 units below its p*K*a). Conversely, at pH value above 12 (1.5 units above its p*K*a), the alkaline salt form of **L1.3-Boc** showed excellent solubility in aqueous layer. These findings suggested that adjusting the reaction mixture to pH 13-14 might enable effective removal of organic impurities by solvent wash. Various organic solvents (Toluene, EtOAc, iPrOAc, 2-MeTHF, MEK, MIBK, etc.) were screened to purge organic impurities from the basic aqueous solution. Toluene purged these impurities but presented challenges with emulsions and layer separation. MEK enabled excellent layer separation

from the aqueous phase. PhMe/MEK (9/1, v/v) removed organic impurities, particularly L1.2-DiMs-DeBo, however, the binary solvent system still suffered from poor layer separation. Among the screened solvents, MTBE was optimal for purging impurities such as L1.2-Boc-DiFd, L1.2-Boc, and Frag B-DiMs-DeBo (all of which lack free methylsulfonamide (-NHMs) groups). MIBK showed excellent solubility for L1.3-K-Boc across the entire pH range. Although ineffective at purging impurities, MIBK exhibited excellent phase separation and proved to be a highly effective solvent for extracting the desired product from the aqueous layer after impurity removal.

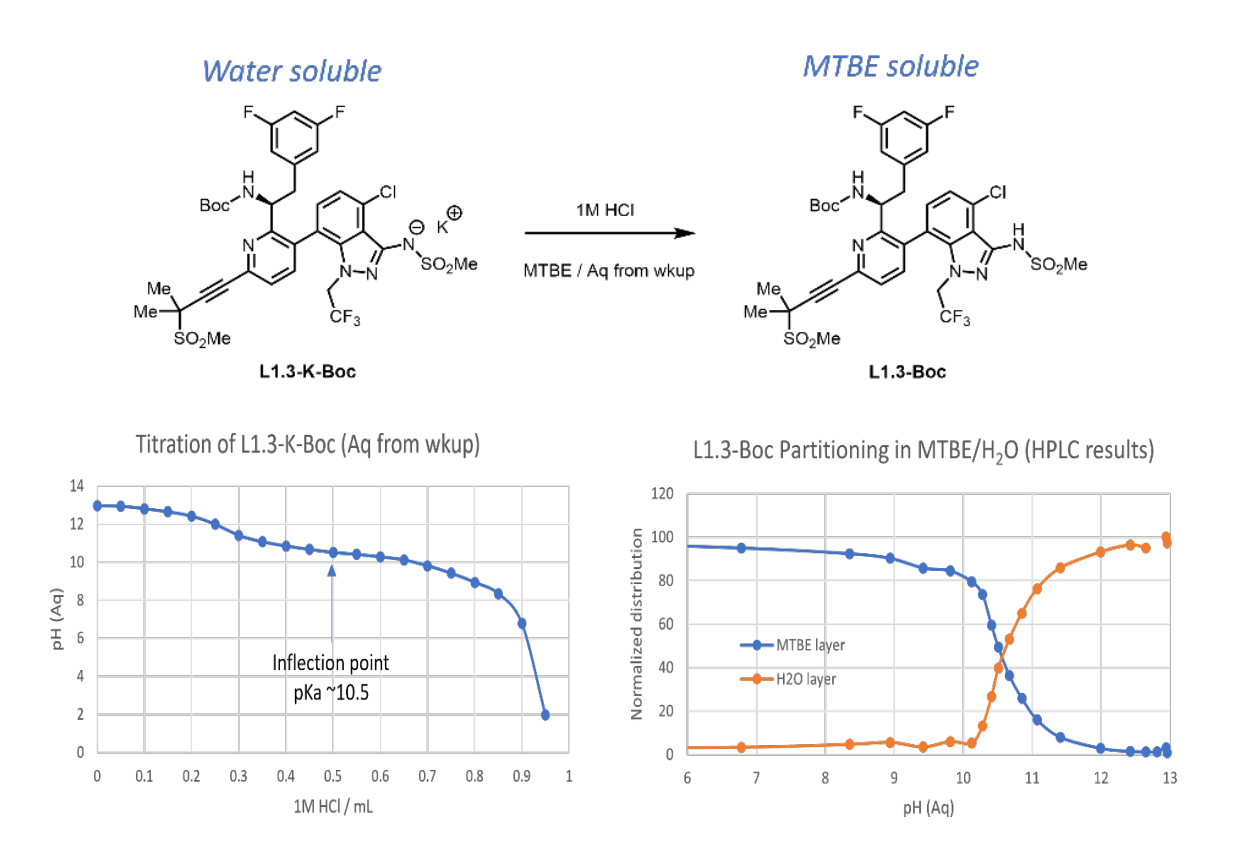


Figure 2.1.1 p*K*a measurement of **L1.3-Boc** and partitioning in MTBE and H₂O layer. MTBE effectively rejects **L1.3-K-Boc**, while readily dissolving organic impurities, at pH > 12.5. Titration experiment: 0.1M **L1.3-K-Boc** in 5 mL MTBE / 10 mL water, titrated with 1M HCl at 21°C, after each 0.1 mL addition of HCl, both organic and aqueous layers were sampled (30 μ L into 1.00 mL CH₃CN) for HPLC analysis. Peak areas were normalized using the first and last data points. Inflection point in the titration curve corresponds to a p*K*a of ~10.5 for **L1.3-Boc**.

Initial application of MTBE in the liquid-liquid extraction (LLE) workup of alkaline L1.3-K-Boc, to purge impurities, met with significant product loss. Residual 2-MeTHF from the telescoped coupling reaction was identified as the primary cause. To address this, azeotropic distillation was employed to remove 2-MeTHF from the system. Its removal effectively minimized product loss in subsequent MTBE washes. Three MTBE washes were sufficient to purge organic impurities, resulting in a crude of ~95 A% (HPLC, 275 nm). Crude **L1.3-K-Boc** was then retrieved from the aqueous layer via two MIBK extractions. To precipitate **L1.3-K-Boc** from the MIBK solution, various anti-solvents and minimal MIBK volumes were evaluated. The optimal precipitation conditions were identified as follows:

- 5 volumes of MIBK: Provided favorable conditions for precipitation
- 10 volumes of heptane: Enable formation of fine precipitates

Based on the established LLE workup and precipitation conditions, **L1.3-K-Boc** was isolated as a light-yellow solid in 62-70% yield, with approximately 90 wt% purity (> 97 A%, 275 nm)^k.

A telescoped Heck-Suzuki sequence was developed using a double-dosed Pd catalyst system: 1 mol% of Pd(PPh₃)₂Cl₂ for the initial Heck reaction, followed by 3 mol% of PdCl₂ and 6 mol% of CataCXium A for the subsequent Suzuki coupling. This strategy enabled the first synthesis of the key intermediate for lenacapavir API. Notably, the advanced Pd-coupling strategy facilitated early-stage Pd removal, aligning with final API specifications.³⁶ In accordance with the ICH Q3D(R2) guideline for elemental impurities, the final API must contain less than 10 ppm of Pd residue for both oral and injectable drug substances.³⁷ Compared with Gilead's 2024 process,²⁰ which incorporates Pd removal at a late stage, the M4ALL route offers a strategic advantage by enabling earlier Pd purging during the synthetic sequence.

Table 2.1.8 Pd scavenger screen for removal of Pd residue from crude L1.3-K-Boc.

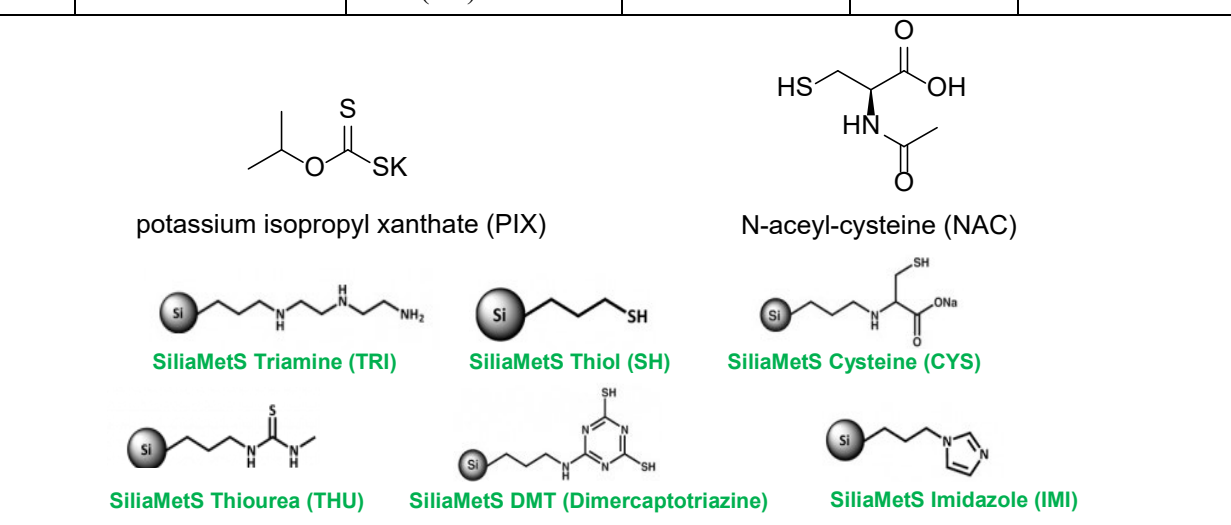
# ^a	Sample ID	Scavenger (0.2 g)	A%, (275 nm)	$Pd (ppm)^b$	Recovery yield
1	DAG173-X47	Source batch	97	395 ^c	NA

ⁱ 2-MeTHF is the reaction solvent during the telescoped coupling reactions. Since **L1.3-K-Boc** is soluble in 2-MeTHF, performing MTBE washes in the presence 2-MeTHF leads to product loss.

^j **L1.3-K-Boc** is crystalline, offering the opportunity to develop recrystallization conditions for purification. Recrystallization of the crude from IPA afforded off-white solid with 89 A% (275 nm); Recrystallization from toluene / heptane afforded pale-yellow solid with 92 A% (275 nm).

^k Refer to Table 2.1.10 for the detailed data.

2^d	DAG173-X47-NAC	aq NAC (20 mol%)	98	61	ND
3^e	DAG173-X47-PIX	aq PIX (20 mol%)	98	89	ND
4	DAG173-X46	Source batch	97	261 ^c	NA
5	RVE196-X27-2	(CYS) Cysteine	95	105	85%
6	RVE196-X27-4	(DMT) Dimercaptotriazine	95	18	88%
7	RVE196-X27-6	(IMI) Imidazole	95	21	88%
8	RVE196-X27-8	(THU) Thiourea	96	16	89%
9	RVE196-X27-10	(TRI) Triamine	94	59	84%
10	RVE196-X27-12	(SH) Thiol	94	13	74%



^aL1.3-K-Boc (200 mg) was stirred with the respective scavenger (1:1, wt/wt) in 10 volumes of MIBK at 50 °C for 2 hours, unless otherwise stated in the table. The resulting slurry was cooled down to 20 °C and filtered using a disposable funnel (10 micron), and the solid was washed with MIBK (3 × 10 volumes). The combined organic filtrate was concentrated under reduced pressure at 50 °C and then dried in a vacuum tray dryer (VTD) at 75 °C for 16 hours for Pd residue measurement; ^bPd content was measured by ICP-OES; ^cNo Pd scavenger treatment; ^dA mixture of L1.3-K-Boc in MIBK and 20 mol% NAC in 3% w/w KOH at 50 °C for 2h; ^eA mixture of L1.3-K-Boc in MIBK and 20 mol% PIX in 3% w/w KOH at 50 °C for 2h.

A range of Pd scavengers was screened to reduce residual Pd in L1.3-K-Boc. As summarized in Table 2.1.8, NAC and PIX treatments reduced Pd content from 395 ppm to 61 ppm and 89 ppm, respectively.^{38,39} While initially promising, further Pd reduction could not be achieved. Neither doubling the scavenger concentration nor extending treatment time yielded additional improvement. SiliaMetS scavengers, however, showed superior performance.^{40,41} Most variants exhibited strong Pd removal capabilities, with SiliaMetS SH achieving a reduction to 13 ppm. Despite its effectiveness, challenges remained: the process required high scavenger loading

(100 wt%) and enabled moderate recovery (74%), which posed limitations for cost-effective process development.

Weight loading and operating temperature of SiliaMetS SH were examined for Pd removal efficiency. Temperature was found to be a crucial factor impacting its Pd scavenging performance (Table 2.1.9). At 50 °C, lower scavenger loadings, such as 75 wt% or 25 wt%, only reduced Pd levels to approximately 100 ppm. Significant enhancement in Pd removal was observed at 80 °C; initial experiments demonstrated that both 5 wt% and 10 wt% scavenger loading effectively reduced Pd levels to below 10 ppm after 20 h of treatment. Furthermore, a shorter treatment duration of 3 h was sufficient to achieve a Pd concentration below 10 ppm. Notably, the Pd treatment process did not introduce any additional impurities, and the purity profile remained unchanged or slightly improved.

To improve L1.3-K-Boc recovery during filtration, 50 wt% of Celite¹ was added as a processing aid. This resulted in a faster filtration and increased the isolated yield to more than 95%. The Pd removal process was thus implemented into the LLE workup and the 10 wt% Pd scavenger loadings was selected for scale-up. During the LLE workup, the resulting MIBK solution was treated with 10 wt% SiliaMetS SH at 80 °C for 3h, utilizing 50 wt% of Celite as a filtration aid. The resulting solution was concentrated to 5 V and precipitated with heptane (10 V), affording L1.3-K-Boc with excellent recovery and < 10 ppm Pd. It is worth noting that the potassium level decreased from 4% to approximately 2%, indicating neutralization occurred during the SiliaMetS SH treatment. Reduction of potassium content also introduced challenges in the subsequent precipitation process. However, a basification step applied to the solution resulting from the SiliaMetS SH treatment successfully restored the potassium level, thereby enabling a smooth and efficient precipitation process.^m

Table 2.1.9 Efficiency improvement of Pd removal in L1.3-K-Boc.

¹ The amount of Celite is relative to the substrate mass. While it might be plausible to reduce the amount of the Celite, its quantity was not optimized due to time constraints.

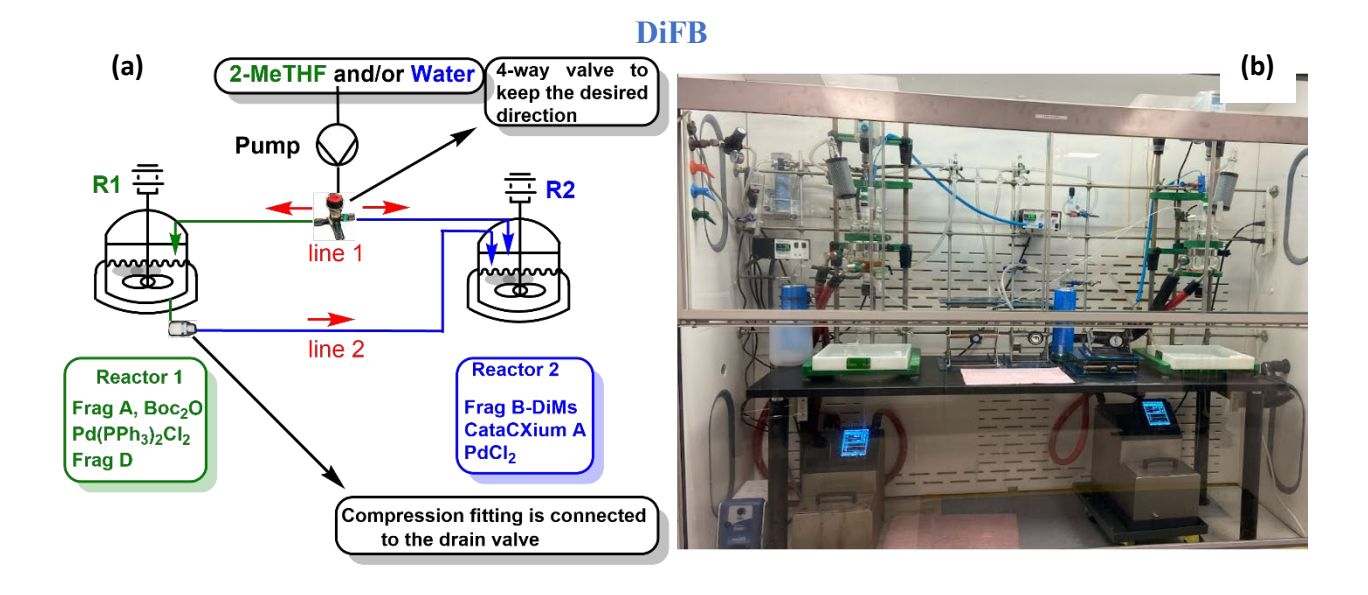
^m The authors hypothesize that further decreases in the loading of SiliaMetS Thiol (e.g., less than 5 wt%) – with the achievement of residual Pd < 10 ppm – is plausible. Further reduction in the Pd sequestrant loading is anticipated to minimize the neutralization phenomenon, possibly negating the subsequent base treatment.

Boc N SO₂Me SiliaMetS SH (x wt%), MIBK
$$(10V)$$
, 80 °C, time $(10V)$,

# ^a	ELN	SiliaMetS SH (wt%)	Temp (°C)	Time (h)	Pd (ppm)	Recovery yield (%)
1^b	AAN174-X33	-		-	500	-
2	RVE196-X27-15	75	50	3	129	95
3	RVE196-X27-13	25	50	3	188	83
4	RVE196-X31-1	5	80	20	<10 (LOQ)	92
5	RVE196-X31-2	10	80	20	<10 (LOQ)	93
6	RVE196-X31-6	5	80	3	<10 (LOQ)	95
7	RVE196-X31-7	10	80	3	<10 (LOQ)	95

"See Table 2.1.8 (note a) for experimental procedure; "Source batch for Pd scavenger weight loading study.

As a result, the finalized process flow diagram of Milestone 1 is presented in Figure 2.1.1. The simplified reaction setup is illustrated in Figure 2.1.1 (a). Milestone 1 requires two reactors: Boc-protection and Heck alkynylation are carried out in the Reactor 1. Upon completion, the reaction mixture is transferred to Reactor 2, where the Suzuki reaction and de-mesylation are performed. Cannular transfer under positive argon pressure is employed to deliver solvents and liquid reagents, as well as to transfer the reaction mixture from Reactor 1 to Reactor 2. A photograph of the two reactors is shown in Figure 2.1.1 (b). All the decagram scale verification and scale-up reactions are conducted using the ChemRxnHub reactor system with Huber circulators as shown in the picture. The detailed process flow diagram of the workup and purification steps is depicted in Figure 2.1.1 (c).



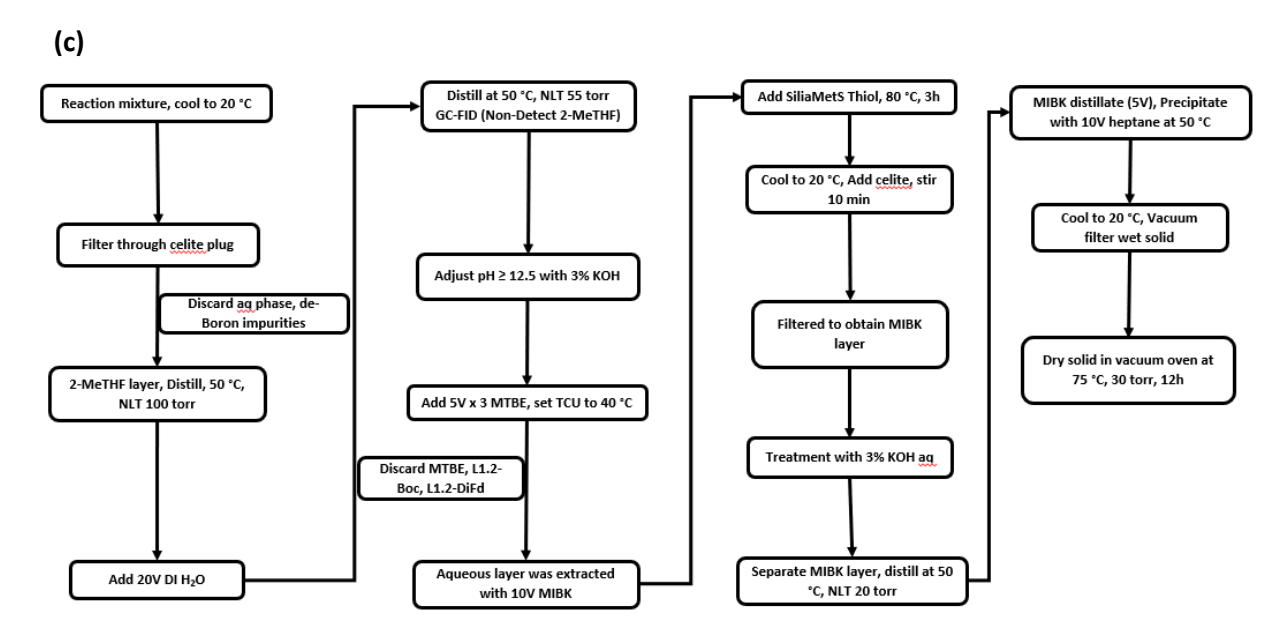


Figure 2.1.2 Batch process and LLE purification of **L1.3-Boc**: a) reactor setup chart; b) reactor pictures; c) process flow diagram.

The process comprises five major operations:

- 1) Azeotropic distillation to remove 2-MeTHF
- 2) MTBE-assisted purging of organic impurities
- 3) MIBK-based extraction of L1.3-K-Boc
- 4) SiliaMetS SH treatment for Pd removal followed by basification

5) Heptane-induced precipitation

Through these five major operations, the telescoped process yielded **L1.3-K-Boc** with an isolated yield of 60-70%, and > 90 wt% purity (>97 A%, 275 nm). The process was verified at decagram scale and documentedⁿ. Overall, the **CPPs** of the telescoped process are summarized below:

- High purity of Frag D° (> 98 wt%) is essential to accurately control the 1.05-1.06 equivalents in the Heck reaction. Lower purity (~90 wt%) has led to inconsistent results.
- Complete conversion of L1.1-Boc is necessary to prevent undesired downstream double Suzuki reactions, the products of which cannot be removed by the aforementioned LLE
- **Formation of the potassium salt** (L1.3-K-Boc) is crucial for solid isolation following LLE workup.
- Azeotropic removal of 2-MeTHF is essential to minimize product loss during LLE workup
- pH adjustment to > 12 enables efficient impurity removal via MTBE extraction while minimizing product loss to the organic layer.
- MIBK-based LLE provides excellent phase separation, allowing for effective recovery of L1.3-K-Boc from the aqueous layer
- SiliaMetS SH treatment at 80 °C streamlines Pd removal in a cost-effective manner. A subsequent base treatment facilitates smooth precipitation.
- Concentration of MIBK solution to 5 V ensures robust precipitation upon the addition of 10 V of heptane.

Table 2.1.10 Decagram-scale verification of one-pot double-dosed Heck-Suzuki Sequence.

ⁿ The scanned documented process was provided in Chapter 3.1.

^o The use of commercial **Frag D** with approximately 90 wt% purity led to inconsistent outcomes in our Heck reactions.

		In-process analysis data (A%) ^b											
		Step 1			Step 2								
#	ELN^a	L1.2 Boc-		L1.3 -K-	L1.2	L1.2- Boc-	FragB- MoMs-	Di- FragB-					
		-Boc	DiFd	\mathbf{Boc}^c - \mathbf{Boc}		DiFd	DeBo	MoMs	7.2	8.8	12.1	12.8	
1	DAG173-X47	95	5	78.5	7.3	4.4	6.4	1.1	0.2	0.2	0.4	0.6	
2	AAN174-X33	94	6	83.3	3.2	5.1	5.5	0.7	0	0	0.4	0.5	
3^d	AAN174-X34 ^e	90	8	49.5	23.2	10.1	10.1	3.5	0.7	ſ	0.2	0.2	
4 g	DAG173-X51 ^e	94	6	84.0	2.3	4.6	5.8	0.6	0.2	0.2	0.6	0.4	

	ELN	Output after LLE purification											
#		HPL			K								
				FragB- Major unknowns MoMs- Retention Time (min)			Mass (g)	wt % ^h	(wt %) ⁱ	IY (%) ^j	Pd (ppm) ^k		
		\mathbf{Boc}^c	DeBo	7.2	8.8	12.1	12.8			, 0)			
5	DAG173-X47	97.7	0.3	ND	0.3	0.6	0.4	15.4	78	4.0	62	395	
6	AAN174-X33	98.7	0.5	ND	0	0.8	0	16.9	79	4.0	69	500	
7 ^d	AAN174-X34 ^e	97	1.0	0.0 6	0.3	0.2	0.2	33.1	81	4.2	34	< 11.4 ^l	
8 ^g	DAG173-X51 ^e	98.1	0.8	ND	ND	1.1	ND	65	86	4.7	70	8"	

^aAll reactions were performed on 10g scale of **Frag A** (1.0 eq), **Frag D** (1.1 eq), Boc₂O (1.1 eq) and Pd(PPh₃)₂Cl₂ (1 mol%), unless otherwise stated; **L1.1-Boc** was completely consumed in all Heck reactions; ^bA% measured at 275 nm by HPLC; ^cTwo atropisomers (minor/major (A%) ~ 1/5) were observed; ^dLow yield due to the failure to achieve complete deoxygenation of the reaction system during Suzuki reaction; ^e40g of **Frag A** was used; ^fOverlaped with **L1.2-Boc-DiFd** (8.5 min); ^g1.05 eq of **Frag D** was used; ^hWt% based on **L1.3-Boc** free base was obtained by HPLC, containing 3-8 wt% of MIBK, 1-2 wt% of water; ⁱPotassium content was measured by LC-ELSD; ^jCorrected by wt%; ^kObtained by ICP-OES; ^hTreated with 100 wt% SiliaMetS SH at 80 °C for 3h; ^mTreated with 10 wt% SiliaMetS SH at 80 °C for 3h. ND = Non-detect.

Several verification batches were conducted at the decagram scale prior to formal process documentation. The results, summarized in the Table 2.1.10 (entries 1-3, 5-7), underscore the efficiency of the telescoped, double-dosed Pd-catalyzed synthesis of L1.3-K-Boc. These trials also guided the fine-tuning of Frag D stoichiometry, with 1.05 equivalents identified as optimal for the finalized process (entries 4 and 8). The two atropisomers of L1.3-Boc remained unchanged before

and after purification, with a consistent minor-to-major isomer ratio of approximately 1:5, based on A% (275 nm). Documentation of the optimized route was completed and archived, with scanned records provided in Chapter 3.1. This work marks the development of the first one-pot catalytic system for constructing the core structure of the complex lenacapavir molecule.

2.1.3 Process safety assessment for Milestone 1

Safety assessment of a chemical process is crucial to determine its suitability for scale-up, particularly for Pd-catalyzed coupling reactions. A Reaction calorimetry provides critical insights by measuring the heat evolved or absorbed during a reaction, including parameters such as adiabatic temperature rise (ΔT_{ad}) and maximum temperature of synthesis reaction (MTSR). Among calorimetric techniques, heat flow calorimetry (HFCal) is particularly valuable as it closely mimics the plant-scale operations. In HFCal, a circulation system maintains isothermal conditions by removing heat at the same rate as it evolves during the reaction. To support safe scale-up, we conducted a comprehensive reaction calorimetry study using Mettler-Toledo EasyMax 102 system. This study measured ΔT_{ad} and MTSR for each step of Milestone 1, providing a detailed thermal assessment of the telescoped process.

Specifically, the dosing of the Boc anhydride/triethylamine in the Heck coupling, the addition of deionized H₂O/2-MeTHF in the Suzuki, and the KOH addition during the hydrolysis were evaluated. The reaction calorimetric analysis for the Heck coupling was conducted using 5 g of **Frag A** in a 100 mL vessel. The Δ H calculations, based on the moles of **Frag A** deployed, are summarized in Table 2.1.11. The addition of Boc anhydride and triethylamine to the reaction mass at 23 °C was found to be minimally exothermic, with a total heat of the reaction (Δ H_r) -16.0 kJ/mol (based on 5g of **Frag A**). The MTSR – defined as the sum of the adiabatic temperature rise (Δ T_{ad}) and the maximum process temperature – was determined to be 70.1 °C (Δ T_{ad} = -3.27 °C). This value is below the boiling point of the reaction solvent 2-MeTHF (i.e., 78.0 °C), indicating a low risk of solvent boiling under cooling failure conditions. The maximum reaction temperature (MRT), representing the peak temperature reached during the process step, was recorded at 69.0 °C. Additionally, the maximum heat generation (MHG) during the addition was measured at 8.36 W. Based on standard reactor cooling capacity thresholds – Low severity: Δ T_{ad} <50 °C and MHG

^p See Appendix for calorimetry experimental details.

<30 W; Medium: ΔT_{ad} 50-200 °C; High: ΔT_{ad} >200 °C and MHG>30 W)⁴³ – the step is classified as low severity, indicating minimal thermal hazard.

Table 2.1.11 Heat evolution during the dosing steps of the Heck coupling.

Process	$\Delta H_{ m r}$	ΔH_{r}	$\Delta H_{ m r}$	ΔT_{ad}	MTSR	MRT	MHG	C _p (J/	g K)	U (W/	m ² K)
Step	(kJ)	(kJ/g)	(kJ/mol)	(°C)	(°C)	(°C)	(W)	Before	After	Before	After
1 ^a	-0.204	-0.041	-16.0	-3.27	68.7	69.0	8.36	3.36	1.73	178.8	139.6

^aAddition of Boc anhydride and triethylamine to the reaction mass at 23 °C, C_p = Specific heat; U = Overall heat transfer coefficient.

Similarly, heat effects for the Suzuki reaction were obtained from a reaction on 7.1 g of **L1.2-Boc**. The ΔH calculations, based on the moles of **L1.2-Boc** are summarized in Table 2.1.12. The addition of deionized $H_2O/2$ -MeTHF and aqueous KOH (3M) to the reaction mass at 72 °C was found to be endothermic. The total ΔH_r was found to be -163.9 kJ/mol and -1217.0 kJ/mol (based on 7.1g of **L1.2-Boc**), for the addition of deionized $H_2O/2$ -MeTHF and aq KOH, respectively. While the MTSR was observed to be -57.7 °C (ΔT_{ad} = -129.7 °C) for the addition of deionized $H_2O/2$ -MeTHF and 64.5 °C (ΔT_{ad} = -7.54 °C) for aqueous KOH addition, which are both lower than the boiling point of the reaction solvent 2-MeTHF. Additionally, the MRT was found to be 69.0 °C for both process steps. Finally, an MHG of -2.92 W and -25.3 W were observed during the addition of deionized $H_2O/2$ -MeTHF and aqueous KOH, respectively. Again, based on prototypical reactor cooling capacity, the severity is considered low for the Suzuki reaction and demesylation step.

Table 2.1.12 Heat evolution during the dosing steps of the Suzuki coupling and demesylation.

Process	$\Delta H_{ m r}$	$\Delta H_{ m r}$	$\Delta H_{ m r}$	ΔT_{ad}	MTSR			$C_p (J/g)$	g K)	U (W/	m ² K)
Step	(kJ)	(kJ/g)	(kJ/mol)	(°C)	(°C)	(°C)	(W)	Before	After	Before	After
1^a	-2.09	-0.298	-163.9	-129.7	-57.7	69.0	-2.92	-0.0475	0.250	207.0	179.2
2^b	-15.5	-1.51	-1217	-7.54	64.5	69.0	-25.3	4.99	27.1	132.4	195.4

^aAddition of deionized H₂O/2-MeTHF to the reaction mass at 72 °C; ^bAddition of KOH to the reaction mass at 72 °C.

Overall, calorimetry data of Milestone 1 shows low severity of the process, indicating its suitability for scale-up from the safety point of view.

2.1.4 Impurities identification and RT marker

The identification, synthesis, and characterization of impurities play a critical role in process development, enabling a comprehensive understanding of the chemical process and, ultimately, robust product quality. ^{44–47} For Milestone 1, impurities associated with the finalized conditions are summarized in Figure 2.1.3. The corresponding HPLC retention times are provided as RT marker to support in-process analysis monitoring and isolated product characterization.

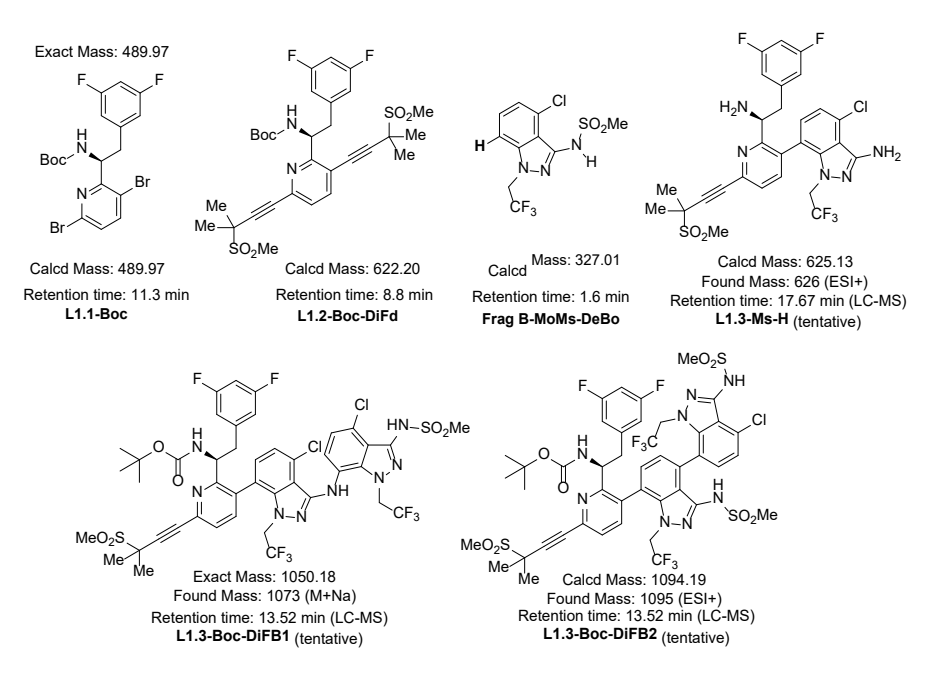


Figure 2.1.3 Identified major impurities and RT marker in Milestone 1.^q

2.2 H₂SO₄-based deBoc reaction and process development (Milestone 2)

With **L1.3-K-Boc** in hand, Boc deprotection was initially carried out using trifluoroacetic acid (TFA),¹⁷ yielding the corresponding amine **L1.3-Ms**. Subsequent coupling with **Frag C** proceeded smoothly, affording Len-API-H in > 90% isolated yield after column chromatography (Scheme 2.2.1).

Scheme 2.2.1 TFA-promoted Boc-deprotection and the subsequent amidation with **Frag** C for **Len-API-H** synthesis.

^q Major impurities **L1.1-Boc**, **L1.2-Boc-DiFd**, and **Frag B-MoMs-DeBo** were synthesized and structurally confirmed by ¹HNMR, ¹³CNMR, ¹⁹FNMR, and LC-MS (See the appendix for detailed synthetic procedures). Small amount (< 1 A% (275 nm) of **L1.3-Ms-H**, **L1.3-Boc-DiFB1** and **L1.3-Boc-DiFB2** was detected by LCMS. Their structures were tentatively proposed based on LCMS data. Please refer to **GFN-002-LEN-ADR** for the detailed analytical methods.

The results supported the feasibility of the proposed synthetic route towards to the API. Despite this initial success, several challenges had to be addressed to enable a process suitable for adoption by generic pharmaceutical companies:

- Although TFA-promoted Boc removal was efficient, complete elimination of residual TFA during workup proved difficult. Remaining TFA reacts with the amino group in L1.3-Ms to form trifluoroacetamide during the subsequent amidation, complicating purification of the final API.
- 2. Increasing regulatory restrictions on PFAS compounds limit the use of TFA in pharmaceutical manufacturing. 48-51

To overcome these issues, alternative Boc-deprotection strategies were explored, with the goal of identifying a practical, scalable, and reliable method for Boc removal.

2.2.1 Condition screening and optimization

Various mineral acids and methanesulfonic acid (MSA) were evaluated for Boc deprotection of L1.3-K-Boc. Sec. As summarized in Table 2.2.1, both H₂SO₄ (9M, 10 equiv) and MSA effectively cleaved the Boc group, affording L1.3-Ms in 96-97 A% (275 nm). In contrast, HCl and H₃PO₄ failed to deprotect L1.3-K-Boc. Notably, MSA produced a gel-like reaction mixture that complicated purification. Optimization revealed that using less than 10 equivalents or a lower concentration of H₂SO₄ was insufficient for complete Boc removal. Solvent screening identified a mixture of toluene (4.5 V) and EtOH (0.5 V) as optimal, providing a homogenous solution of L1.3-K-Boc prior to acid addition. Upon addition of H₂SO₄, a heterogenous mixture formed, but the subsequent workup proceeded smoothly, yielding L1.3-Ms. Single solvents such as MEK and MIBK provided high yields with H₂SO₄; concerns over the potential imine formation between the ketone solvent and L1.3-Ms ultimately led to their de-prioritization. EtOH enabled smooth deprotection, but the presence of inorganic salts in the final product led to low wt% purity. Ultimately, the combination of toluene (4.5 V) and EtOH (0.5 V) was selected for the preferred solvent system for the Boc deprotection process.

Table 2.2.1 Acid screening and optimization for Boc deprotection of L1.3-K-Boc.

L1.3-K-Boc (0.1 g, 1.0 eq)

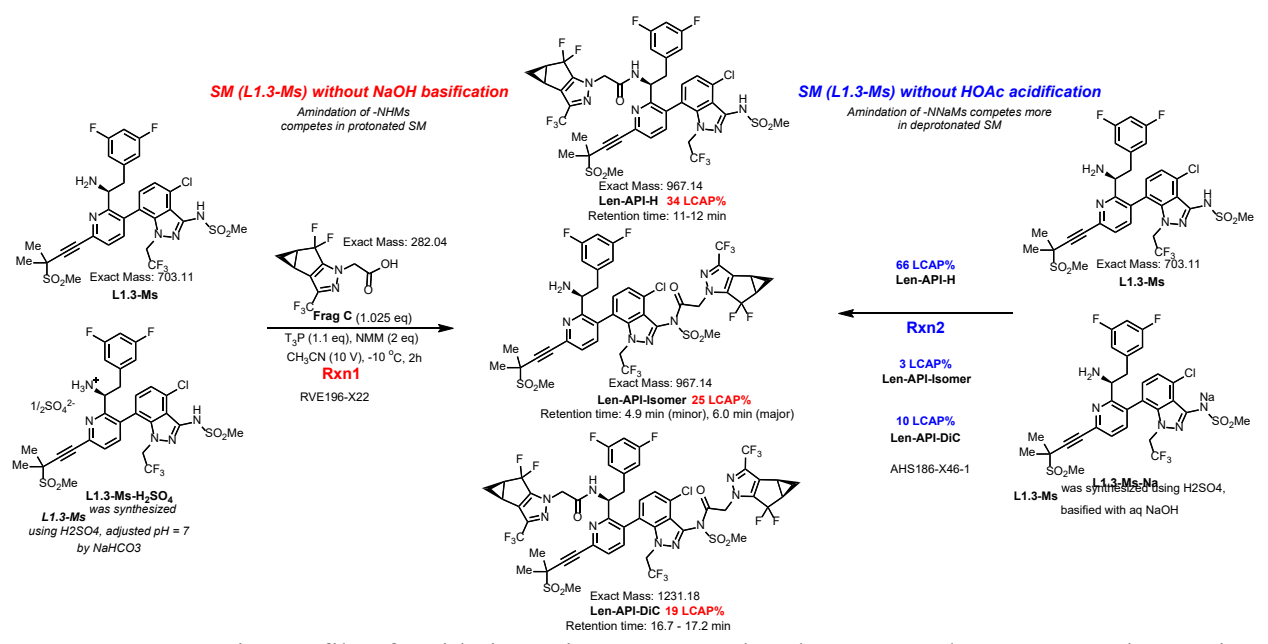
L1.3-Ms

				Time	In-proce	ss A % ^b	
#"	ELN No.	Acid	Solvent	(h)	L1.3- Boc ^c	L1.3- Ms ^c	Remarks
1	RVE196-X5-5	HCl in MeOH (3M, 20 eq)	DCM (5V)	24	61	30	Low
2	RVE196-X5-6	aq H ₃ PO ₄ (4M, 20 eq)	DCM (5V)	24	94	ND	conversion
3	RVE196-X18-1	MSA (10 eq)	Toluene (5V)	5	ND	97	Gel formation
4	RVE196-X18-2	aq H ₂ SO ₄ (9M, 10 eq)	Toluene (5V)	5	ND	97	Biphasic, heat needed to dissolve SM
5	AHS186-X38-1	aq H ₂ SO ₄ (9M, 2 eq)	Toluene (5V)	20	24	75	Incompletion
6	AHS186-X38-2	aq H ₂ SO ₄ (2M, 5 eq)	Toluene (5V)	20	97	0.3	No reaction
7	AHS186-X38-3	aq H ₂ SO ₄ (5.5M, 8 eq)	Toluene (5V)	20	80	17	Incompletion
8	RVE196-X18-3	aq H2SO4 (16M, 10 eq)	Toluene (5V)	5	ND	97	Biphasic
9	AHS186-X40	aq H ₂ SO ₄ (9M, 10 eq)	MEK (5V)	3	ND	97	Dipliasic
10	RVE196-X18-4	aq H ₂ SO ₄ (9M, 10 eq)	water (5V)	22	96	<1	No reaction
11	RVE196-X18-5	aq H ₂ SO ₄ (9M, 10 eq)	EtOH (5V)	6	<1	96	SM soluble
12	RVE-196-X23- 4	aq H ₂ SO ₄ (9M, 10 eq)	MIBK (5V)	1	ND	98	Biphasic
13	AHS186-X54- 1g	aq H ₂ SO ₄ (9M, 10 eq)	Toluene/EtO H (4.5V/0.5V)	1	ND	97	SM soluble,
14	AHS186-X54- 10g	aq H ₂ SO ₄ (9M, 10 eq)	Toluene/EtO H (4.5V/0.5V)	1	ND	97	reaction mixture

^aAll reactions were performed on 100 mg scale of **L1.3-Boc**; ^bA% measured at 275 nm, several other minor peaks observed; ^cTwo atropisomers (minor/major (A%) \sim 1/5) were observed.

The free base (neutral) form of L1.3-Ms was found to be critical for the success of the subsequent amidation step. Both protonated and deprotonated congeners of L1.3-Ms led to increased formation of regioisomer (Len-API-Isomer) and Len-API-DiC impurities (Scheme 2.2.2). Moreover, the ratio of protonated to deprotonated L1.3-Ms was highly sensitive to the acid-

base workup conditions, making it difficult to control and resulting in inconsistent amidation outcomes.



Scheme 2.2.2 Purity profile of amidation using protonated or deprotonated L1.3-Ms as the starting material. Major impurities of Len-API-Isomer and Len-API-DiC were formed.

To address this issue, isolating the free base of L1.3-Ms became essential. Initially, careful basification was performed to remove residual H_2SO_4 , followed by controlled acidification using AcOH to neutralize the deprotonated L1.3-Ms. Excess AcOH was then quenched with NaHCO₃, a weak base that was not expected to deprotonate L1.3-Ms. While this sequence yielded neutral L1.3-Ms and thus, a clean reaction profile in amidation, consistently achieving precise acid-base treatments proved challenging. The resulting L1.3-Ms continued to show variability in amidation performance. Consequently, a more practical and robust workup process – based on pKa-guided pH adjustment for free base isolation – was developed (vide infra) to ensure reproducibility and scalability.

2.2.2 Practical workup and purification for scalability

To facilitate pH adjustment for isolating the free base form of **L1.3-Ms**, its pKa was measured in iPrOAc via acid-base titration and determined to be between 9.8 and 10.2. Partitioning behavior between iPrOAc and water across varying pH levels was also evaluated by HPLC (Figure 2.2.1). As shown in Figure 2.2.1, **L1.3-Ms** preferentially partitioned into iPrOAc at pH values below 9 (i.e., \sim 1 order of magnitude below its pKa). In contrast, at pH values above 9, its

partitioning into aqueous phase increased. These findings suggested that adjusting the reaction mixture to pH 7-8 may promote effective formation of free base version of **L1.3-Ms**, while also enabling efficient extraction into organic solvent.

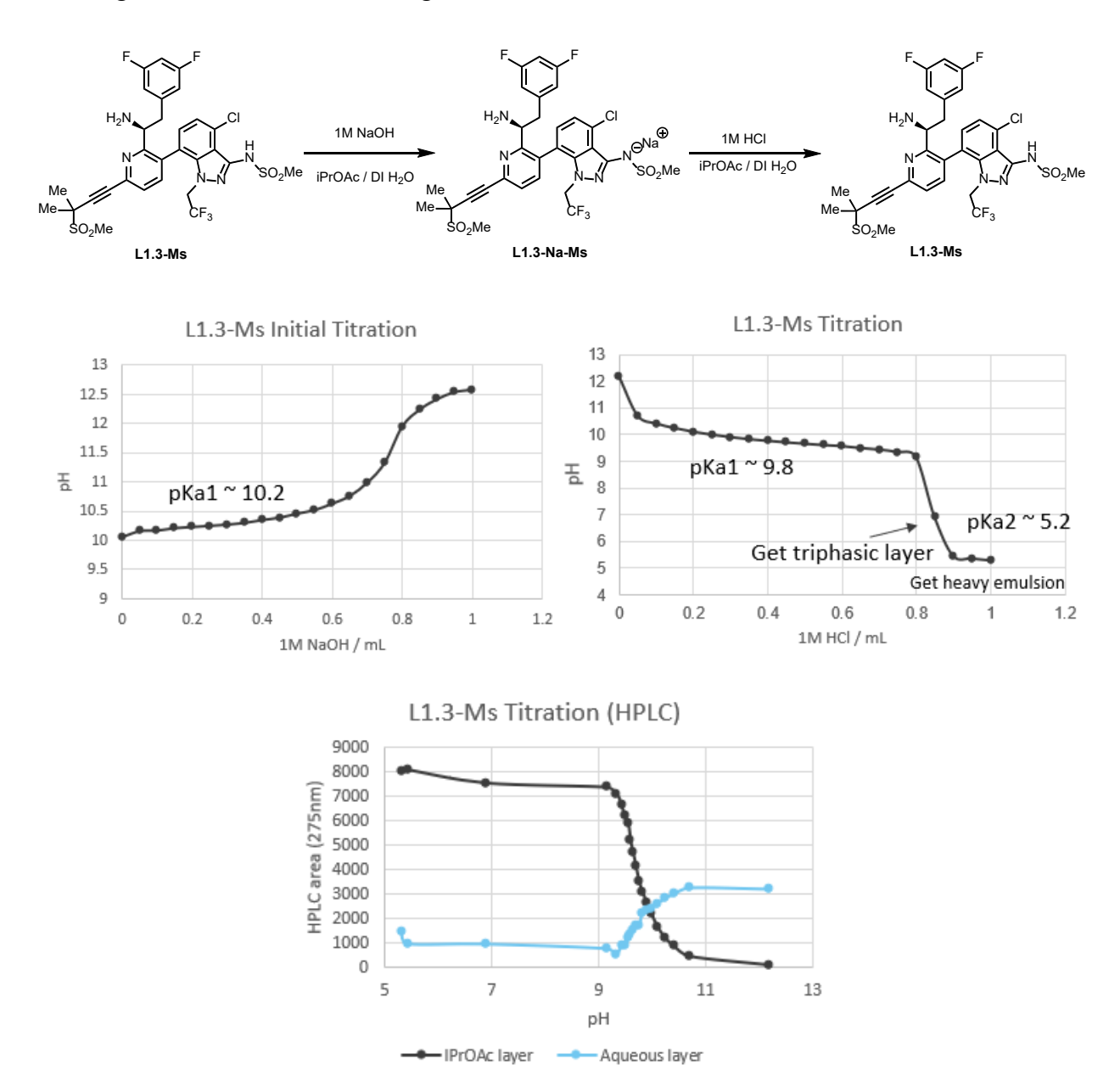


Figure 2.2.1 pKa measurement of **L1.3-Ms** and partitioning in iPrOAc and H₂O layer. iPrOAc effectively dissolves **L1.3-Ms** at pH < 9. Titration experiment: 0.1M **L1.3-Ms** in 5 mL iPrOAc / 10 mL water, titrated with 1M HCl at 21°C, after each 0.05 mL addition of HCl, both organic and aqueous layers were sampled (30 μ L into 1.00 mL CH₃CN) for HPLC analysis. Inflection point in the titration curve corresponds to a pKa of ~10.2 for **L1.3-Ms** during basification, while a pKa of ~9.8 was observed during acidification.

To optimize LLE, various organic solvents (e.g., EtOAc, iPrOAc, and 2-MeTHF) were screened at pH 7.5. Among them, EtOAc demonstrated excellent solubilization for **L1.3-Ms** and enabled clean phase separation. What is more, a single EtOAc extraction efficiently retrieved **L1.3-Ms** from the reaction mixture. This pKa-guided pH adjustment strategy proved to be a highly effective and robust approach for the purification of **L1.3-Ms**.

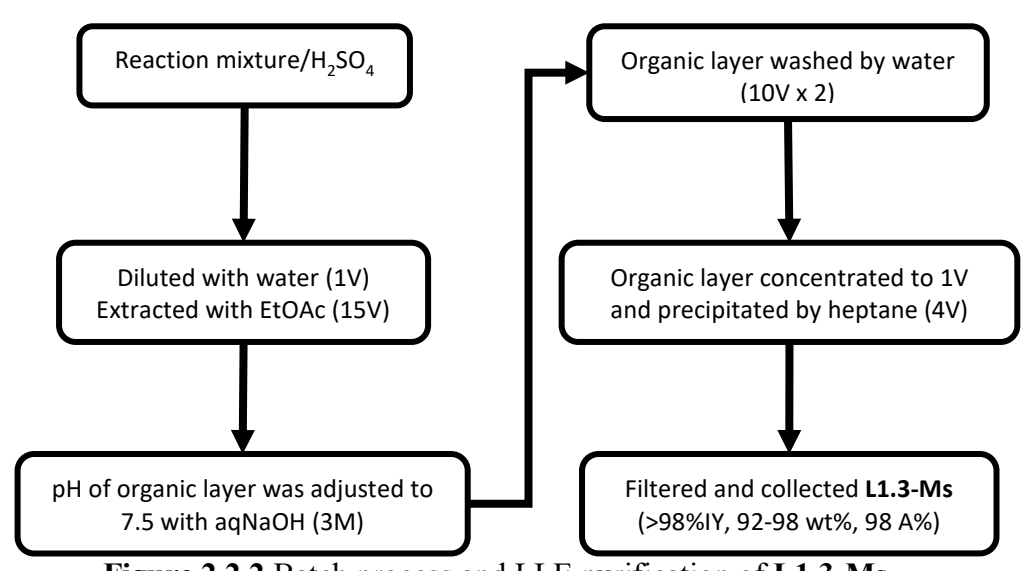


Figure 2.2.2 Batch process and LLE purification of L1.3-Ms.

As shown in Figure 2.2.2, upon completion of Boc deprotection, the reaction mixture was diluted with water (1 V) to facilitate efficient phase separation during subsequent EtOAc (15 V) extraction. The acidic organic layer was then treated with NaOH (3M) to achieve pH 7-8. To ensure complete removal of residual Na⁺ and SO₄²⁻ ions, two water washes were performed, with ELSD monitoring confirming their absence. The resulting organic layer was concentrated and precipitated by the addition of heptane, yielding **L1.3-Ms** with 92-97 wt% purity and 94-97% isolated yield. The pKa-guided LLE strategy streamlined the workup, enhancing reproducibility and product quality for the subsequent amidation step. The process was successfully demonstrated on decagram scales, consistently delivered high yields and purity of **L1.3-Ms**, as summarized in Table 2.2.2.

Table 2.2.2 Results summary of Boc deprotection and pKa-guided LLE purification of **L1.3-Ms** (decagram scale).

$$\begin{array}{c} \text{Me} \\ \text{Me} \\ \text{Me} \\ \text{SO}_2\text{Me} \\ \text{Exact Mass: 841.12} \\ \textbf{L1.3-K-Boc} \end{array} \begin{array}{c} \text{H}_2\text{SO}_4 & \text{(9M, 10 eq)} \\ \text{H}_2\text{SO}_4 & \text{(9M, 10 eq)} \\ \text{Indicate (4.5V)} \\ \text{EtOH (0.5V)} \\ \text{25 °C, 3h} \end{array} \begin{array}{c} \text{Exact Mass: 703.11} \\ \text{Exact Mass: 703.11} \\ \text{Exact Mass: 703.11} \end{array}$$

	ELN		Output after LLE purification											
# ^a		1	A% (LCM	S, 275 nm	$)^{b,c}$	Mass (g)	Wt% ^d	IY (%) ^e	Pd	Res.	Water (KF)	salts		
		L1.3 -Ms	L1.3- Ms-Ac	L1.3- Ms-Et	L1.3- DiFB1				(ppm) ^f	Sol.				
1	SRK18 5-X78	94	1	1	1	18	97	94	< 10	ND	1	ND		
2	SRK18 5-X79	96	0.6	1	0.6	18	92	95	10	-	-	ND		
3	SRK18 5-X80	97	0.1	0.5	1.5	39	94	97	18	3	1	ND		

^aAll reactions were performed at rt using **L1.3-K-Boc** (25 g for entries 1, 2; 50 g for entry 3) and H₂SO₄ (9M, 10 eq), refer to Appendix for experimental details; ^bA% measured at 275 nm by HPLC, multi-small peaks (< 0.1 A%) were observed; Tentative structures of **L1.3-Ms-Ac**, **L1.3-Ms-Et**, and **L1.3-DiFB1** were shown in Figure 2.2.3; ^cTwo atropisomers (minor/major (A%) ∼ 1/5) were observed; ^dWt% was obtained by HPLC; ^eCorrected by wt%; ^fObtained by ICP-OES. IY: isolated yield; Res. Sol.: residual solvents; ND = Non-detect.

As shown in the table, Boc deprotection using H₂SO₄ acid, combined with the pKa-guided LLE purification process, consistently yielded L1.3-Ms with isolated yield of 95-97 %, and 92 - 97 wt% purity (94-97 A%, 275 nm). L1.3-Ms was obtained as a mixture of two atropisomers, with a minor-to-major isomer ratio of approximately 1:5 (based on A% at 275 nm), mirroring the profile observed for its precursor, L1.3-K-Boc. All batches of L1.3-Ms demonstrated excellent reactivity in the subsequent amidation step (vide infra).

The **CPPs** for this step are summarized below:

- Use of ≥9M H₂SO₄ is essential for efficient Boc deprotection
- Toluene with a small amount of EtOH is required to fully dissolve L1.3-K-Boc prior to acid addition

- **EtOAc extraction** ensures clear phase separation and minimizes product loss during the workup
- pH adjustment to 7-8.5^r is critical to obtain the free-base form of L1.3-Ms
- Complete removal of residual of Na⁺ and SO₄²⁻ is vital for achieving high wt% purity and confirming full neutralization.

2.2.3 Safety assessment of the process

Similar to safety assessment for synthesis of L1.3-K-Boc (section 2.1.3), a reaction calorimetric evaluation was undertaken to understand the hazard potential of the Boc deprotection reaction. Specifically, the rate at which sulfuric acid was dosed into the PhMe/EtOH solution of L1.3-K-Boc was evaluated (see appendix for experimental details).

Table 2.2.3 Heat evolution during the dosing step of the Boc deprotection.

Process	ΔH_r ΔH_r	$\Delta H_{ m r}$	$\Delta H_{ m r}$	$\Delta { m T}_{ m ad}$	MTSR	MRT		C _p (J/g K)		U (W/m ² K)	
Step	(kJ)	(kJ/g)	(kJ/mol)	(°C)	(°C)	(°C)		Before	After	Before	After
1 ^a	2.27	0.211	178.1	13.7	33.7	31.1	47.3	2.10	1.94	139.9	117.0
2^b	3.34	0.311	261.7	20.1	40.1	25.4	15.8	2.10	2.00	145.9	103.1
3 ^c	1.35	0.135	113.6	14.7	34.7	23.0	2.39	2.43	1.26	126.3	56.0

^aMEK (5V) was used as a solvent, aq 9M H₂SO₄ was added to **L1.3-K-Boc** (10.7g) in 2 minutes to the reaction mass at 23 °C; ^bMEK (5V) was used as a solvent, aq 9M H₂SO₄ was added to **L1.3-K-Boc** (10.7g) in 12 minutes to the reaction mass at 23 °C; ^cToluene/EtOH (5/2, 7V) was used as solvents, aq 9M H₂SO₄ was added to **L1.3-K-Boc** (10g) in 45 minutes to the reaction mass at 23 °C.

41

^r At lower pH, **L1.3-Boc** becomes protonated, whereas at higher pH, it may be deprotonated. Both conditions can lead to undesired side-reactions during amidation.

The reaction calorimetric evaluation was conducted to assess the heat effects associated with Boc deprotection of L1.3-K-Boc (10.7 g, 0.01275 moles), using varying H₂SO₄ addition rates: 2 min (fast), 12-minute (intermediate) and 45-minute (slow). ΔH was calculated based on the molar quantity of L1.3-K-Boc and is summarized in Table 2.2.3. Addition of 9M H₂SO₄ to the reaction mass at 23 °C exhibited increasingly exothermic behavior with faster addition rates. The total ΔH_r was 261.7 kJ/mol for the 2-minute addition, 178.1 kJ/mol for the 12-minute addition, and 113.6 kJ/mol for the 45-minute addition. The maximum temperature of the synthesis reaction (MTSR) and adiabatic temperature rise (ΔT_{ad}) were also dependent on the addition rate. For the 2-minute, 12-minute, and 45-minute additions, the MTSR values were 40.1 °C, 33.7 °C, and 34.7 °C, respectively, with ΔT_{ad} values of 20.1 °C, 13.7 °C, and 14.7 °C. Importantly, all MTSR values remained below the boiling point of the reaction solvent, indicating that thermal runaway was unlikely under these conditions. The measured reaction temperatures (MRT) were 31.1 °C for the 2-minute addition, 25.4 °C for the 12-minute addition, and 23.0 °C for the 45-minute addition. Correspondingly, maximum heat generation (MHG) rates were 47.3 W, 15.8 W, and 2.39 W for the 2-, 12-, and 45-minute additions, respectively. Based on typical reactor cooling capacity criteria – where severity is classified as low ($\Delta T_{ad} < 50$ °C and MHG < 30 W), medium ($\Delta T_{ad} = 50$ – 200 °C), or high ($\Delta T_{ad} > 200$ °C and MHG > 30 W) – the 2-minute addition is considered high severity, while the 12- and 45-minute additions fall within the low severity range. In general, controlling the H₂SO₄ addition rate to maintain the MRT at or below 25 °C effectively minimized thermal hazard during scale-up.

2.2.4 Impurities identification and RT marker

For Boc deprotection (Milestone 2, step 2), impurities associated with the finalized conditions are summarized in Figure 2.2.3. The corresponding HPLC retention times are provided as RT marker to support in-process analysis monitoring and isolated product characterization.

Figure 2.2.3 Identified major impurities and RT marker in Milestone 2 (Boc deprotection).

2.3 T3P-promoted amidation and process development (Milestone 2)

The synthesis of sodium (4-chloro-7-(2-((S)-1-(2-((3bS,4aR)-5,5-difluoro-3-(trifluoromethyl)-3b,4,4a,5-tetrahydro-1H-cyclopropa[3,4]cyclopenta[1,2-c]pyrazol-1-yl)acetamido)-2-(3,5-difluorophenyl)ethyl)-6-(3-methyl-3-(methylsulfonyl)but-1-yn-1-yl)pyridin-3-yl)-1-(2,2,2-trifluoroethyl)-1H-indazol-3-yl)(methylsulfonyl)amide (**Len-API**) was accomplished via a T3P-promoted amide coupling between **L1.3-Ms** and **Frag C**, using N-methylmorpholine (NMM) as the base (Scheme 2.3.1). Following recrystallization from EtOH/heptane, **Len-API** was obtained with ~ 99 A% (235 nm), with the major impurity **L1.3-Ms-Ac** present at 0.4 – 0.6 A%. The Pd content of the final API was measured to be below 10 ppm.

Scheme 2.3.1 T3P-promoted amide coupling for synthesis of Len-API.

Several critical process parameters (CPPs) were identified for the amidation step as shown below:

- The use of the free-base (neutral) form of L1.3-Ms was essential for successful coupling.
- NMM, a weak base, was critical for the desired amidation.
- Stepwise (semi-batch) addition of T3P was crucial for complete conversion of L1.3-Ms. An initial portion of T3P (1.0 eq) was added at low temperature to control reactivity and

^s Impurity L1.3-Ms-Ac was synthesized and structurally confirmed by ¹HNMR, ¹³CNMR, ¹⁹FNMR, and LC-MS (See the appendix for detailed synthetic procedures). L1.3-Ms-DiFB1 and L1.3-Ms-Et was detected by LCMS. Their structures were tentatively proposed based on LCMS data. Please refer to GFN-002-ELN-ADR for the detailed analytical methods.

^t L1.3-Ms-Ac was generated during the EtOAc workup in Boc deprotection step and subsequently carried through into the final API. See footnote s for details on issue resolution.

suppress side reactions. Subsequent stirring at 60 °C, followed by incremental additions of 0.1–0.3 equivalents of T3P, ensured full consumption of **L1.3-Ms**.

- Full conversion of L1.3-Ms (> 99.8%) was critical for achieving high purity of Len-API after recrystallization.
- Recrystallization from EtOH/heptane was effective in purifying the product, and performing the recrystallization twice consistently yielded Len-API with high purity.

2.3.1 Condition screening and optimization

Amidation of L1.3-Ms with Frag $C^{24,53}$ represents the final step in the synthesis of the target API, making it critical to establish reaction conditions that yield a clean purity profile and controllable impurity levels. Our initial approach to Len-API synthesis employed T3P-based amide coupling conditions pioneered by Gilead Sciences Inc.²⁰ Amidation of L1.3-Ms with Frag C was carried out at 20°C using T3P (1.5 eq) as the coupling reagent and TEA (1.5 eq) as the base (Table 2.3.1, entry 1). The desired Len-API was obtained in 85.9 A% (235 nm), accompanied by 1.3 A% (235 nm) of an over-amidation side-product Len API-DiC, and 2.3 A% (235 nm) of residual L1.3-Ms. No mono-amidation product on the methylsulfonamide (-NHMs) group was detected. Increasing TEA to 3 equivalents, in a bid to reduce residual L1.3-Ms, led to substantial quantities of Len-API-DiC, even at 0 °C (Table 2.3.1, entry 2). Although subsequent base treatment successfully decomposed Len-API-DiC and removed Frag C after liquid-liquid extraction (LLE) workup, L1.3-Ms persistent. Given the pKa of \sim 10 for the -NHMs group in L1.3-Ms, the authors hypothesized that TEA (pKa = 10.8) could potentially deprotonate -NHMs and thereby promote the undesired amidation to Len-API-DiC. To achieve complete conversion of L1.3-Ms while suppressing side reactions at the -NHMs site, our efforts focused on systematic base screening and reaction condition optimization (Table 2.3.1). Side-reactions at the -NHMs moiety increased with temperature. At 50 °C, TEA (1.5 eq) generated 12.9 A% (235 nm) of Len-API-DiC (Table 2.3.1, entry 3). DIPEA (3.0 eq), a similar pKa to TEA, resulted in 15.4 A% (235) nm) Len-API-DiC (Table 2.3.1, entry 4). NMM (pKa = 7.4) emerged as the most reliable base. At -10 °C, 3.0 equivalents of NMM delivered Len-API in 88 A%, with only 1.9 A% (235 nm) Len-API-DiC (Table 2.3.1, entry 5). However, at 20 °C under similar conditions, Len-API-DiC increased to 12.1 A% (235 nm) (Table 2.3.1, entry 6). Using pyridine (pKa = 5.2) as the base, amidation proceeded slowly, yielding Len-API in 59 A% (235 nm), with significant residual L1.3**Ms** and 8.4 A% (235 nm) **Len-API-DiC** (Table 2.3.1, entry 7). These findings underscore the importance of using NMM at low temperature to suppress **Len-API-DiC** formation.

Further optimization focused on varying the equivalents of NMM and T3P (Table 2.3.1, entries 8-11). The optimal conditions – 2.2 equivalents of NMM and 1.25 equivalents of T3P at -10 °C – enabled reproducible high conversion of **L1.3-Ms** with acceptable levels of **Len-API-DiC**. Under these conditions, **Len-API** was obtained in 86.7 A% (235 nm), with 1.2 A% (235 nm) residual **L1.3-Ms**, 2.5 A% (235 nm) **Len-API-DiC** and 0.3 A% (235 nm) **Len-API-DiC** (Table 2.3.1, entry 11). Prolonging the reaction time did not improve conversion; the product profile after 5 min was identical to that observed after 1h (Table 2.3.1, entry 12), indicating that the amidation proceeds rapidly under optimized conditions.

Table 2.3.1 Base screening and reaction condition optimization for synthesis of Len-API-H.

$$\begin{array}{c} \text{F} \\ \text{F} \\ \text{N} \\ \text{OH} \\ \text{Exact Mass: } 282.0428 \\ \text{Base (x eq), } T_3 P \text{ (y eq)} \\ \text{Emp, } 3\text{-5 h} \\ \text{Exact Mass: } 703.1113 \end{array}$$

# ^a	ELN	Base	T3P	Temp	In-process A% (235 nm) ^b					
117	LLIV	(eq)	(eq)	(°C)	L1.3-Ms	Frag-C	Len-API ^c	Len-API-DiC		
1	RVE196-X12	TEA (1.5)	1.5	20	2.3	-	85.9	1.3		
2	AHS186-X37-3	TEA (3.0)	1.5	0	0.3	-	71.6	22.2		
3	AHS186-X36-3	TEA (1.5)	1.5	50	0.7	3.2	74.7	12.9		
4	AHS186-X37-1	DIPEA (3.0)	1.5	-10	0.4	0.7	78.2	15.4		
5	AHS186-X37-2	NMM (3.0)	1.5	-10	2.2	2.0	88.0	1.9		
6	AHS186-X37-5	NMM (3.0)	1.5	20	3.6	1.7	66.7	12.1		
7	AHS186-X37-4	Py (3.0)	1.5	0	14.2	3.7	59.0	8.4		
8	AHS186-X37-8	NMM (1.0)	1.0	-10	25.5	5.2	65.6	0.45		
9	AHS186-X37-10	NMM (2.0)	1.25	-10	5.8	2.1	85.1	1.1		
10	AHS186-X37-11	NMM (2.0)	1.25	-10	5.4	3.6	82.9	1.1		
11	RVE196-X19-1	NMM (2.2)	1.25	-10	1.2	2.0	86.7	2.5		
12^d	RVE196-X19-2	NMM (2.2)	1.25	-10	1.2	2.0	86.7	2.6		

^aAll reactions were performed with L1.3-Ms (0.5 g, 1 eq), Frag C (1.05 eq), T3P (50 wt% in DMF), base under conditions shown in the table; ^bA% measured at 275 nm by HPLC, several other

small unknown impurities along with 0.2-0.3 A% **L1.3-Ms-Ac** (see Scheme 2.3.2 for structure) in all reactions; c Two atropisomers (minor/major (A%) $\sim 1/6$) were observed; d 5min reaction time.

Despite achieving an acceptable level of **Len-API-DiC**, the presence of 1-2 A% (235 nm) **L1.3-Ms** became a challenge for **Len-API** purification. Following LLE workup and recrystallization, **L1.3-Ms** could only be diminished to 0.2-0.5 A% (235 nm). Therefore, reducing **L1.3-Ms** during amidation proved critical to achieving levels below 0.1 A% (235 nm) in the final API. Further optimization of the reaction conditions revealed that stepwise addition of T3P was essential to suppress **L1.3-Ms** below 0.1 A% (235 nm). Specifically, an initial charge of T3P (1.0 eq) was added to a mixture of **L1.3-Ms** (1.0 eq), **Frag C** (1.02 eq), and NMM (3.0 eq) at -10 °C, followed by heating to 60 °C for 4-5h. In-process analysis (HPLC) of the reaction mixture showed approximately 2-3 A% (235 nm) of **L1.3-Ms** remained. A second portion of T3P (0.3 eq) was then introduced at 60 °C, which enabled complete conversion of **L1.3-Ms** after 18h. " However, under these conditions, the **L1.3-Ms-Ac** * emerged as the predominant impurity (~0.9 A%, 235 nm) (Scheme 2.3.2). Its level was reduced to below 0.5 A% (235 nm) after two recrystallizations from EtOH/heptane (vide infra). Additional optimization is required to fully purge the impurity to below 0.1 A% (235 nm).

_

[&]quot; If trace amounts of **L1.3-Ms** persisted, a third portion of T3P (0.2 eq) was added at 60 °C to drive the reaction to completion. The reaction time has not been optimized, though we anticipate that shorter reaction times may be feasible.

^v It was found that **L1.3-Ms-Ac** was formed during the EtOAc workup in Boc deprotection step and subsequently carried over into the API. Due to time constraints, further optimization, such as switching EtOAc to other solvents for workup during Boc-deprotection step or refining second recrystallization conditions for API purification, was initiated but not fully pursued to enhance API purity at this stage (vide infra).

Scheme 2.3.2 Controlled stepwise T3P addition enables full conversion of **L1.3-Ms** in **Len-API** synthesis.

2.3.2 Practical workup and purification Len-API

Full conversion of **L1.3-Ms** was successfully achieved under optimized amidation conditions. The formation of the sodium salt is a critical step in the API synthesis, as it not only supports downstream processing but also enables high-yield recrystallization. During solvent screening for sodium salt formation, CH₃CN, EtOH, and 2-MeTHF provided satisfactory, delivered expected levels of Na⁺. Treatment of **Len-API-H** with 6 equivalents of NaOH (1M) in each one of these solvents provided a sodium content of 2 wt% (vs theoretical 2.3 wt%) (Table 2.3.2). However, a single water wash (performed in MIBK) lowered the Na content to 1.4-1.5 wt%.

Table 2.3.2 Base screening and reaction condition optimization for synthesis of **Len-API-H**.

# ^a	ELN	Solvent	Output Len-API (Na salt) b				
	LLIV	Borvent	freebase assay (wt%)	Na assay (wt%)			
1	RVE196-X38-5	THF	87	1.8			
2	RVE196-X38-2	2-MeTHF	86	2.1			
3	RVE196-X38-3	EtOH	87	2.0			
4	RVE196-X38-1	CH ₃ CN	84	2.1			
5	RVE196-X38-4	Acetone	84	1.7			

^aAll reactions were performed using **Len-API-H** (0.5 g, 1 eq, 85 wt%) and NaOH (1M, 5 eq) at 45 °C for 3h, with the solvents shown in the table; ^bNa content was measured by LC-ELSD, and wt% of the material was measured by HPLC (235nm), theoretical Na content of pure API is 2.3 wt%, for a wt% assay of 85%, the expected Na content is approximately 2%.

To streamline the process, the basification step was applied to the crude reaction mixture.^w After amidation, the mixture was treated with 1M aqueous NaOH (10 eq) at 45 °C for 2h,^x followed by partitioning into MIBK. Without a water wash, the MIBK layer was concentrated and precipitated with heptane to yield the crude API with a sodium content of 2 wt% (measured by LC-ELSD), consistent with theoretical expectations based on the crude API composition (85 wt%). The crude product showed 94-97 A% (235 nm), containing 0.5-1 A% (235 nm) L1.3-Ms-Ac and ~1 A% (235 nm) of other minor impurities (Table 2.3.3).

Table 2.3.3 Synthesis of Len-API-H and its transformation to Len-API sodium salt.

-													
	# ^a		Input L1.3-Ms			Output crude Len-API ^{b, c}							
		ELN	Mass (g)	Wt%	A%	IY%	Mass (g)	A%	Wt%	Na wt%	L1.3-Ms- Ac (A%)	L1.3-Ms (A%)	
I	1	JMS176-X37	10	98	96	81	13.4	97.3	83 ^d	1.8	0.5	0.13	
	2	AHS186-X73	11	92	98	85	15	94.0	81	2.0	0.5	< 0.2	
	3	RVE196-X40	35	94	97	92	53	93.7	81	2.0	1.0	0.3	

^aAll amidations were carried out with L1.3-Ms (1.0 eq) and Frag C (1.025 eq) under conditions shown in the scheme and table, the batch process of entry 3 was documented, see Appendix for

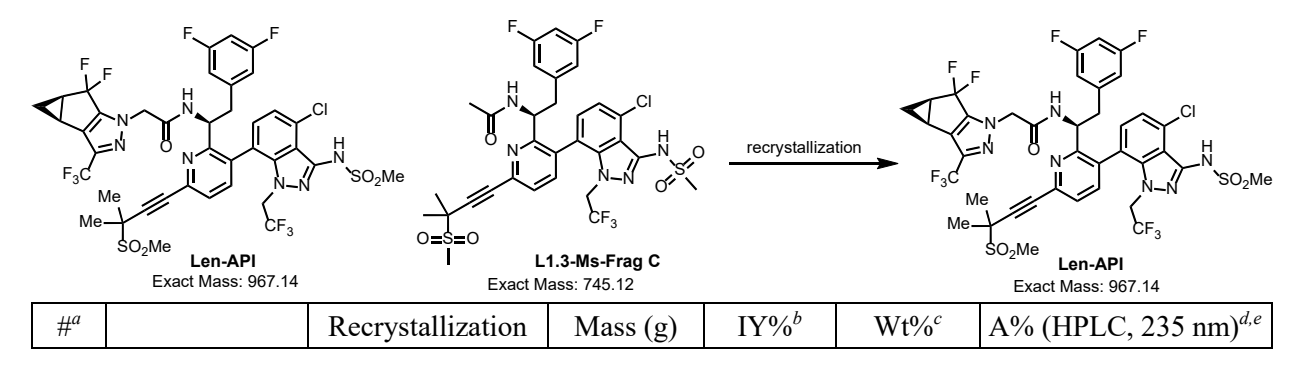
^wThe reaction solvent CH₃CN effectively facilitates the telescoped NaOH treatment.

^{*} To quench T3P and eliminate residual Frag C and Len-API-DiC, 10 equivalents of NaOH (1M) were employed.

experimental details; b Na content was measured by LC-ELSD, and wt% of the free base material was measured by HPLC unless otherwise stated, A% measured at 235 nm by HPLC, corrected isolated yield (IY); c Two atropisomers (minor/major (A%) $\sim 1/6$) were observed; d Wt% of the free base was measured by qNMR.

The crude API was further purified via recrystallization. As detailed in Table 2.3.4, the binary solvent system of EtOH (10V) / heptane (20 V) delivered the best results. The system increased API purity to 99.0 A% (235 nm), effectively reducing impurities such as L1.3-Ms (< 0.1 A%, 235 nm) and L1.3-Ms-Ac (0.6 A%, 235 nm). A second recrystallization using the same solvent system further improved purity to 99.2 A% (235 nm), with L1.3-Ms-Ac as the sole major impurity (~0.5 A%, 235 nm). Other solvent systems, including iPrOH, toluene/heptane, EtOH, MTBE, and 2-MeTHF, were ineffective in removing the L1.3-Ms-Ac impurity. The two atropisomers of Len-API was observed, with a minor-to-major isomer ratio of approximately 1:6 based on A% (275) nm). The proportion of the major isomer was slightly higher than that observed in its precursor L1.3-Ms (1:5). A second lot of API was recovered from the mother liquor with an approximate yield of 20%. The mother liquor was concentrated, treated with NaOH, and purified via two recrystallizations following the standard protocol, affording API with ~99 A% (235 nm). The overall yield of the amidation reached up to 80%. The process was verified at a 10-35g scale, consistently delivering similar yield and purity. Results are summarized in the Table 2.3.4 and the full characterization data was summarized in Table 2.3.5. Further efforts, such as refining second recrystallization conditions, will be needed to enhance API purity.^y

Table 2.3.4 Recrystallization of crude Len-API sodium salt.



y It was believed that **L1.3-Ms-Ac** was formed during the EtOAc workup in Boc deprotection step and subsequently carried over into the API. Replacing EtOAc with 2-MeTHF suppressed the formation of **L1.3-Ms-Ac** during Boc deprotection, resulting in an amidation step free of this impurity. Following the standard purification protocol, the API achieved > 99.7A%. Alternatively, a new recrystallization solvent system (MIBK/toluene (5V/5V)) reduced **L1.3-Ms-Ac** levels to < 0.2 A%. However, the scalability of both approaches remains unverified due to time constraints.

49

	ELN					Len-API
1	IMC176 V27	Input crude	13.4	-	83 ^e	97.3
1	JMS176-X37	Output for 2 nd RC	8.5	60	> 98	98.9
		Input crude	15	-	81	94.0
2	AHS186-X73	Output for 1st RC	10.6	-	-	98.0
		Output for 2 nd RC	10	70	>99.9	98.9
3	RVE196-X40	Input crude	53	-	81	93.7
3	KVE190-A40	Output for 2 nd RC	37.5	78	>99.9	98.8

^aBatch process of entry 3 was documented, see Appendix for experimental details (recovered material from mother liquor is not included in the table); ^bCorrected isolated yield (IY) after recrystallization; ^cWt% was measured by HPLC; ^dA% measured at 235 nm by HPLC; ^eWt% of the free base was measured by qNMR; ^dTwo atropisomers (minor/major (A%) \sim 1/6) were observed.

Table 2.3.5 Characterization data of purified Len-API sodium salt.

							A% (HPLC, 235 nm)					
#*	ELN	Wt%	Pd (ppm)	Na wt%	Water wt%	Solvent (wt%)	Len- API ^b	L1.3- Ms	L1.3- Ms-Ac	Unknown at 12.89 min		
1	JMS176-X37	> 98	< 3.7	1.8	0.8	Heptane: 0.1	98.9	0.2	0.4	0.3		
2	AHS186-X73	>99.9	< 4.2	1.96	0.25	Ethanol: < 0.14 Heptane: 0.06	98.9	0.1	0.6	0.3		
3	RVE196-X40	>99.9	< 4.2	1.88	0.3	Ethanol: 0.3 Heptane: 0.06	98.8	0.2	0.6	0.4		

^aAll final API recrystallized twice from EtOH/heptane, Na content was measured by LC-ELSD, and wt% of the free base was measured by HPLC, A% measured at 235 nm by HPLC, Pd content measured by ICP-OES; b Two atropisomers (minor/major (A%) $\sim 1/6$) were observed.

2.3.3 Safety assessment of the process

As with the preceding steps, a reaction calorimetric evaluation was conducted to assess the hazard potential associated with the amidation process. The dosing profiles of N-methylmorpholine (NMM) and propanephosphonic acid anhydride (T3P) were examined (see Appendix for experimental details). The amidation reaction was performed in a 100 mL glass reactor using 10.0g (0.0142 mol) of **L1.3-Ms** as the substrate. Heat effects were quantified based on this amount, and the corresponding ΔH values are summarized in Table 2.3.5. Addition of T3P at -10 °C was found to be highly exothermic, whereas the addition of NMM at -10 °C and T3P at

60 °C exhibited only mild exothermicity. The total ΔH_r were calculated as 0.528 kJ/mol, 192.3 kJ/mol, and 24.2 kJ/mol for dosing of NMM, T3P at -10 °C, and T3P at 60 °C, respectively. Maximum temperature of the synthesis reaction (MTSR) values were recorded as -9.99 °C (ΔT_{ad} = 3.01 °C), 4.6 °C (ΔT_{ad} = 17.6 °C), and 61.0 °C (ΔT_{ad} = 0.99 °C) for the respective dosing conditions. All MTSR values remained below the boiling point of the reaction solvent, acetonitrile (82.0 °C), indicating manageable thermal behavior. Corresponding maximum reactor temperature (MRT) were -10.0 °C, 1.15 °C, and 61.0 °C, while the maximum heat generation (MHG) rates were 4.01 W, 36.0 W, and 8.04 W for NMM, T3P at -10 °C, and T3P at 60 °C dosing, respectively. Based on standard reactor cooling capacity criteria – where severity is Low (ΔT_{ad} <50 °C and MHG <30 W), Medium (ΔT_{ad} 50-200 °C), and High (ΔT_{ad} >200 °C and MHG >30 W) – the thermal severity for all dosing conditions is considered low.

Table 2.3.5 Heat evolution during the dosing steps of the L1.3-Ms amidation.

Process	ΔH_{r}	ΔH_{r}	$\Delta H_{ m r}$	ΔT_{ad}	MTSR	MRT (°C)	MHG (W)	C_p (J/g K)		$U\left(W/m^2K\right)$	
Step	(kJ)	(kJ/g)	(kJ/mol)	(°C)	(°C)			Before	After	Before	After
1^a	0.075	0.0075	0.528	3.01	-9.99	-10.0	4.01	1.66	2.00	13.6	205.9
2^b	2.73	0.0273	192.3	17.6	4.6	1.15	36.0	2.00	2.70	205.9	192.1
3 ^c	0.343	0.0343	24.2	0.99	61.0	61.0	8.04	2.70	2.13	152.6	145.5

^aAddition of NMM to the reaction mass at -10 °C; ^bAddition of T3P to the reaction mass at -10 °C; ^cAddition of T3P to the reaction mass at 60 °C.

In conclusion, based on the safety data, each step in the synthesis of **Len-API** – including Heck coupling, Suzuki coupling, Boc deprotection, and T3P-mediated amidation – is considered as non-critical and therefore safe. However, for plant-scale operations, it is strongly recommended that reagents, particularly 9M H₂SO₄ during Boc deprotection and T3P during amidation, be dosed slowly to avoid sudden spikes in heat generation. In the event of a cooling failure or agitation issue,

reagent addition must be halted immediately and should not resume until the system is fully restored. Such disruptions may elevate the batch temperature toward its MTSR, posing a potential safety risk. Consequently, extra care and a very keen observation are required throughout the reaction period. The cooling system must be capable of managing the thermal load during each phase of the process. Active cooling and a high-efficiency condenser are critical for safely executing these steps.

2.3.4 Impurities identification and RT marker

For amidation (Milestone 2, step 3), impurities associated with the finalized conditions are summarized in Figure 2.3.3. The corresponding HPLC retention times are provided as RT marker to support in-process analysis monitoring and isolated product characterization.

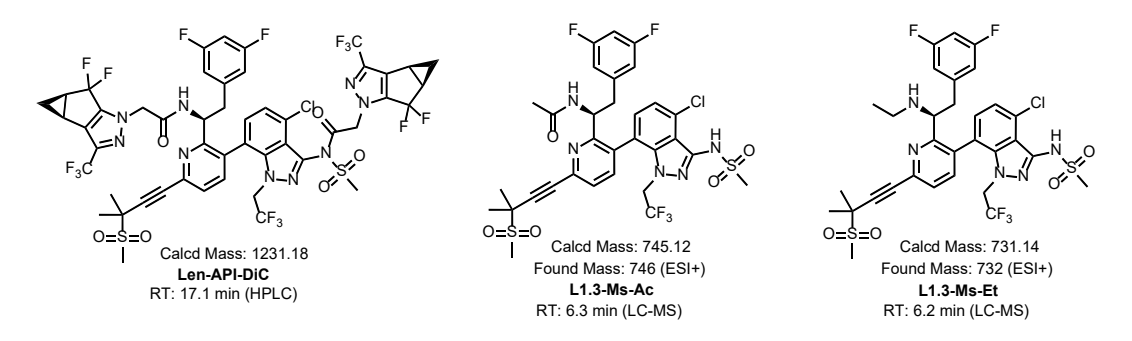


Figure 2.3.1 Identified major impurities and RT marker in Milestone 2 (Amidation).^z

2.4 Conclusions

We successfully developed a novel, streamlined, and efficient synthetic process for production of lenacapavir API, incorporating minor variations in key intermediates to enhance accessibility for generic pharmaceutical manufacturers. A sequential Heck-Suzuki coupling strategy was employed for the first-time synthesis of the key intermediate **L1.3-K-Boc**. A cost-effective and process-friendly Boc deprotection method was established, followed by a final-step amidation with **Frag C** to complete the synthesis of lenacapavir API.

^z Major impurities **Len-API-DiC** and **L1.3-Ms-Ac** were synthesized and structurally confirmed by ¹HNMR, ¹³CNMR, ¹⁹FNMR, and LC-MS (See the appendix for detailed synthetic procedures). Impurity **L1.3-Ms-Et**, (< 0.1 A%, 235 nm) was detected by LCMS, and its structure was tentatively proposed based on LCMS data. Please refer to **GFN-002-LEN-ADR** for the detailed analytical methods.

An early-stage Pd removal step ensured that the final API contained less than 10 ppm of residual Pd. This overall process delivers lenacapavir API in 50-55% overall yield with a purity up to > 99.9 wt% and ~ 99 A% (235 nm) after two recrystallizations. Comprehensive process documentation supports seamless adoption by generic manufacturers.

Technoeconomic (TE) cost analysis indicates that, compared to Gilead's route, M4ALL's new process achieves a 20-30% reduction in raw material cost (RMC). We hope these results will empower generic pharmaceutical companies to produce lenacapavir more efficiently and affordably, ultimately expanding access to patients in low- and middle-income countries.

3 Appendix

3.1 Process documentation (PDFs embedded)

A batch sheet record is a comprehensive document that captures the full manufacturing history of a specific pharmaceutical product batch.⁵⁴ It documents raw materials, equipment used, personnel involved, processing steps, and quality control checks. This record ensures traceability, accountability, and compliance with industry regulations, like Good Manufacturing Practices (GMP). Batch records play a critical role in verifying that products are made correctly, supporting quality assurance efforts, facilitating audits and investigations, and demonstrating adherence to stringent safety and quality standards. Although our primary focus was on R&D process development, we documented the optimized procedure in accordance with batch sheet record standards. The complete documentation of each step in API synthesis is attached below.

Step 1 Coupling Fragments A, D and B-DiMs



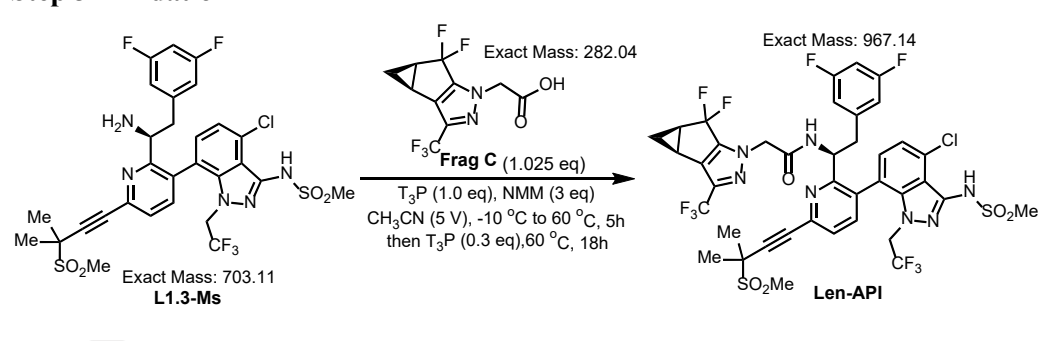
Step 2 Boc deprotection

$$\begin{array}{c} \text{Me} \\ \text{Me} \\ \text{SO}_2\text{Me} \\ \text{Exact Mass: 841.12} \\ \textbf{L1.3-K-Boc} \\ \end{array} \begin{array}{c} \text{H}_2\text{SO}_4 & \text{(9M, 10 eq)} \\ \text{H}_2\text{SO}_4 & \text{(9M, 10 eq)} \\ \text{In toluene (4.5V) / Me} \\ \text{EtOH (0.5V)} \\ \text{25 °C, 3h} & \text{Exact Mass: 703.11} \\ \textbf{L1.3-Ms} \\ \end{array}$$



Step 2-Process Documentation

Step 3 Amidation





Step 3-Process Documentation

3.2 Experimental details

General Methods

Reagents and solvents were obtained from commercial suppliers and used as received unless otherwise indicated. Where applicable, reactions were conducted in oven-dried (120 °C)

glassware, which was assembled while hot, and cooled to ambient temperature under an inert atmosphere. Reactors were pre-rinsed with reaction solvent and subjected to evacuation/back-fill cycles (3×) as necessary. All reactions were conducted under an inert atmosphere (Nitrogen) unless otherwise noted. Reactions were monitored by TLC (precoated silica gel 60 F254 plates, EMD Chemicals), Agilent HPLC, GCMS, or Agilent GC-FID using various methods. GC-FID was used for analysis of heptane and toluene levels. The sample was prepared in an acetonitrile/methanol mixed diluent, in duplicate. Quantitation was performed using a calibration curve. Ethyl acetate was used as an internal standard and QC standards were analyzed throughout the sequence. The samples for Pd analysis were prepared in 10% HCl and analyzed by ICP-OES. A calibration curve for analysis was prepared with QC standards analyzed throughout the sequence. Weight Assay was measured by LC-DAD. Salt Content was measured by LC-ELSD. Water content was measured by KF titration. A% was measured by HPLC at 275 nm or 235 nm. Melting point was measured with a Stuart SMP10 melting point apparatus. TLC was visualized with UV light or by treatment with phosphomolybdic acid (PMA), ninhydrin, and/or KMnO₄. ¹H NMR and ¹³C NMR spectra were routinely recorded on Bruker Avance III HD Ascend 600 MHz spectrometer. All chemical shifts are reported in parts per million (ppm) relative to residual DMSO (2.50 ppm for ¹H, 39.52 ppm for ¹³C) or CHCl₃ (7.26 ppm for ¹H, 77.16 ppm for ¹³C). Coupling constants J are reported in hertz (Hz). The following abbreviations were used to designate signal multiplicity: s, singlet; d, doublet; t, triplet; q, quartet, p, pentet; dd, doublet of doublets; ddd, doublet of doublet of doublets; dt, double of triplets; ddt, doublet of doublet of triplets; m, multiplet; br, broad. Advanced intermediates Frag A, Frag B, and Frag C-EE were prepared according to Y1 Len PDRs. 22-24

Synthesis of key intermediates

Synthesis of N-(4-chloro-7-(4,4,5,5-tetramethyl-1,3,2-dioxaborolan-2-yl)-1-(2,2,2-trifluoroethyl)-1H-indazol-3-yl)-N-(methylsulfonyl)methanesulfonamide (Frag B-DiMs)

A 5L ChemRxnHub reactor was degassed with N₂ and charged with **Frag B**²³ (222.00 g, 561.53 mmol, 95.0 wt%), 2-MeTHF (2.2 L, 10V), and triethylamine (250.0 mL, 1.80 mol, 3.2 eq) at 25 °C. The mixture was stirred, and the temperature control unit (TCU) was set to -3.0 °C. Once the internal temperature reached NMT 1.0 °C, methanesulfonyl chloride (109.0 mL, 1.40 mol, 2.5 eq) was added slowly over 20 minutes, maintaining the internal temperature at NMT 10.0 °C. The mixture was heated to 20 °C and stirred at the same temperature for 2 h. After the reaction was complete (monitored by TLC and ¹H NMR), the resulting suspension was filtered and the filter cake was washed with heptane (890 mL, 4V). The solid was then transferred to the reactor, stirred in 2-MeTHF (890 mL, 4V) for 30 min, and filtered. The filter cake was washed with 2-MeTHF (230 mL, 1V). The filtrate was concentrated to 2-3V, precipitated by addition of heptane (5V). The suspension was stirred for 30 min and then filtered. The resulting solid was transferred to the reactor, stirred in deionized H₂O (5V) for 30 min, and filtered. The filter cake was washed with heptane (1V) and dried *in vacuo* at 60 °C until constant weight to yield **Frag B-DiMs** (281.00 g, 100 wt% by qNMR) as a white solid (94.1% corrected yield).

¹H NMR (600 MHz, DMSO- d_6) δ 7.95 (d, J = 7.6 Hz, 1H), 7.50 (d, J = 7.6 Hz, 1H), 5.94 (q, J = 8.7 Hz, 2H), 3.66 (s, 6H), 1.37 (s, 12H).

¹³C NMR (151 MHz, DMSO- d_6) δ 170.9, 143.6, 135.0, 125.9 (q, J = 281 Hz), 118.5, 110.7, 60.3, 49.9 (q, J = 35 Hz), 43.0, 21.2, 14.5.

¹⁹F NMR (565 MHz, DMSO- d_6) δ -69.70 (t, J = 8.8 Hz, 3F).

A% (275 nm): 97.7 %

HPLC wt% purity (275 nm): 100.3 %

KF water content analysis: 0.023 %

LC-MS (m/z) (M+H): 532

IR (ATR) vmax: 3045, 3017, 2988, 2935, 1573, 1416, 1398, 1368, 1351, 1331, 1314, 1264, 1245, 1206, 1161, 1105, 1090, 988, 967, 939, 887, 857, 833, 813, 773, 757, 703, 691

HRMS (ESI) m/z: calcd for $C_{17}H_{22}BClF_3N_3O_6S_2 \cdot Na^+ = [M+Na]^+ 554.0576$, found 554.0588

Melting point: 220-222 °C.

Synthesis of 2-((3bS,4aR)-5,5-difluoro-3-(trifluoromethyl)-3b,4,4a,5-tetrahydro-1H-cyclopropa[3,4]cyclopenta[1,2-c]pyrazol-1-yl)acetic acid (Frag C)

To a three-neck 1000 mL round-bottom flask was added **Frag C-EE**²⁴ (56.00 g, 172.4 mmol, 1.0 eq, 95.5 wt%, 100%ee), EtOH (33.6 mL, 0.6V) and 224 mL of H₂O (4V). Then, an aqueous solution of KOH (31.4 mL, 31 wt%, 224.1 mmol, 1.3 eq) was added, and the mixture was stirred at 50 °C for overnight. After reaction was complete, the mixture was added dropwise to a precooled aqueous HCl solution (1.7M, 263.7 mL, 448.2 mmol, 2.6 eq) at 0 °C. The resulting suspension was filtered, and the filter cake was washed with H₂O (250 mL, 4.5V) and dried under vacuum to yield **Frag C** (44.00 g, 95.8 wt% by qNMR, 100% ee) as a white solid (86.7% corrected yield).

¹H NMR (600 MHz, DMSO- d_6) δ 13.52 (brs, 1H), 5.02 (dd, J = 18.0, 44.0 Hz, 2H), 2.70 – 2.60 (m, 2H), 1.44 – 1.48 (m, 1H), 1.05 – 1.03 (m, 1H).

¹³C NMR (151 MHz, DMSO- d_6) δ 167.8, 142.7 (t, J = 29.0 Hz), 134.0 (q, J = 39.0 Hz), 132.4 (m), 120.7 (q, J = 268.3 Hz), 120.2 (t, J = 243.4 Hz), 52.2, 27.6 (dd, J = 29.0, 5.7 Hz), 23.4, 11.7. ¹⁹F NMR (565 MHz, DMSO- d_6) δ -60.3 (s, 3F), -79.8 (d, J = 253.0 Hz, 1F), -102.8 (d, J = 253.0 Hz, 1F).

A% (235 nm): 99.0 %

HPLC wt% purity (235 nm): 100.2 %

KF water content analysis: 0.009 %

LC-MS (m/z) (M+H): 283

IR (ATR) vmax: 3075, 3014, 2965, 1767, 1735, 1538, 1443, 1411, 1390, 1344, 1321, 1273, 1241, 1182, 1129, 1109, 1047, 1016, 952, 926, 839, 805, 759, 714, 669

HRMS (ESI) m/z: calcd for $C_{10}H_7F_5N_2O_2\cdot H^+=[M+H]^+283.0506$, found 283.0504

Melting point: 149-151 °C.

Synthesis of 3-methyl-3-(methylsulfonyl)but-1-yne (Frag D)¹⁶

To a 500 mL round-bottom flask was added sodium methanesulfinate (36.29 g, 341.26 mmol, 1.4 eq, 96 wt%), copper (II) acetate (2.26 g, 12.19 mmol, 0.05 eq, 98 wt%), TMEDA (3.67 mL, 24.38 mmol, 0.1 eq, 99.5 wt%), and isopropyl acetate (175 mL, 7V). The suspension was agitated at <25 °C, and 3-chloro-3-methylbut-1-yne (25.00 g, 27.4 mL, 243.76 mmol) was added dropwise to maintain a temperature < 25 °C. The reaction mixture was then heated at 30 °C for 16 h, cooled to RT, diluted with isopropyl acetate (125 mL, 5V), and washed twice with deionized H₂O (125 mL, 5V each). The combined aqueous layers were extracted thrice with isopropyl acetate (125 mL, 5V), and concentrated in vacuo to give a solid. The solid was then dried under a high vacuum at RT to yield **Frag D** (17.00 g, 94.05 wt% purity by GCMS) as a white solid (45% corrected yield).

All Frag D batches and commercial batches of Fragment D (Ambeed) were combined and purified through recrystallization to afford a singular batch to use in API process development.

Procedure: **Frag D** (165 g, 88 wt% by qNMR) was suspended in MTBE (1.65 L, 10V). The mixture was heated to 55 °C until dissolved, stirred for 20 minutes, and filtered (hot-filtration) to remove a brown sticky solid. The solution was cooled to 0 °C and stirred for an additional 2 h. The resultant solid was filtered and washed with cold MTBE. The solid was dried overnight in a high vacuum to yield purified **Frag D** (130 g, 97.3 wt% by GCMS) as a white solid.

¹H NMR (600 MHz, DMSO- d_6) δ 3.70 (s, 1H), 3.10 (s, 3H), 1.54 (s, 6H)

¹³C NMR (151 MHz, DMSO-*d*₆) δ 82.1, 77.4, 56.5, 34.5, 22.3.

GCMS TIC A%: 99.2%

GCMS wt% purity: 97.3 wt%

GC-FID solvent analysis: MTBE 0.67 wt%

IR (ATR) vmax: 3263, 3034, 3017, 2991, 2937, 1452, 1415, 1316, 1293, 1217, 1165, 1113, 964, 945, 800, 757, 719, 669

Melting point: 123-125 °C.

Synthesis of *tert*-butyl (1-(3,6-dibromopyridin-2-yl)-2-(3,5-difluorophenyl)ethyl)carbamate (rac-L1.1-Boc):

To a 250 mL round-bottom flask was charged **Frag A** (10.0 g, 25.51 mmol) and DCM (100 mL, 10V). The reaction mixture was cooled to 0 °C, TEA (5.33 mL, 38.3 mmol, 1.5 eq) and di-tert-butyl dicarbonate (8.35 g, 38.3 mmol, 1.5 eq) were added in order. The reaction mixture was allowed to warm to RT while stirring for 17 hours. After completion, the solvent was evaporated via distillation to afford a crude solid. The crude solid was dissolved in EtOAc (2V), and hexane (8V) was added dropwise to precipitate **L1.1-Boc** (7.90 g, 95.0 wt% by qNMR) as a white solid (60.0% corrected yield).

¹H NMR (600 MHz, DMSO- d_6) δ 7.99 (d, J = 8.25 Hz, 1H), 7.51 (dd, J = 8.44, 12.65 Hz, 2H), 7.07 (t, J = 9.35 Hz, 1H), 7.01 (d, J = 6.60 Hz, 2H), 5.05 (dt, J = 4.40, 9.08 Hz, 1H), 2.86-2.99 (m, 2H), 1.29 (s, 9H).

¹³C NMR (151 MHz, CDC13-d) δ 162.9 (d, J = 13.2 Hz), 161.3 (d, J = 13.2 Hz), 160.0, 155.2, 143.6, 142.7 (t, J = 9.5 Hz), 139.6, 128.5, 119.3, 112.3 (dd, J = 20.0, 4.4 Hz), 101.9 (t, J = 25.8 Hz), 56.6, 55.6, 38.3, 28.0, 27.6.

¹⁹F NMR (565 MHz, DMSO-d6) δ -110.59 (s, 2F).

A% (275 nm): 99.4 %

LC-MS (m/z) $[M+H]^+$: 491

IR (ATR) vmax: 3379, 2982, 2935, 1690, 1629, 1593, 1459, 1441, 1420, 1368, 1347, 1308, 1269, 1252, 1239, 1174, 1129, 1111, 1055, 1008, 971, 928, 891, 848, 829, 777, 762, 725

HRMS (ESI) m/z: calcd for $C_{18}H_{18}Br_2F_2N_2O_2\cdot Na^+=[M+Na]^+$ 512.9595, found 512.9452

Melting point: 130-132 °C.

Synthesis of *tert*-butyl (1-(3-bromo-6-(3-methyl-3-(methylsulfonyl)but-1-yn-1-yl)pyridin-2-yl)-2-(3,5-difluorophenyl)ethyl)carbamate (rac-L1.2-Boc)

To a 25 mL round-bottom flask was charged rac-**Frag A** (1.0 g, 2.55 mmol), **Frag D** (410.2 mg, 2.81 mmol, 1.1 eq), bis(triphenylphosphine)palladium (II) dichloride (10.7 mg, 15.3 μmol, 0.006 eq), and degassed 2-MeTHF (5.0 mL, 5V). The mixture was evacuated and backfilled with N₂ three times. Then degassed TEA (1.78 mL, 12.8 mmol, 5.0 eq) was added under N₂ atmosphere at 20 °C, followed a solution of di-tert-butyl dicarbonate (612.4 mg, 2.81 mmol, 1.1 eq) in degassed 2-MeTHF (1 mL, 1V). The reaction mixture was heated to 68 °C and maintained for 2 h. Upon completion, the reaction mixture was partitioned between EtOAc (20V) and deionized H₂O (20V). The aqueous layer was extracted thrice with EtOAc (10V each). The combined organic layers were washed thrice with deionized H₂O (10V each), brine (10V), and concentrated to dryness. The resulting crude solid was dissolved in EtOAc (2V), and then hexane (8V) was added dropwise to yield rac-**L1.2-Boc** as a brown solid (1.04 g, 73.4 % uncorrected yield).

¹H NMR (600 MHz, DMSO- d_6) δ 8.10 (d, J = 8.07 Hz, 1H), 7.47 (dd, J = 8.40, 13.20 Hz, 2H), 7.07 (t, J = 9.45 Hz, 1H), 7.02 (d, J = 6.42 Hz, 2H), 5.08 - 5.13 (m, J = 4.03 Hz, 1H), 3.20 (s, 3H), 2.86 - 2.97 (m, 2H), 1.68 (s, 6H), 1.28 (s, 9H).

¹³C NMR (151 MHz, DMSO-*d*₆) δ 163.0, 161.3, 159.2, 155.2, 142.9, 141.3, 139.7, 128.0, 120.1, 112.4, 101.9, 88.0, 84.1, 78.1, 69.0, 57.2, 55.8, 38.5, 35.0, 28.0, 22.3, 22.2.

¹⁹F NMR (565 MHz, DMSO- d_6) δ -110.64 (m, 2F).

A% (275 nm): 97.6 %

LC-MS (m/z) (M+H): 557

IR (ATR) vmax: 3373, 3008, 2982, 2932, 1702, 1627, 1597, 1519, 1448, 1431, 1392, 1366, 1305, 1269, 1256, 1241, 1165, 1116, 1060, 1038, 1016, 971, 855, 766

Telescoped synthesis of L1.3-K-Boc (Step 1: Coupling Fragments A, D, and B-DiMs)

Synthesis of potassium (S)-(7-(2-(1-((tert-butoxycarbonyl)amino)-2-(3,5-difluorophenyl)ethyl)-6-(3-methyl-3-(methylsulfonyl)but-1-yn-1-yl)pyridin-3-yl)-4-chloro-1-(2,2,2-trifluoroethyl)-1H-indazol-3-yl)(methylsulfonyl)amide (L1.3-K-Boc)

A 1L ChemRxnHub reactor was successively charged with **Frag A**²² (40.00 g, 100.1 mmol, 98.1 wt%, 98.8 %ee), **Frag D** (15.84 g, 105.1 mmol, 1.05 eq, 97 wt%), and bis-(triphenylphosphine)palladium (II) dichloride (0.70 g, 1.0 mmol, 0.01 eq). The reactor was evacuated and backfilled with Argon four times, then charged with degassed 2-MeTHF (360 mL, 7V), a solution of di-tert-butyl dicarbonate (24.27 g, 110.1 mmol, 1.1 eq) in 2-MeTHF (40 mL, 1V), and triethylamine (70 mL, 500 mmol, 5.0 eq). The contents were stirred and heated to 68 °C and held for 2-3 hours. Once the Heck coupling was complete, degassed deionized H₂O (40 mL, 1V) was added to the reaction mixture.

A 2L ChemRxnHub reactor was successively charged with **Frag B-DiMs** (63.87 g, 120.1 mmol, 1.2 eq, 100 wt%), CataCXium A (2.27 g, 6.00 mmol, 0.06 eq), and palladium (II) dichloride (0.53 g, 3.00 mmol, 0.03 eq). The reactor was evacuated and backfilled with Argon four times, then charged with degassed 2-MeTHF (80 mL, 2V), and the contents stirred at 20 °C. The contents in Reactor 1 were then transferred to Reactor 2. Following complete transfer, a deionized H₂O (40 mL, 1V) rinse was added to Reactor 1 and transferred to Reactor 2. The contents of Reactor 2 were heated to 68 °C and stirred for 3 hours. Once the Suzuki reaction was complete, 3M KOH

(200 mL, 600 mmol, 6.0 eq) was added to Reactor 2 and stirred for 1 hour at the same temperature. Upon hydrolysis completion, the contents were cooled to 20 °C.

The contents were filtered through a celite plug (20 g) and returned to a clean reactor. Once the aqueous phase was separated, the organic phase was concentrated at 50 °C (NLT 100 torr), diluted with deionized H₂O (800 mL, 20V), and further concentrated until the volatile organics were removed (NLT 55 torr). The aqueous phase was pH-adjusted to pH \geq 12.5 with aq. KOH (160 mL, 3 wt%) and washed thrice with MTBE (200mL, 5V each). The aqueous phase was then extracted once with MIBK (400 mL, 10V), and the organic phase was treated with SilaMetS Thiol (8.40 g, 10 wt% of theoretical yield) as a slurry at 80 °C for 3 hours. The contents were cooled to 20 °C, filtered through a celite plug (20 g), and rinsed with MIBK (200 mL, 5V). The filtrate is returned to a clean reactor, washed successively with 3M KOH (40 mL, 1V) and deionized H₂O (40 mL, 1V), concentrated at 50 °C (NLT 30 torr) to ~200 mL batch volume, and precipitated with heptane (400 mL, 10V) over NLT 10 minutes. The contents were cooled to 20 °C, filtered, and the solid was dried in a vacuum oven at 75 °C, 30 torr, for NLT 12 hours to yield L1.3-K-Boc (65.05 g, 90.4 wt% by HPLC) as a light-yellow solid (69.7% corrected yield).

¹H NMR (600 MHz, DMSO- d_6) δ 7.74 – 7.67* (m, 2H), 7.41 – 7.26* (d, J = 6 Hz, 1H), 7.08 – 6.94* (m, 3H), 6.51 – 6.41* (m, 2H), 4.33 – 4.03* (m, 3H), 3.36 (s, 3H), 3.24 – 3.23* (m, 3H), 2.86 – 2.77* (m, 4H), 1.72 (brs, 6H), 1.26 – 1.21* (s, 9H). *Signals from minor atropisomer included.

¹³C NMR (151 MHz, DMSO- d_6) δ 208.3, 162.8 (d, J = 13.6 Hz), 161.2 (d, J =13.6), 160.7, 155.5, 152.1, 143.2 – 143.1 (m), 140.9, 139.8, 139.3, 131.4, 129.9, 128.2, 126.3, 124.7, 122.8, 119.2, 117.6, 117.5, 111.9 – 111.8 (m), 102.0 – 101.6 (m), 87.5, 84.8, 78.2, 57.3, 55.5, 51.8, 35.1, 30.1, 28.1, 24.9, 23.9, 22.5, 22.3.

¹⁹F NMR (565 MHz, DMSO- d_6) δ -68.3 (t, J = 8.7 Hz, 1F), -68.6 (m, 0.3H)*, -68.8 (t, J = 9.3 Hz, 3F), -110.4 – -110.5 (m, 2F), -110.6 – -110.7* (m, 0.5F), -110.8 – -110.9* (m, 0.2F), -111.0 – -111.1* (m, 0.2F). *Signals from minor atropisomer included.

A% (275 nm): 98.1%

Atropisomeric ratio based on A% (275 nm): major: 83.2% (retention time: 10.11min); minor atropisomer: 16.8% (retention time: 9.76 min)

HPLC wt% purity (275 nm): L1.3-Boc free acid (85.7 wt%)

GC-FID solvent analysis: MIBK (3.90 wt%); Heptane (0.13 wt%)

ICP-OES metals analysis: Pd (7.9 ppm)

KF water content analysis: H₂O (1.32 wt%)

ELSD salt content analysis: 4.7 wt%

LC-MS (m/z) [M-K+H]⁺: 804

IR (ATR) vmax: 2978, 2935, 1703, 1625, 1595, 1577, 1508, 1482, 1366, 1305, 1228, 1198, 1157, 1103, 1042, 977, 841, 760

HRMS (ESI) m/z: calcd for $C_{34}H_{34}C1F_5KN_5O_6S_2 \cdot H^+= [M+H]^+ 842.1269$, found 842.1264

Melting point: 210-215 °C.

Synthesis of L1.3-Ms (Step 2: Boc-Deprotection of L1.3-K-Boc)

Synthesis of (S)-N-(7-(2-(1-amino-2-(3,5-difluorophenyl)ethyl)-6-(3-methyl-3-(methylsulfonyl)but-1-yn-1-yl)pyridin-3-yl)-4-chloro-1-(2,2,2-trifluoroethyl)-1H-indazol-3-yl)methanesulfonamide (L1.3-Ms).

To a 300 mL ChemRxnHub reactor was added L1.3-K-Boc (50.00g, 53.66 mmol, 1.0 eq, 90.4 wt%), toluene (225 mL, 4.5V), and EtOH (25 mL, 0.5V). The reaction was stirred for 20-30 min at 20 °C under N₂ atmosphere to obtain a clear solution. After which, 9M sulfuric acid (59.6 mL, 536.6 mmol, 10 eq) was added dropwise via syringe, and the reaction was stirred at 20 °C until Boc-deprotection was completed. After 2 hours, EtOAc (750 mL, 15V) and H₂O (75 mL, 1.5V) were added and stirred for 10 minutes. The layers were separated, and the organic layer was

basified (pH ~8.5) using 3M NaOH (20 mL, 0.4V). The layers were separated, and the organic layer was washed two times with deionized H₂O (250 mL, 5V each). The final organic layer was concentrated at 55 °C (NLT 50 torr) to ~50 mL batch volume (1V). Heptane (500 mL, 10V) was added, and the slurry was stirred for 30 minutes. After which, the solid was collected via filtration using a disposable funnel, suction dried for 30 minutes and then dried in a vacuum oven at 75 °C, 30 torr, for NLT 12 hours to afford **L1.3-Ms** (39 g, 94.1 wt% by HPLC) as a light-yellow solid (97 % corrected yield).

¹H NMR (600 MHz, DMSO- d_6) (**Major isomer**) δ: 7.74 (d, J = 8.0 Hz, 1H), 7.71 (d, J = 7.9 Hz, 1H), 7.21 (d, J = 7.6 Hz, 1H), 7.03 – 6.93 (m, 1H), 6.63 (d, J = 7.6 Hz, 1H), 6.31 (dd, J = 8.3, 2.1 Hz, 2H), 4.91 (td, J = 16.8, 8.5 Hz, 1H), 4.32 (td, J = 16.9, 8.5 Hz, 1H), 3.62 (t, J = 6.8 Hz, 1H), 3.25 (s, 3H), 3.16 (s, 3H), 2.91 – 2.74 (m, 2H), 1.73 (s, 6H).

¹H NMR (600 MHz, DMSO- d_6) (**Minor isomer**) δ: 7.82 (d, J = 8.0 Hz, 1H), 7.71 (d, J = 7.9 Hz, 1H), 7.42 (d, J = 7.7 Hz, 1H), 7.36 (d, J = 7.7 Hz, 1H), 7.02 – 6.93 (m, 1H), 6.60 (dd, J = 8.3, 2.0 Hz, 1H), 6.31 (dd, J = 8.3, 2.1 Hz, 1H), 4.50 (dt, J = 24.3, 8.3 Hz, 1H), 4.10 – 3.96 (m, 1H), 3.70 (dd, J = 8.6, 5.1 Hz, 1H), 3.25 (s, 3H), 3.16 (s, 3H), 2.98 (dd, J = 13.4, 8.7 Hz, 1H), 2.90 – 2.83 (m, 1H), 1.73 (s, 6H).

¹³C NMR (151 MHz, DMSO- d_6) δ 163.3 (d, J = 13.3 Hz), 161.7 (d, J = 13.4 Hz), 161.1, 143.0, 142.2, 141.5 (d, J = 177.2 Hz), 140.1, 139.95 – 139.8 (m), 139.7, 131.1 (d, J = 106.3 Hz), 129.0 (d, J = 104.6 Hz), 124.6, 122.7, 122.4, 119.7, 118.2, 117.8, 112.4 (d, J = 24.3 Hz), 102.2 (t, J = 25.6 Hz), 88.6, 85.1, 57.8, 55.3, 50.7 (d, J = 33.5 Hz), 44.4, 41.6 (s), 41.4, 35.5 (d, J = 3.6 Hz), 31.7, 28.8, 22.8 – 22.7 (m), 22.6, 14.4. (Atropisomers cannot be differentiated in ¹³CNMR).

¹⁹F NMR (565 MHz, DMSO- d_6) (**Major isomer**) δ -68.95 (t, J = 8.6 Hz, 3F), -110.42 (t, J = 7.8 Hz, 2F).

¹⁹F NMR (565 MHz, DMSO- d_6) (**Minor isomer**) δ -68.75 (t, J = 8.3 Hz, 3F), -110.42 (t, J = 7.8 Hz, 2F).

A% (275 nm): 96.8 %

Atropisomeric ratio based on A% (275 nm): major: 83.0% (retention time: 7.77 min); minor atropisomer: 17.0% (retention time: 6.14 min)

HPLC wt% purity (275 nm): 94.1 %

GC-FID solvent analysis: 2.49 % Heptane; 0.40 % Toluene

ICP-OES metals analysis: 18.2 ppm

KF water content analysis: 0.83 %

ELSD salt content analysis: Not detected

LC-MS (m/z) $[M+H]^+$: 704

IR (ATR) vmax: 3360, 3248, 3021, 2935, 1625, 1593, 1577, 1500, 1446, 1357, 1303, 1262, 1239, 1154, 1115, 1044, 973, 937, 885, 848, 829, 759

HRMS (ESI) m/z: calcd for $C_{29}H_{27}ClF_5N_5O_4S_2 \cdot H^+ = [M+H]^+ 704.1186$, found 704.1183

Melting point: 126-127 °C.

Synthesis of Len-API (Step 3: Amidation of L1.3-Ms with Frag C)

Synthesis of Sodium (4-chloro-7-(2-((S)-1-(2-((3bS,4aR)-5,5-difluoro-3-(trifluoromethyl)-3b,4,4a,5-tetrahydro-1H-cyclopropa[3,4]cyclopenta[1,2-c]pyrazol-1-yl)acetamido)-2-(3,5-difluorophenyl)ethyl)-6-(3-methyl-3-(methylsulfonyl)but-1-yn-1-yl)pyridin-3-yl)-1-(2,2,2-trifluoroethyl)-1H-indazol-3-yl)(methylsulfonyl)amide (Len API)

To a 1000 mL ChemRxnHub Reactor 1 was added **L1.3-Ms** (35g, 1eq, 46.72 mmol, 94 wt%) and **Frag C** (13.5g, 1.025 eq, 47.89 mmol, 100 wt%). Reagent-grade acetonitrile (175mL, 5V) was added to Reactor 1, and the mixture is stirred at 25 °C under N₂. The mixture was then cooled to an internal temperature of -10 °C. 4-Methylmorpholine (15.9mL, 3.0 eq, 140.2 mmol) was added slowly (8 mL/min) to Reactor 1, at -10 °C (internal) under N₂ and stirred for NLT 10 minutes, after which, a 50% solution of T3P (27.8mL, 1.0 eq, 46.72 mmol, 50 wt%) in DMF was added slowly (8 mL/min) to Reactor 1, at -10 °C under N₂. The reactor was then warmed to 25 °C and further heated to NLT 60 °C and stirred for NLT 4.5 hours. After the allotted time, a second lot of

50% T3P (8.2 mL, 0.3 eq, 14.0mmol, 50wt%) in DMF was added slowly (8 mL/min) to Reactor 1 at 60 °C under N₂. The reactor was maintained under these conditions for NLT 18 hours. After 18h, a third lot of 50% T3P (5.44 mL, 0.2 eq, 9.3mmol, 50wt%) in DMF was added slowly (8 mL/min) to Reactor 1 at 60 °C under N₂. The reactor was maintained under these conditions for NLT 1 hour.

The reaction mixture was basified (pH ~13.7) with 1M NaOH (383mL, 8 eq. 374mmol), then stirred and heated to 45 °C (internal) for NLT 3 hours. To this reaction mixture was added MIBK (358mL, 10V), and the mixture was stirred for NLT 15 minutes. A phase separation was undertaken, and the aqueous layer was discharged. The organics were concentrated via distillation (250 to 50 mbar) to 40mL, ~1V, and then heptane (530mL, 15V) was added, stirred for 1 hour. The resulting solid was filtered using a disposable fritted funnel and suction-dried for 1 hour. The solid was transferred to 2000 mL ChemRxnHub Reactor 2. To this, EtOH (530mL, 10V based on crude solid) was added and stirred at 70 °C for 15 min until a clear solution was observed. Then heptane (1060mL, 20V based on crude solid) was added dropwise over 3h maintaining temperature 70 °C. The mixture was stirred at 70 °C for 30 minutes, and then slowly cooled to room temperature over 16 hours. The solid was filtered with a disposable fritted funnel, washed with 1:2 EtOH: Heptane (530mL, 10V), suction dried for NLT 1h. The obtained solid was charged back to Reactor 2. To this, EtOH (600mL, 10V based on crude solid) was added and stirred at 70 °C for 15 min until a clear solution was observed. Then heptane (1200mL, 20V based on crude solid) was added dropwise over 3h maintaining temperature 70 °C. The mixture was stirred at 70 °C for 30 minutes, and then slowly cooled to room temperature over 16 hours. The solid was filtered with a disposable fritted funnel, washed with 1:2 EtOH:Heptane (600mL, 10V), suction dried for NLT 1h and finally oven dried at 75 °C under vacuum (30 torr) for NLT 12 h until constant weight to obtain pure Len API sodium salt as a yellow solid in (37.5 g, 78.4% corrected yield, 102.48wt%) ¹H NMR (600 MHz, DMSO- d_6) (**Major isomer**) δ : 9.08 (d, J = 8.0 Hz, 1H), 7.69 (s, 2H), 7.04 –

6.96 (m, 1H), 6.93 (d, J = 7.6 Hz, 1H), 6.67 (d, J = 7.6 Hz, 1H), 6.44 (d, J = 6.3 Hz, 2H), 4.89 (d, J = 16.5 Hz, 1H), 4.76 (d, J = 16.5 Hz, 1H), 4.69 (td, J = 8.4, 5.1 Hz, 1H), 4.19 (dq, J = 16.6, 8.3 Hz, 1H), 3.81 (dq, J = 17.6, 8.9 Hz, 1H), 3.25 (s, 3H), 2.93 (ddd, J = 22.5, 13.6, 7.0 Hz, 2H), 2.78 (s, 3H), 2.61 – 2.51 (m, 2H), 1.74 (s, 3H), 1.73 (s, 3H), 1.39 (dd, J = 13.4, 7.2 Hz, 1H), 0.94 (d, J = 3.3 Hz, 1H).

¹H NMR (600 MHz, DMSO- d_6) (**Minor isomer**) δ: 8.92 (d, J = 8.5 Hz, 1H), 7.75 (dd, J = 21.8, 7.9 Hz, 2H), 6.95 (d, J = 12.0 Hz, 1H), 6.91 – 6.85 (m, 2H), 6.52 (d, J = 6.3 Hz, 2H), 4.83 – 4.78 (m, 2H), 4.63 (d, J = 16.5 Hz, 1H), 4.28 (dd, J = 16.0, 8.2 Hz, 1H), 3.73 (dd, J = 16.5, 8.1 Hz, 1H), 3.24 (s, 3H), 3.09 – 3.00 (m, 2H), 2.83 – 2.79 (s, 3H), 2.62 – 2.51 (m, 2H), 1.73 (d, J = 3.6 Hz, 6H), 1.45 – 1.41 (m, 1H), 0.98 (s, 1H).

¹³C NMR (151 MHz, CDCl3-*d*) δ 164.4, 163.4, 163.0, 162.9, 161.3, 161.2, 158.9, 158.2, 152.6, 151.9, 143.0 – 142.9 (m), 142.9 – 142.8 (m), 142.8 – 142.7 (m), 142.6, 142.4, 142.4 – 142.2 (m), 142.1 (d, J = 9.4 Hz), 141.4 (s), 141.1, 139.6 (s), 139.4, 134.0 (d, J = 38.6 Hz), 133.6, 133.2 – 133.0 (m), 132.1, 131.9, 131.7, 129.7, 129.6, 128.2, 127.9, 126.9, 126.8, 124.5, 123.5 – 123.1, 122.7, 121.6, 121.6 – 121.5 (m), 119.9, 119.9, 119.8, 118.9, 118.2 (d, J = 21.1 Hz), 117.5, 117.2, 117.0, 112.1, 111.97, 111.8, 102.2, 102.0, 101.8, 88.1, 88.0, 84.7, 57.3, 56.0, 53.2, 53.0, 52.8, 52.4, 49.5 (d, J = 32.1 Hz), 40.0, 38.6, 35.1, 27.7, 27.6, 27.3, 23.2, 22.3 (d, J = 18.7 Hz), 11.6. (Atropisomers cannot be differentiated in ¹³CNMR).

¹⁹F NMR (565 MHz, DMSO- d_6) (**Major isomer**) δ: -60.01 (s, 3F), -68.55 (s, 3F), -79.33 (d, J = 254.0 Hz, 1F), -102.61 (d, J = 253.9 Hz, 1F), -109.89 (s, 2F).

¹⁹F NMR (565 MHz, DMSO- d_6) (**Minor isomer**) δ: -59.97 (s, 3F), -68.03 (s, 3F), -79.58 (d, J = 254.2 Hz, 1F), -102.58 (d, J = 253.7 Hz, 1F), -109.97 (s, 2F).

A% (235 nm): 98.8A%

Atropisomeric ratio based on A% (235 nm): major: 85.9% (retention time: 11.96 min); minor atropisomer: 14.1% (retention time: 11.42 min)

HPLC wt% purity (235 nm): 100.6%±2.8%

GC-FID solvent analysis: 0.3%±0.04% (EtOH); 0.06%±0.01% (Heptane)

ICP-OES metals analysis (Pd content): < 4.2 ppm

KF water content analysis: 0.3%±0.01%

ELSD salt content analysis: 1.88%±0.08%

LC-MS $(m/z) [M - Na + H]^+: 968$

IR (ATR) vmax: 3651, 3366, 3021, 2943, 1702, 1627, 1590, 1515, 1485, 1459, 1385, 1366, 1351, 1314, 1260, 1236, 1148, 1131, 1109, 1042, 1018, 978, 945, 842, 807, 762

HRMS (ESI) m/z: calcd for $C_{39}H_{31}C1F_{10}N_7NaO_5S_2 \cdot H^+ = [M+H]^+ 990.1327$, found 990.1326

Melting point: 238-240 °C.

 $[\alpha]_D^{20}$ (deg·mL·g⁻¹·dm⁻¹) (MeOH (10mg/mL) at 20 °C under 589nm): -93.044

Synthesis and characterization of major impurities

N-(4-chloro-1-(2,2,2-trifluoroethyl)-1H-indazol-3-yl)methanesulfonamide (Frag B-MoMs-Debo)

$$\begin{array}{c} \text{SO}_2\text{Me} \\ \text{SO}_2\text{Me} \\ \text{SO}_2\text{Me} \\ \text{SO}_2\text{Me} \\ \text{Frag B-DiMs-DeBo} \\ \text{CF}_3 \\ \end{array}$$

To a two-neck 100 mL round-bottom flask was added **Frag B-DiMs-DeBo** (1.5 g, 3.7 mmol, 1 eq), 2-MeTHF (7.5 mL, 5V) and KOH (3M, 6.2 mL, 18.5 mmol, 5 eq) at room temperature. The reaction mixture was heated at 70 °C for 2 h. Upon completion of the reaction (monitored by TLC), the mixture was cooled to 20 °C. The mixture was extracted twice with EtOAc (15 mL each, 10V). The organic layers were combined and washed with 5% acetic acid (7.5 mL, 5V), followed by deionized water (7.5 mL, 5V) to pH = 7.0. The organic layer was concentrated and treated with heptane (10.5 mL, 7 V). The slurry was filtered to afford **Frag B-MoMs-DeBo** as a solid (0.70 g, 2.1 mmol, 57.8 % uncorrected yield).

¹H NMR (600 MHz, DMSO- d_6) δ 9.94 (s, 1H), 7.80 (d, J = 8.5 Hz, 1H), 7.55 – 7.41 (m, 1H), 7.29 (d, J = 7.4 Hz, 1H), 5.49 (q, J = 9.0 Hz, 2H), 3.22 (s, 3H).

¹³C NMR (151 MHz, DMSO- d_6) δ 142.8, 138.7, 128.7, 125.3, 127.4 – 119.8 (q, 280Hz), 122.5, 116.7, 109.4 (s), 49.0 (q, J = 33.6 Hz), 41.4.

¹⁹F NMR (565 MHz, DMSO- d_6) δ -69.58 (t, J = 9.1 Hz).

A% (275 nm): 98.2 %

LC-MS (m/z) $[M+H]^+$: 328

IR (ATR) vmax: 3274, 3224, 3021, 2968, 2939, 1740, 1612, 1572, 1526, 1500, 1451, 1429, 1388, 1347, 1299, 1261, 1246, 1183, 1155, 1090, 1060, 978, 941, 892, 855, 833, 782, 762, 738

HRMS (ESI) m/z: calcd for $C_{10}H_9CIF_3N_3O_2S\cdot Na^+=[M+Na]^+349.9948$, found 349.9997

Melting point: 166 -168 °C.

tert-butyl (S)-(1-(3,6-bis(3-methyl-3-(methylsulfonyl)but-1-yn-1-yl)pyridin-2-yl)-2-(3,5-difluorophenyl)ethyl)carbamate (L1.2-Boc-DiFd)

A 100 mL two-neck round-bottom flask was charged with **Frag A** (2.00 g, 5.1015 mmol, 1.0 eq), **Frag D** (1.49 g, 10.203 mmol, 2.0 eq), PdCl₂ (45.2 mg, 0.255 mmol, 0.05 eq), and XPhos (243.2 mg, 0.510 mmol, 0.1 eq). The above reaction mixture was degassed and backfilled with nitrogen three times. Then degassed 2-MeTHF (3.0 mL, 8V) was added. To the stirred mixture was slowly added a solution of di-tert-butyl dicarbonate (1.22 g, 5.6117 mmol, 1.1 eq) in degassed 2-MeTHF (2.0 mL, 1V), then degassed triethylamine (3.56 mL, 25.508 mmol, 5 eq) was added slowly. The reaction mixture was heated at 68 °C and stirred for 2 h under N₂ atmosphere. Upon completion of the reaction, 2-MeTHF was removed under vacuum at 50 °C. The solid was then suspended in deionized H₂O (20 mL,10V) and stirred for 20 min. The solid was collected by filtration and washed with heptane (20 mL, 10 V). The solid was dried at 65 °C to afford **L1.2-Boc-DiFd** as a light brown solid (1.4 g, 2.1918 mmol, 42.9 % uncorrected yield).

¹H NMR (600 MHz, DMSO- d_6) δ 8.97 (bs, 1H), 7.90 (d, J = 7.8 Hz, 1H), 7.54 (d, J = 7.8 Hz, 1H), 7.42 (d, J = 7.8 Hz, 1H), 7.16 – 7.01 (m, 1H), 6.96 (d, J = 6.4 Hz, 1H), 5.22z (d, J = 6.5 Hz, 1H), 5.09* (s), 3.21 (s, 6H), 3.12* (d, J = 13.6 Hz), 3.05 (s, 1H), 2.98 (d, J = 9.1 Hz, 1H), 2.69 – 2.68 (m, 1H), 1.68 (d, J = 6.3 Hz, 12H), 1.57* (m), 1.28 (s, 9H), 1.16* (s).

¹³C NMR (151 MHz, DMSO- d_6) δ 163.3, 161.6, 155.6, 143.1, 141.2, 140.8, 126.7, 117.0, 113.0, 102.3, 96.2, 89.4, 85.1, 81.6, 78.9, 78.5, 69.5, 58.0, 57.9, 57.78, 55.1, 46.2, 35.7, 35.5 (d, J = 3.8 Hz), 28.6, 28.3 – 28.0 (m), 22.8 (d, J = 4.8 Hz), 22.7, 22.5.

¹⁹F NMR (565 MHz, DMSO- d_6) δ -110.7*, -110.8 (d, J = 7.8 Hz).

A% (275 nm): 98.6 %

LC-MS (m/z) $[M+H]^+$: 623

IR (ATR) vmax: 3371, 2982, 2935, 1707, 1627, 1597, 1498, 1448, 1366, 1299, 1163, 1113, 1012, 949, 844, 762

HRMS (ESI) m/z: calcd for $C_{30}H_{36}F_2N_2O_6S_2 \cdot H^+ = [M+H]^+ 623.2056$, found 623.2055

Melting point: 121-123 °C.

N-(4-chloro-7-(2-((S)-1-(2-((3bS,4aR)-5,5-difluoro-3-(trifluoromethyl)-3b,4,4a,5-tetrahydro-1H-cyclopropa[3,4]cyclopenta[1,2-c]pyrazol-1-yl)acetamido)-2-(3,5-difluorophenyl)ethyl)-6-(3-methyl-3-(methylsulfonyl)but-1-yn-1-yl)pyridin-3-yl)-1-(2,2,2-trifluoroethyl)-1H-indazol-3-yl)-2-((3bS,4aR)-5,5-difluoro-3-(trifluoromethyl)-3b,4,4a,5-tetrahydro-1H-cyclopropa[3,4]cyclopenta[1,2-c]pyrazol-1-yl)-N-(methylsulfonyl)acetamide (Len-API-DiC)

A 50 mL round-bottom flask was charged with **Len API-H** (500 mg, 0.51 mmol, 1.0 eq), **Frag C** (145.7 mg, 0.516 mmol, 1.0 eq), and 5.0 mL of CH₃CN (10V) under N₂ atmosphere. The mixture was stirred at 20 °C, and then TEA (0.22 mL, 1.55 mmol, 3.0 eq) was added slowly under N₂. The mixture was stirred for 5 minutes and then a solution of T3P in DMF (50 wt%, 0.6 mL 1.03 mmol, 2.0 eq) was added slowly. The mixture was stirred for another 4 h. After completion, 10 mL of ice-cold H₂O was added, and the mixture was stirred for 10 minutes. The mixture was extracted

twice with EtOAc (30 mL each). The organic layers were combined and washed with brine (20 mL). The EtOAc layer was separated and rotovapped to dryness. The residue was precipitated with heptane (5 mL, 10 V). The solid was collected by filtration and dried under vacuum at 60 °C for 7 h to afford 0.37 g of **Len-API-DiC** as a light-yellow solid (58.1% uncorrected yield).

¹H NMR (600 MHz, DMSO- d_6) (**Major isomer**) δ: 9.10 (d, J= 8.5Hz, 1H), 7.81 (d, J = 7.9 Hz, 1H), 7.48 (dd, J = 15.6, 5.7 Hz, 1H), 6.93 (t, J = 9.2 Hz, 1H), 6.89 (d, J = 7.7 Hz, 1H), 6.54 – 6.45 (m, 1H), 6.39 (d, J = 6.5 Hz, 2H), 4.98 – 4.83 (m, 2H), 4.81 – 4.53 (m, 3H), 4.03 (m, 1H), 3.63 (s, 3H), 3.26 (s, 3H), 3.02 (m, 2H), 2.73 – 2.55 (m, 2H), 2.43 (dd, J = 22.4, 9.8 Hz, 2H), 1.75 (s, 6H), 1.41 (ddd, J = 24.4, 13.6, 6.7 Hz, 2H), 1.30 – 1.19 (m, 1H), 0.97 (s, 2H).

¹H NMR (600 MHz, DMSO- d_6) (**Minor isomer**) δ: 9.21 (t, J = 10.1 Hz, 1H), 7.92 (d, J = 7.9 Hz, 1H), 7.76 (dd, J = 20.7, 8.0 Hz, 1H), 7.54 – 7.44 (m, 1H), 7.00 (dd, J = 17.7, 8.4 Hz, 1H), 6.99 – 6.95 (m, 1H), 6.54 – 6.44 (m, 2H), 4.86 (ddd, J = 32.8, 22.0, 12.7 Hz, 2H), 4.80 – 4.51 (m, 3H), 4.22 – 4.05 (m, 1H), 3.63 (s, 3H), 3.26 (s, 3H), 3.00 (m,2H), 2.72 – 2.56 (m, 2H), 2.43 (dd, J = 22.4, 9.8 Hz, 2H), 1.75 (s, 6H), 1.41 (ddd, J = 24.4, 13.6, 6.7 Hz, 2H), 1.21 (m, 1H), 1.01 (d, J = 14.1 Hz, 2H).

¹³C NMR (151 MHz, DMSO- d_6) δ 170.78, 166.56, 166.07, 165.08, 164.90, 163.42, 163.39, 162.75, 161.79, 161.70, 159.29, 158.84, 143.13, 143.02, 142.76, 142.10, 140.76, 140.72, 139.76, 139.45, 135.36, 133.10, 132.25, 130.12, 127.51, 125.858, 125.29, 124.10, 123.96, 122.24, 122.01, 121.92, 120.50, 120.38, 120.30, 120.14, 119.10, 118.54, 112.54, 112.37, 112.20, 102.62, 102.45, 89.05, 88.86, 84.93, 60.19, 57.88, 57.81, 87.79, 54.29, 53.82, 53.43, 53.18, 52.32, 51.13, 50.90, 42.04, 41.86, 36.20, 35.63, 35.55, 35.52, 31.18, 28.01, 27.82, 23.63, 23.43, 22.83, 22.79, 22.76, 22.72, 22.49, 21.1514.48, 12.12. (Atropisomers cannot be differentiated in ¹³CNMR.)

¹⁹F NMR (565 MHz, DMSO- d_6) δ: -59.35 – -61.26 (m), -68.08 – -70.14 (m), -78.66 – -81.57 (m), -101.67 – -104.58 (m), -109.71 – -111.06 (m). (Atropisomers cannot be differentiated in ¹⁹FNMR.) LC-MS (m/z) [M+H]⁺: 1232

Atropisomeric ratio based on A% (235 nm): major: 91.5% (retention time: 17.45 min); minor atropisomer: 8.5% (retention time: 17.37 min)

HRMS (ESI) m/z: calcd for $C_{49}H_{37}C1F_{15}N_9O_6S_2\cdot Na^+=[M+Na]^+1254.1649$, found 1254.1644

(S)-N-(1-(3-(4-chloro-3-(methylsulfonamido)-1-(2,2,2-trifluoroethyl)-1H-indazol-7-yl)-6-(3-methyl-3-(methylsulfonyl)but-1-yn-1-yl)pyridin-2-yl)-2-(3,5-difluorophenyl)ethyl)acetamid (L1.3-Ms-Ac)

To a two-neck 50 mL round-bottom flask was added L1.3-Ms (500 mg, 0.7 mmol, 1.0 eq), followed by acetic acid (0.06 mL, 1.04 mmol, 1.50 eq) to this was added acetonitrile (2.5 mL, 5V) at room temperature under N₂. N-Methylmorpholine (0.23 mL, 2.1 mmol, 3.0 eq, 2.1 mmol) was added slowly over a period of 5 minutes at -12 °C under N₂ and stirred for 30 seconds. Then, 50 % T3P (0.5 mL, 0.87 mmol, 1.25 eq) in DMF was added, and the reaction was allowed to stir at RT for 1 h under N₂. Upon completion, monitored via HPLC-UV, the reaction was distilled out completely, and diluted with MIBK (5.0 mL, 10V) and 1M NaOH (4.4 mL, 13.2 mmol, 3M, 19 eq) was added to adjust the pH to between 7-8. The organic layer was separated, distilled out completely, and subject to purification via SiO₂ column chromatography (0-80 % EtOAc in heptanes), to afford L1.3-Ms-Ac as a semi-solid (0.25 g, 0.325 mmol, 46.8 % uncorrected yield). ¹H NMR (600 MHz, DMSO- d_6) δ 10.09 (d, J = 39.0 Hz, 1H), 8.67 (d, J = 7.9 Hz, 1H), 8.35* (d, J = 39.0 Hz, 1H), 8.67 (d, J = 7.9 Hz, 1H), 8.35* = 8.2 Hz), 7.82 (dd, J = 15.8, 8.0 Hz, 1H), 7.74 (dd, J = 7.9, 4.3 Hz, 1H), 7.39 (dd, J = 12.1, 7.7 Hz, 1H), 7.28* (d, J = 7.7 Hz), 7.13 (d, J = 7.6 Hz, 1H), 7.05 - 6.92 (m, 1H), 6.56* (d, J = 6.2 Hz), 6.49 (dd, J = 8.3, 2.1 Hz, 2H), 4.81 (dq, J = 16.6, 8.4 Hz, 1H), 4.76 – 4.67* (m), 4.47 (ddd, J =9.5, 8.0, 4.7 Hz, 1H), 4.17 - 4.06 (m, 1H), 3.27 - 3.23 (s, 3H), 3.21 (s, 3H), 2.89 (ddd, J = 23.1, 13.6, 7.0 Hz, 1H), 1.73 (d, J = 2.5 Hz, 6H), 1.68 (s, 3h), 1.59* (s). ¹³C NMR (151 MHz, DMSO- d_6) δ 169.0, 168.2, 162.8 (d, J = 13.3 Hz), 161.2 (d, J = 13.3 Hz),

160.1 (s), 142.7, 141.8, 139.6, 139.3, 139.2, 131.2, 130.2, 126.3 (t, J = 27.7 Hz), 125.1 (d, J = 27.7 Hz), 125.1 (d, J = 27.7 Hz)

302.5 Hz), 122.2, 119.4, 117.4, 111.9 (d, J = 24.4 Hz), 102.0 (t, J = 25.7 Hz), 88.2, 84.6, 57.3, 53.0, 52.6, 50.5 (dd, J = 65.6, 34.4 Hz), 41.4, 35.1 (d, J = 5.2 Hz), 22.3 (t, J = 9.3 Hz), 22.0.

¹⁹F NMR (565 MHz, DMSO- d_6) δ -68.78 (t, J = 9.2 Hz), -110.32 (d, J = 9.9 Hz).

A% (275 nm): 95.5 %

Atropisomeric ratio based on A% (275 nm): major: 83.2% (retention time: 6.16 min); minor atropisomer: 16.8% (retention time: 4.85 min)

LC-MS (m/z) $[M+H]^+$: 746

IR (ATR) vmax: 3358, 3028, 3000, 2939, 1736, 1654, 1627, 1595, 1576, 1500, 1446, 1373, 1300, 1261, 1239, 1153, 1112, 1041, 974, 851, 829, 758

HRMS (ESI) m/z: calcd for $C_{31}H_{29}C1F_5N_5O_5S_2 \cdot H^+ = [M+H]^+ 746.1292$, found 746.1292

Melting point: 117-121 °C.

Process safety assessment by EasyMax- detailed procedure for calorimetry data collection

Synthesis of potassium (S)-(7-(2-(1-((tert-butoxycarbonyl)amino)-2-(3,5-difluorophenyl)ethyl)-6-(3-methyl-3-(methylsulfonyl)but-1-yn-1-yl)pyridin-3-yl)-4-chloro-1-(2,2,2-trifluoroethyl)-1H-indazol-3-yl)(methylsulfonyl)amide (L1.3-K-Boc)

To a 100 mL glass reactor was added **Frag A** ((*S*)-A1.5, 5.0 g, 12.7 mmol, 1.0 eq), 2.06 g of **Frag D** (13.2 mmol, 94 wt%, 1.04 eq), 53.7 mg of bis(triphenylphosphine)palladium (II) dichloride (76.5 μ mol, 0.6 mol%), and 7V of 2-MeTHF (35.0 mL). The vessel was evacuated via a vacuum pump and filled with N₂ four times. A baseline HFCal determination was performed (Quick Cal

1) for 1 hour and 10 minutes. Then, Boc anhydride (3.06 g, 14.0 mmol, 1.1 eq) in 1V of degassed 2-MeTHF (5.0 mL), was added dropwise via syringe at RT. Next, 8.9 mL of degassed triethylamine (63.7 mmol, 5 eq), was added dropwise via syringe at RT. The reaction mixture was heated to 68-70 °C ($T_j = 72$ °C) and stirred for 15 minutes. After which, an HFCal determination was performed (Quick Cal 2) for 1 hour and 10 minutes. The reaction was analyzed via TLC for completion and then transferred to the Suzuki reaction (reactor 2) as detailed below.

While the Heck coupling was running (reactor 1), a second 100 mL reaction vessel (reactor 2) was filled with 8.14 g of **Frag B-DiMs** (15.3 mmol, 1.2 eq), 67.8 mg of palladium (II) chloride (382.6 μ mol, 3 mol%), and 274.4 mg of di((38,58,78)-adamantan-1-yl)(butyl)phosphane (765.2 μ mol, 6 mol%). The vessel was evacuated via a vacuum pump and filled with N₂ four times, then the Heck reaction mixture (reactor 1) was charged via syringe and 22G needle. The reaction mixture was heated to 68-70 °C ($T_j = 72$ °C) and stirred for 10 minutes. A baseline HFCal determination was performed (Quick Cal 1) for 1 hour and 10 minutes. After which, 10 mL each of deionized H₂O and 2-MeTHF were added, and the mixture was stirred for 10 minutes. An HFCal determination was performed (Quick Cal 2) for 1 hour and 10 minutes. The reaction was then analyzed via TLC for completion. Upon Suzuki reaction completion, an HFCal determination was performed (Quick Cal 1) for 1 hour and 10 minutes, then 21.256 mL of aqueous 3M potassium hydroxide (63.7 mmol, 5.0 eq) was added to the hot mixture and stirred for 20 minutes. Another HFCal determination was performed (Quick Cal 2) for 1 hour and 10 minutes, and the reaction was analyzed via TLC for completion, then cooled to RT ($T_j = 25$ °C) and ceased.

Synthesis of (S)-N-(7-(2-(1-amino-2-(3,5-difluorophenyl)ethyl)-6-(3-methyl-3-(methylsulfonyl)but-1-yn-1-yl)pyridin-3-yl)-4-chloro-1-<math>(2,2,2-trifluoroethyl)-1H-indazol-3-yl)methanesulfonamide (L1.3-Ms)

$$\begin{array}{c} \text{Me} \\ \text{Me} \\ \text{Me} \\ \text{SO}_2\text{Me} \end{array} \\ \text{L1.3-K-Boc} \\ \begin{array}{c} \text{Aq H}_2\text{SO}_4 \text{ (9M, 10 eq)} \\ \text{9:1 Toluene:EtOH (5V)} \\ \text{20 °C, 2 hr} \\ \end{array} \\ \begin{array}{c} \text{Me} \\ \text{Me} \\ \text{SO}_2\text{Me} \\ \text{SO}_2\text{Me} \\ \end{array} \\ \text{L1.3-Ms} \\ \end{array}$$

To a 100 mL glass reactor was added of L1.3-K-Boc (10.7 g, 12.7 mmol, 1 eq) and 5V of methyl

ethyl ketone (53.7 mL) or **L1.3-K-Boc** (10.0 g, 11.87 mmol, 1 eq) and 7V of 5:2 toluene:EtOH (70.0 mL) under N_2 at 20 °C ($T_j = 20$ °C). The mixture was stirred for 10 minutes, and then a HFCal determination was performed (Quick Cal 1) for 1 hour and 10 minutes. After which, 14.1 mL of aqueous 9M sulfuric acid (127.5 mmol, 10 eq) was added dropwise over various rates (i.e., 2, 12, and 45 minutes) and stirred for 10 minutes under N_2 at 20 °C ($T_j = 20$ °C). A HFCal determination was performed (Quick Cal 2) for 1 hour and 10 minutes, and the reaction was analyzed for completion via TLC, and then ceased.

Synthesis of Sodium (4-chloro-7-(2-((S)-1-(2-((3bS,4aR)-5,5-difluoro-3-(trifluoromethyl)-3b,4,4a,5-tetrahydro-1H-cyclopropa[3,4]cyclopenta[1,2-c]pyrazol-1-yl)acetamido)-2-(3,5-difluorophenyl)ethyl)-6-(3-methyl-3-(methylsulfonyl)but-1-yn-1-yl)pyridin-3-yl)-1-(2,2,2-trifluoroethyl)-1H-indazol-3-yl)(methylsulfonyl)amide (Len API)

To a 100 mL glass reactor was added **L1.3-Ms** (10.0 g, 14.2 mmol, 1 eq), 4.1 g of **Frag C** (14.5 mmol, 1.025 eq), and 5V of acetonitrile (50.0 mL) under N₂ at 20 °C ($T_j = 20$ °C) and stirred for 10 minutes. The reaction mixture was cooled to -10 °C ($T_j = -13$ °C) and stirred for 10 minutes. After which, a HFCal determination was performed (Quick Cal 1) for 1 hour and 10 minutes. Then, 4.6844 mL of NMM (42.6 mmol, 3.0 eq) was dosed over 2 minutes and then stirred for 10 minutes at -10 °C ($T_j = -13$ °C). Next, 8.2611 mL of T3P (14.2 mmol, 1.0 eq) was dosed over 2 minutes at -10 °C ($T_j = -13$ °C). The reaction was then heated to 60 °C ($T_j = 65$ °C) and stirred for 10 minutes. A HFCal determination was performed (Quick Cal 2) for 1 hour and 10 minutes, and then the reaction was held at 60 °C ($T_j = 65$ °C) for 2 hours. After the allotted time a HFCal determination was performed (Quick Cal 1) for 1 hour and 10 minutes, and then 2.5 mL of T3P (4.26 mmol, 0.3 eq) was dosed over 0.5 minutes at 60 °C ($T_j = 65$ °C). A final HFCal determination was performed (Quick Cal 2) for 1 hour and 10 minutes, and the reaction was held at 60 °C ($T_j = 65$ °C) for 15 hours. After which, the reaction was analyzed for completion via HPLC, cooled to RT ($T_j = 20$ °C), and then ceased.

3.3 NMR Spectra

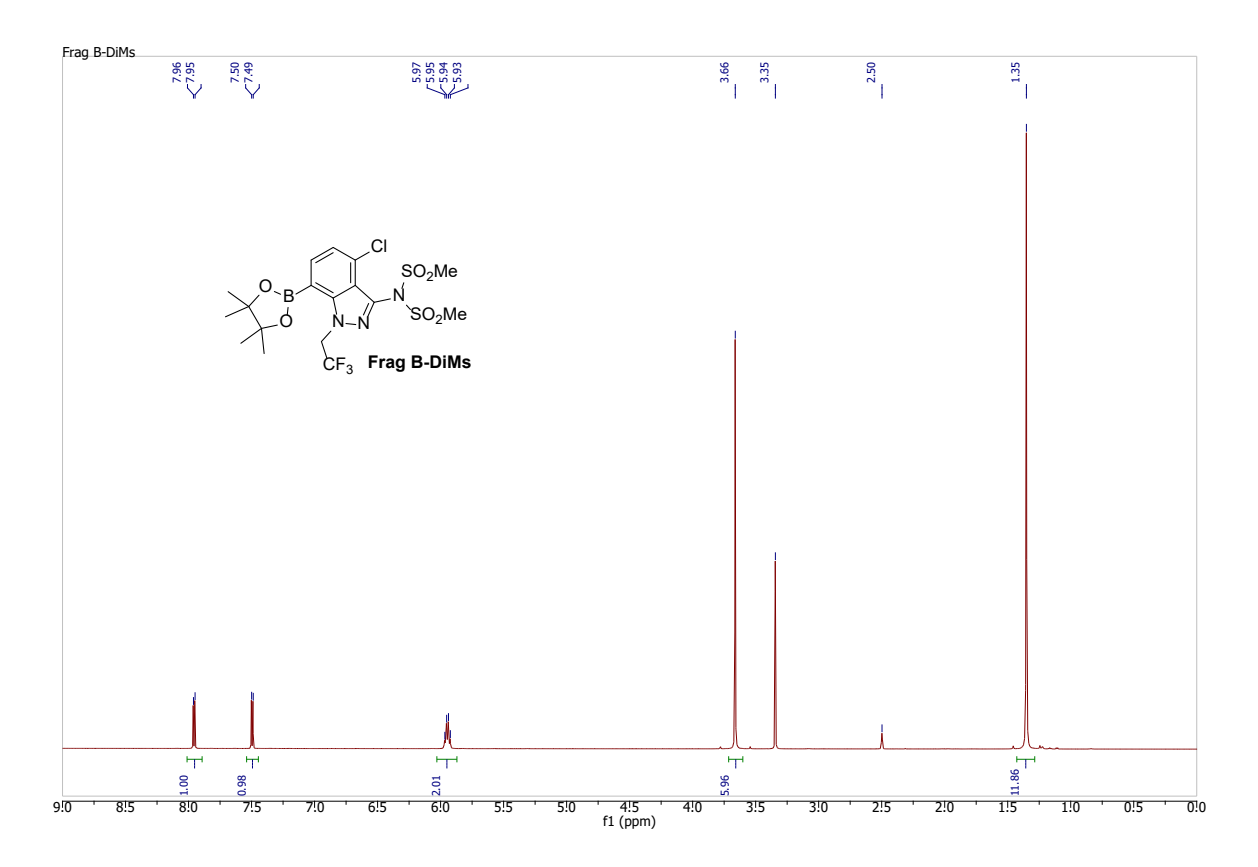


Figure 3.3.1. ¹HNMR (600MHz, DMSO-d₆) of **Frag-B-DiMs**.

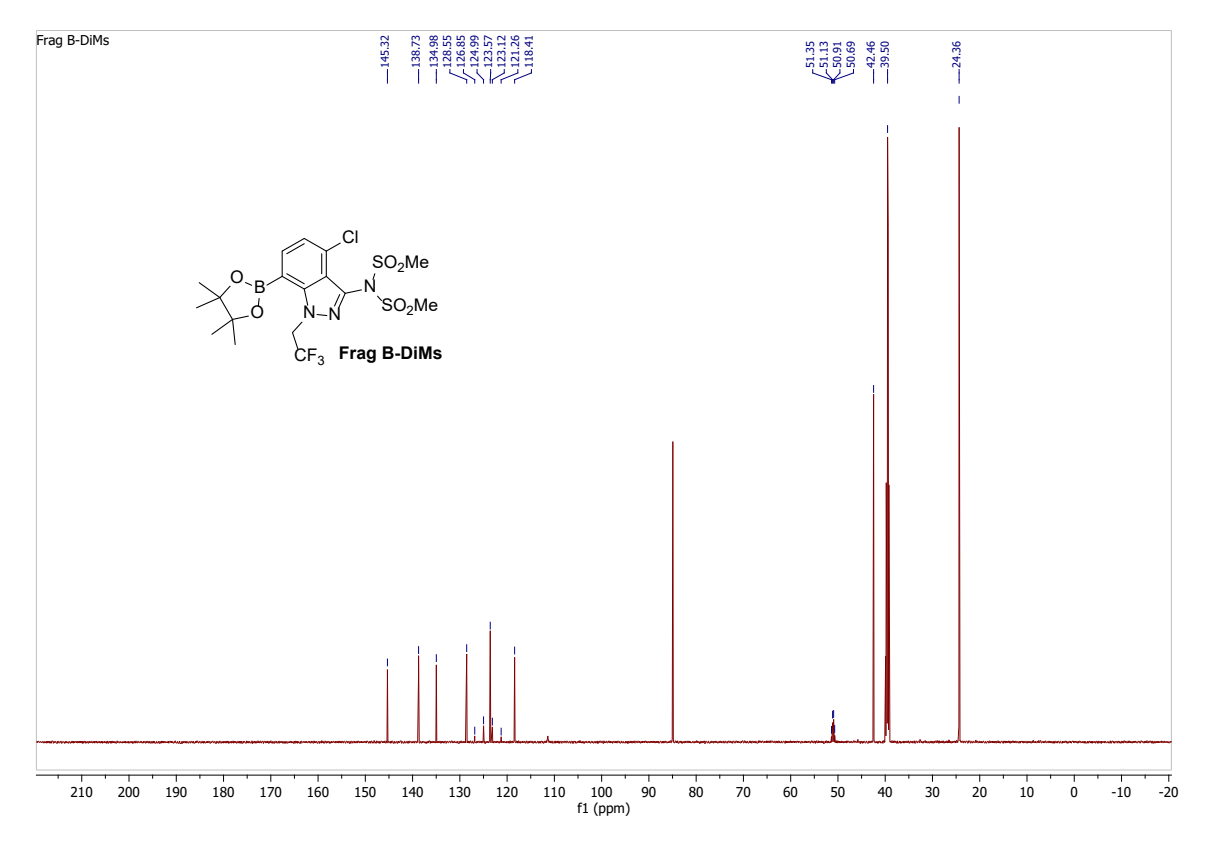


Figure 3.3.2. ¹³CNMR (151MHz, DMSO-d₆) of **Frag-B-DiMs**.

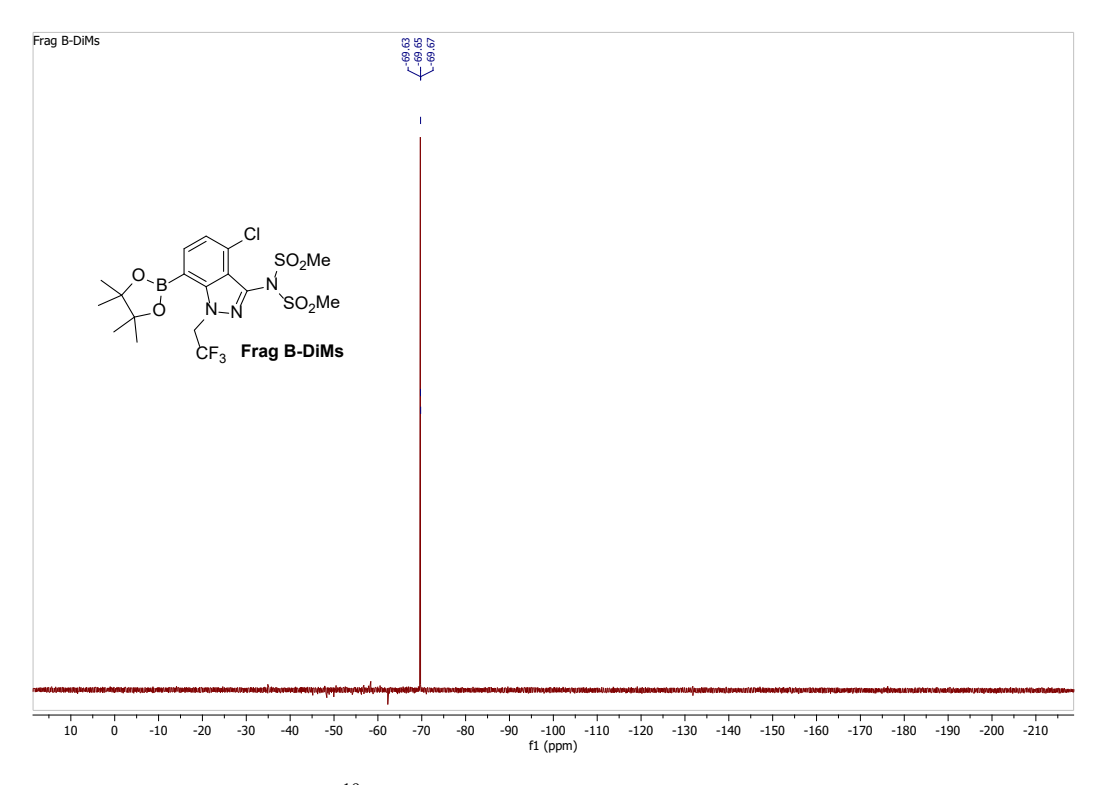


Figure 3.3.3. ¹⁹FNMR (565MHz, DMSO-d₆) of **Frag-B-DiMs**.

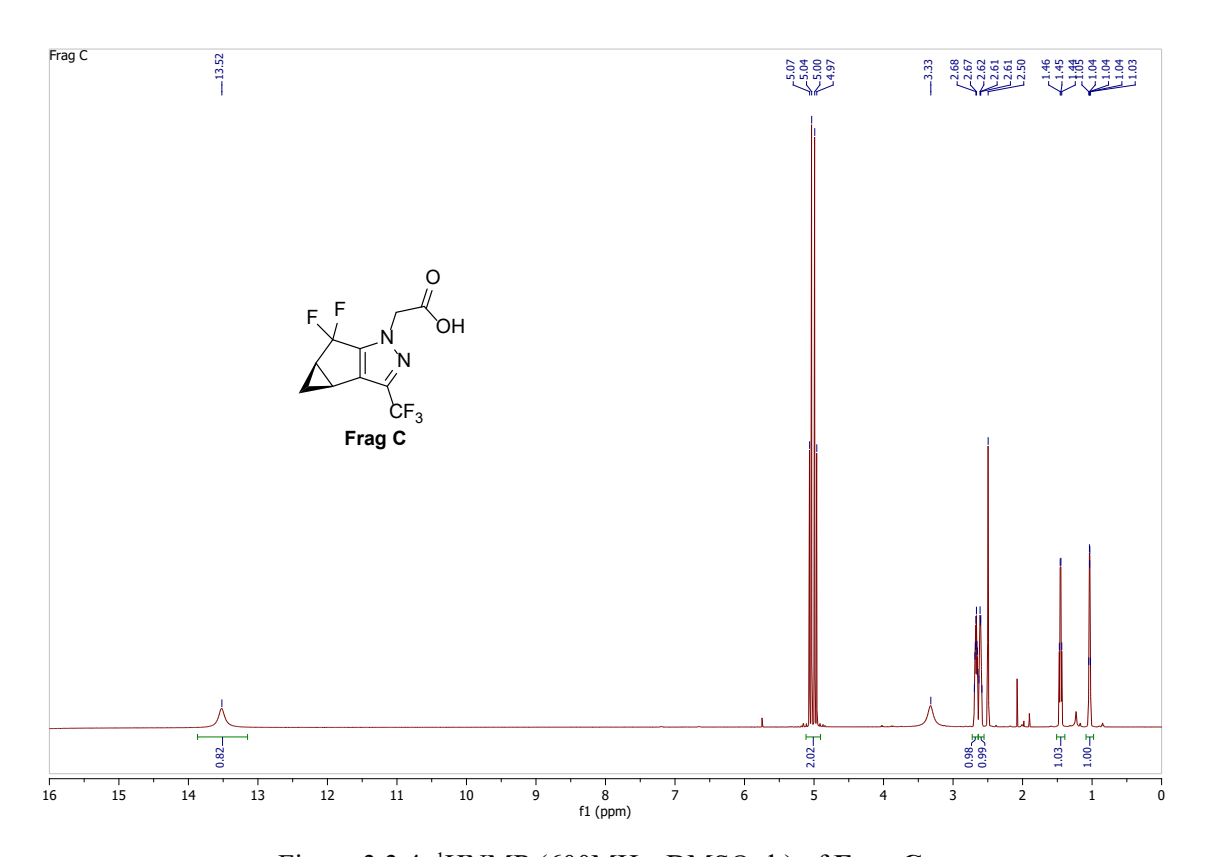


Figure 3.3.4. ¹HNMR (600MHz, DMSO-d₆) of Frag C.

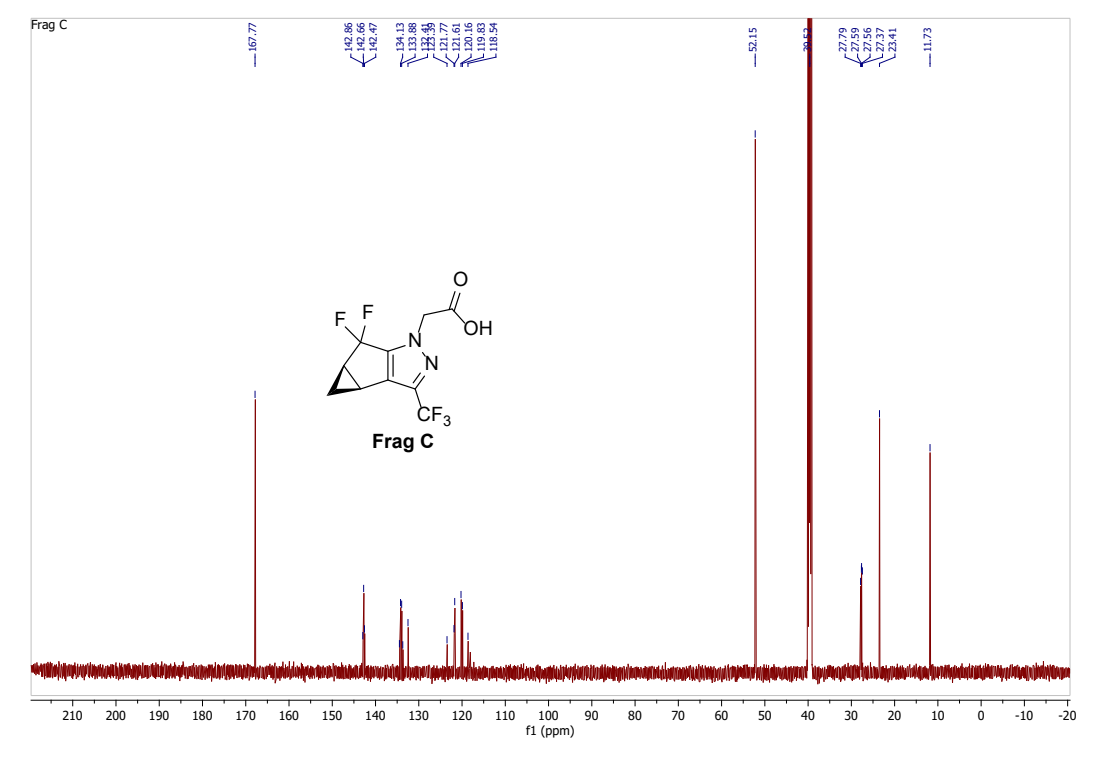


Figure 3.3.5. ¹³CNMR (151MHz, DMSO-d₆) of **Frag C**.

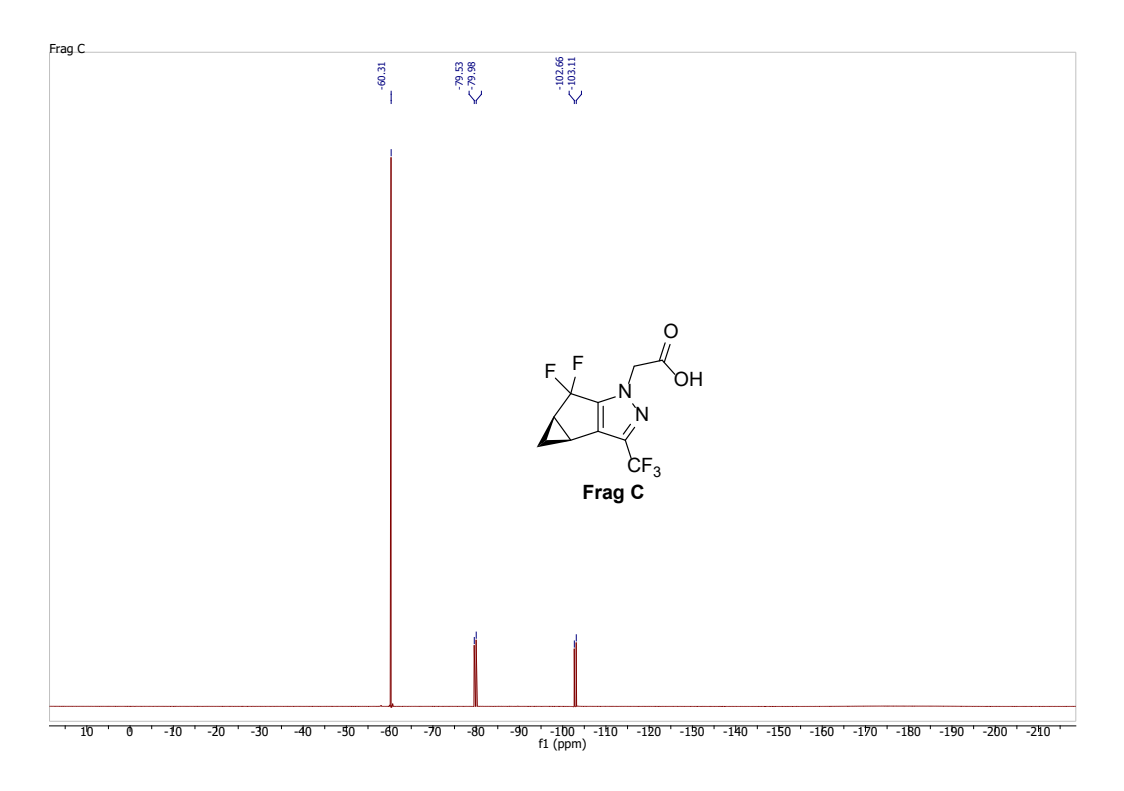


Figure 3.3.6. $^{19}\mbox{FNMR}$ (565MHz, DMSO-d6) of Frag C.

Retention Times					
Compound Time (min)					
Frag C Enantiomer 1	3.53				
Frag C Enantiomer 2	8.52				
Notes: Stereochemical assignments unknown					

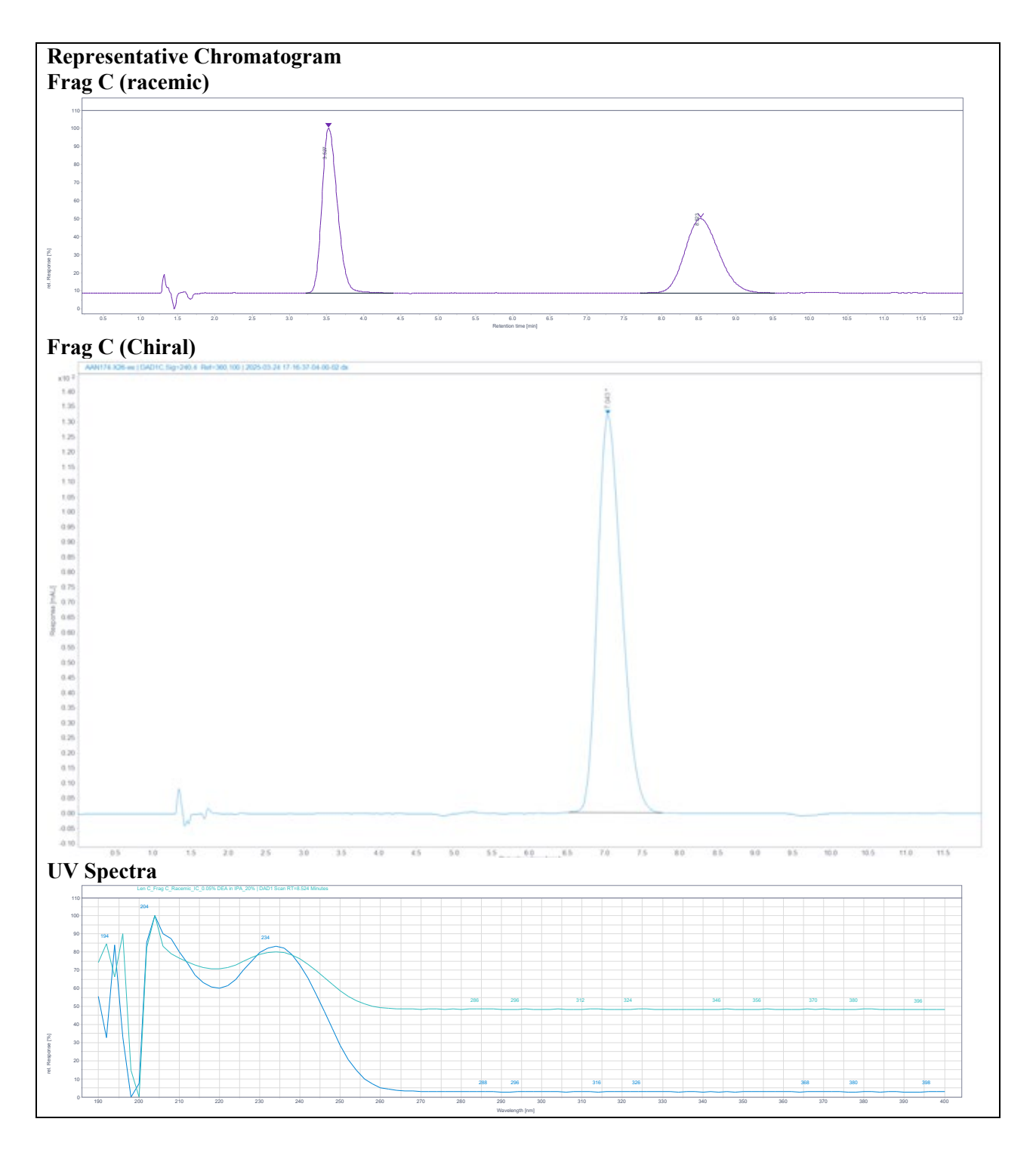


Figure 3.3.7. Chiral GC (GC-FID) spectrum of Frag C.

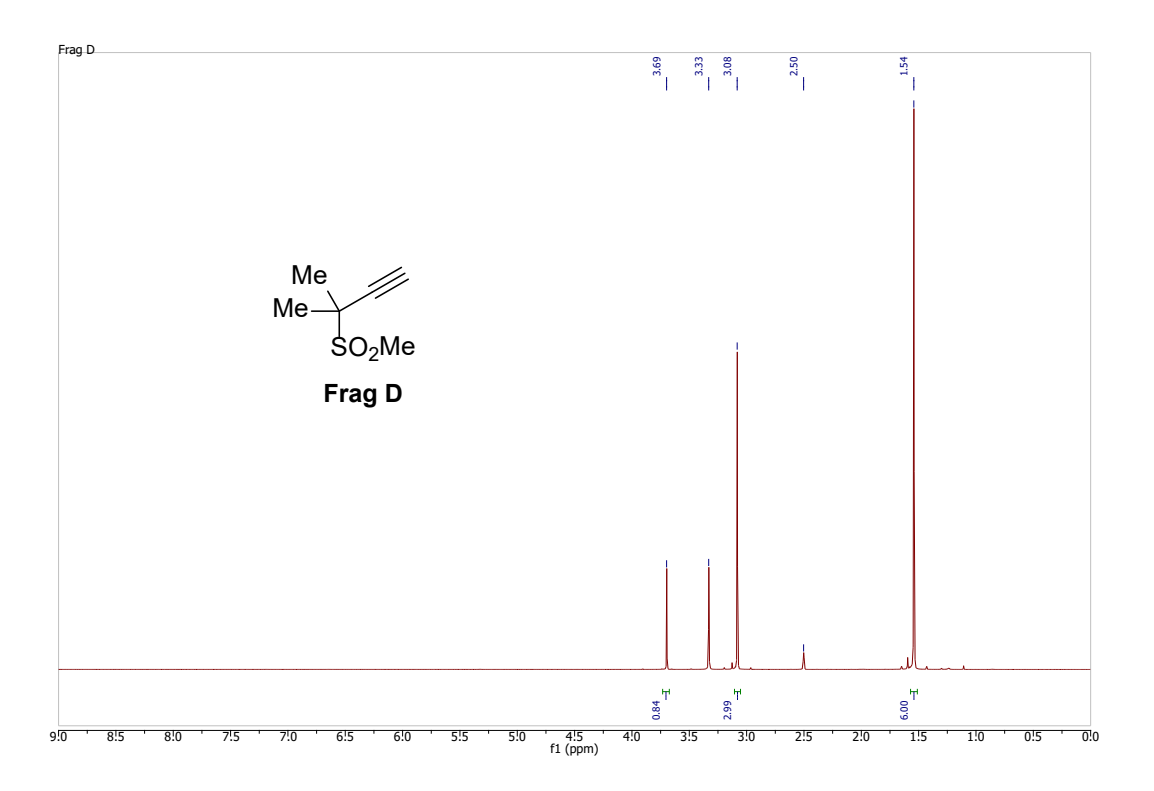


Figure 3.3.8. ¹H NMR (600 MHz, DMSO-*d6*) of **Frag D**.

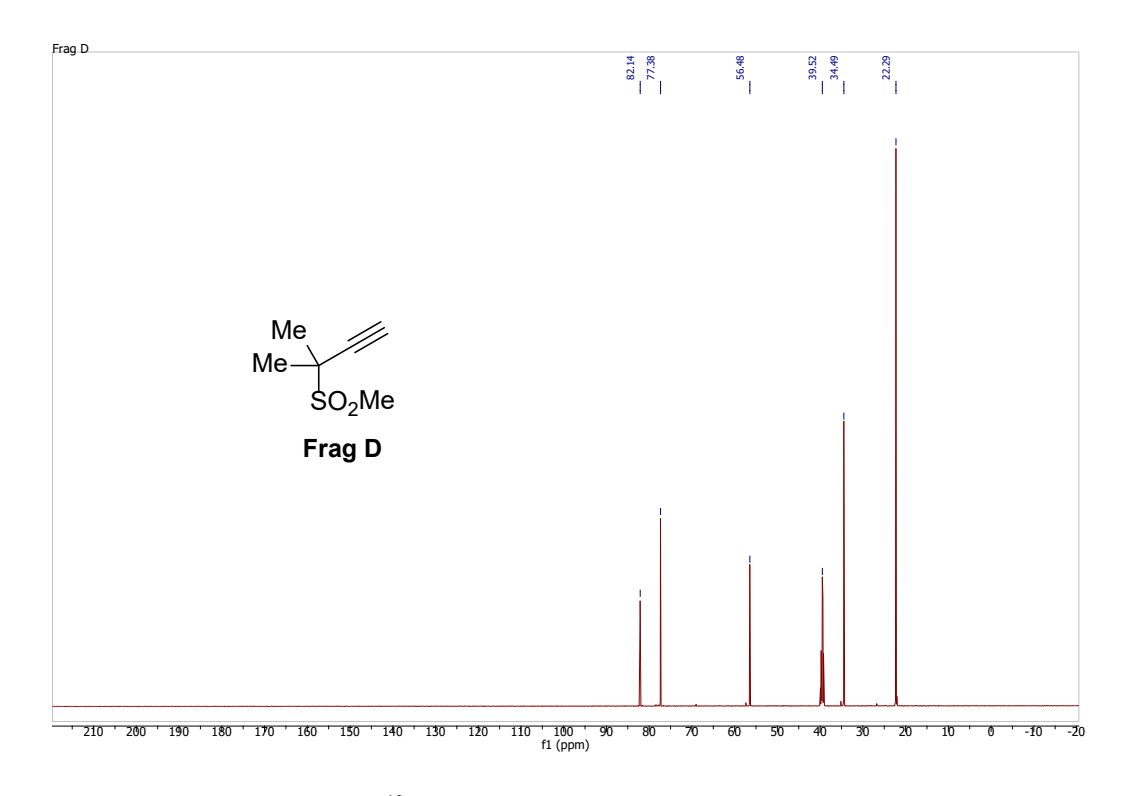


Figure 3.3.9. 13 C NMR (150 MHz, DMSO- d_6) of **Frag D**.

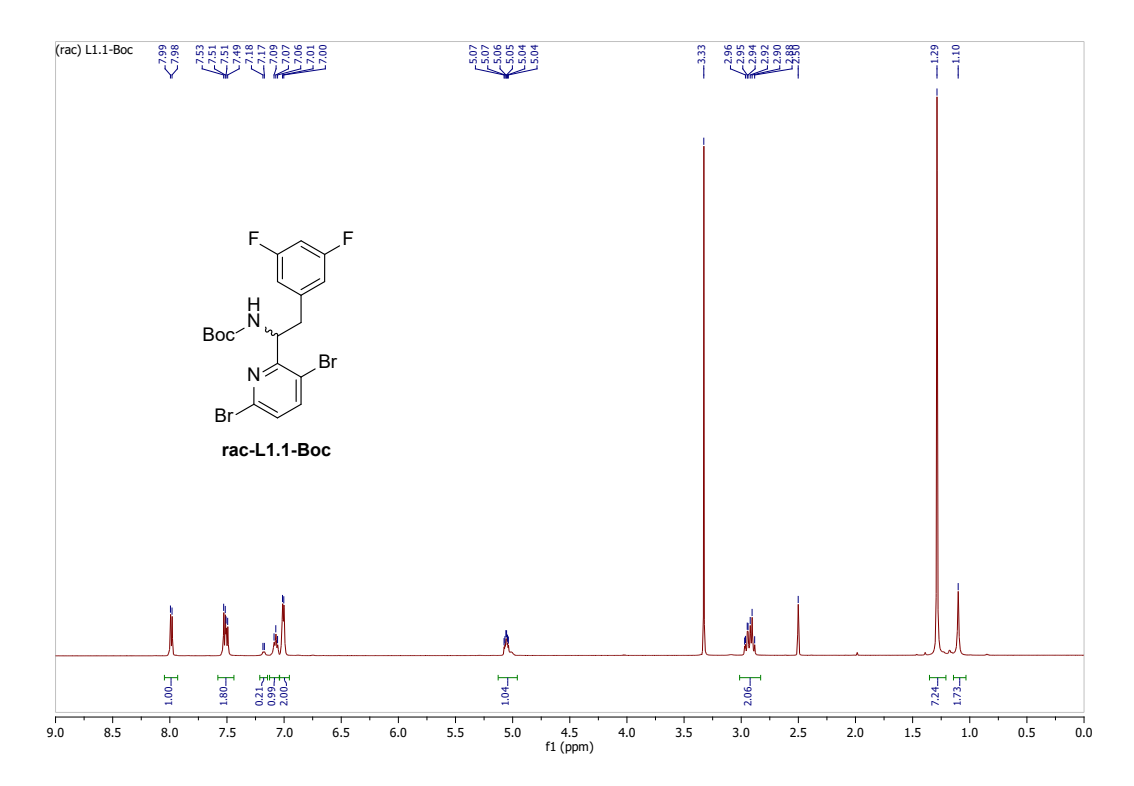


Figure 3.3.10. ¹H NMR (600 MHz, DMSO-*d*₆) of rac-**L1.1-Boc**.

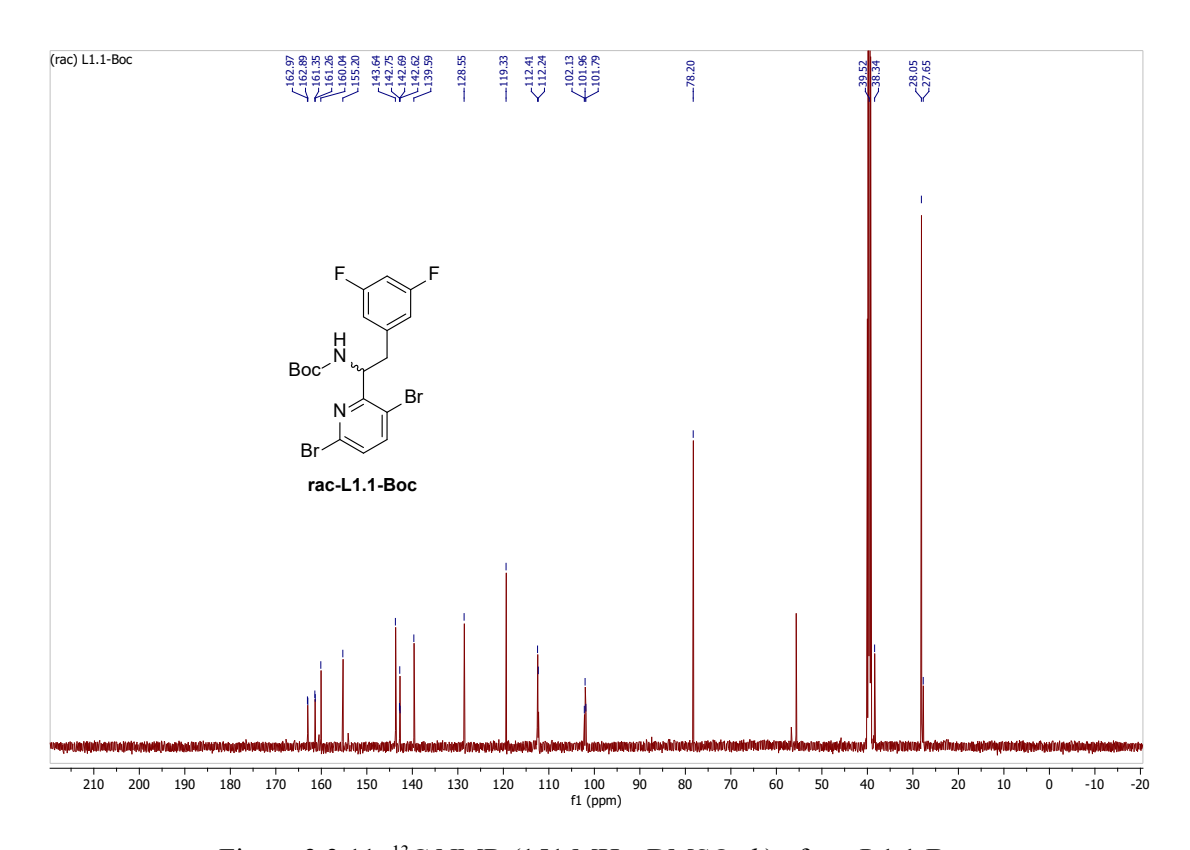


Figure 3.3.11. 13 C NMR (151 MHz, DMSO- d_6) of rac-L1.1-Boc.

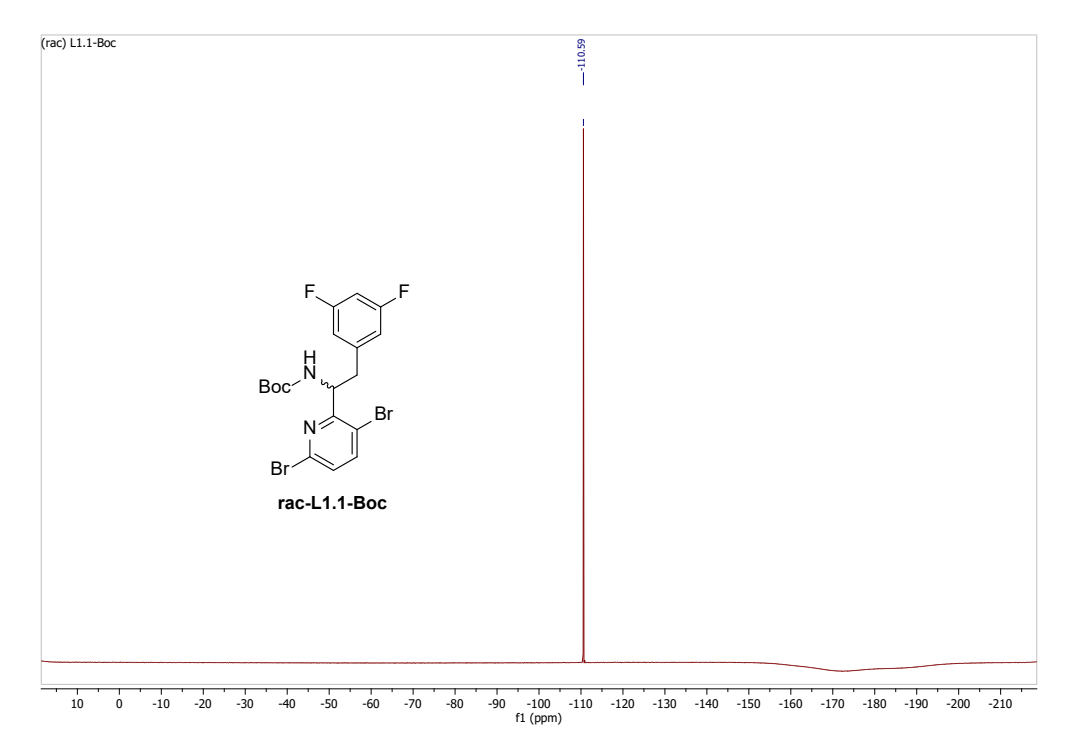


Figure 3.3.12. 19 F NMR (565 MHz, DMSO- d_6) of rac-**L1.1-Boc.**

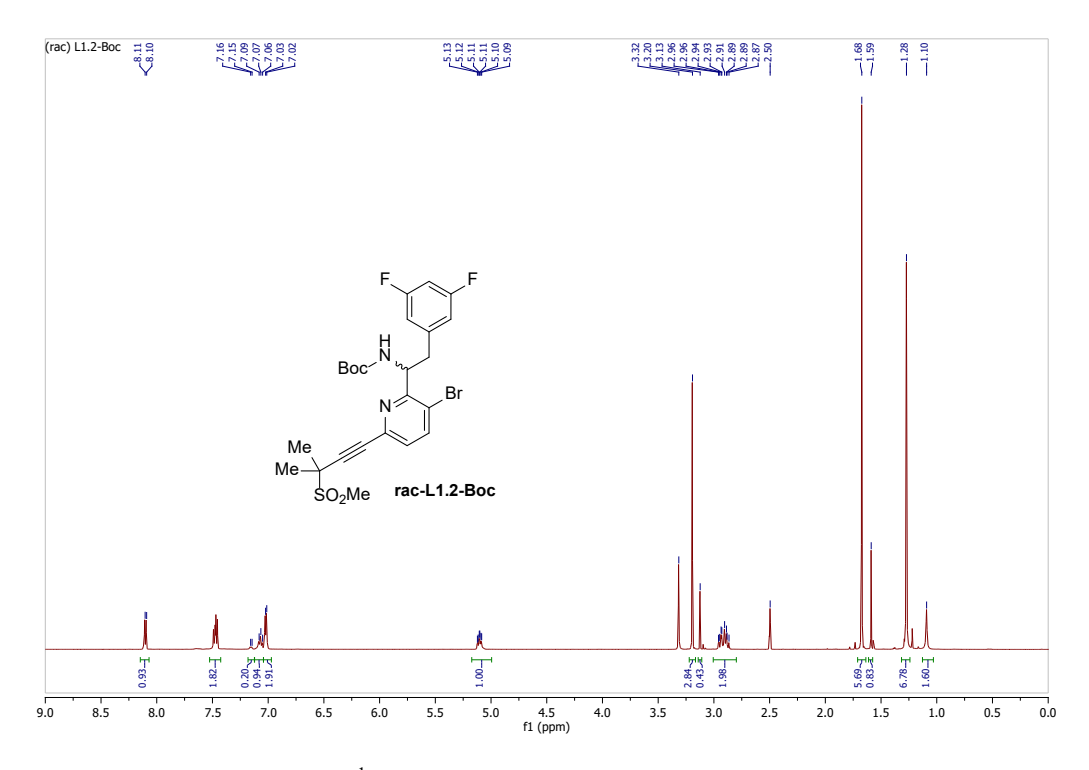


Figure 3.3.13. ¹H NMR (600 MHz, DMSO-*d*₆) of rac-**L1.2-Boc**.

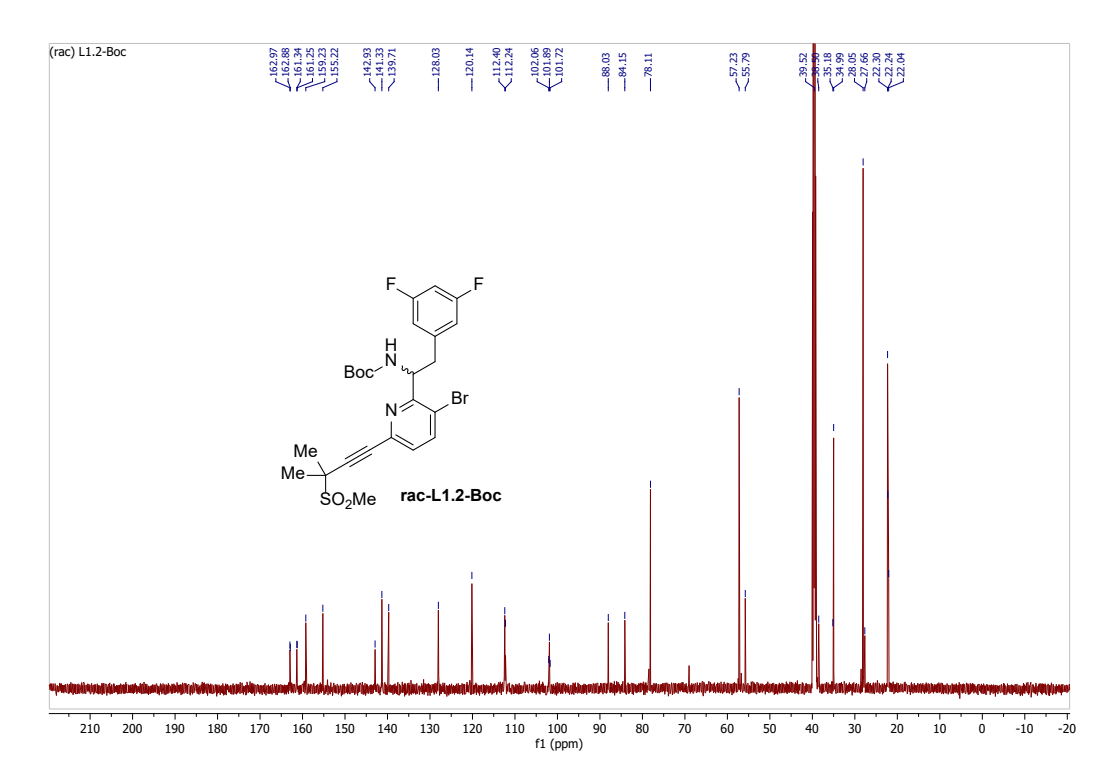


Figure 3.3.14. 13 C NMR (151 MHz, DMSO- d_6) of rac-**L1.2-Boc**.

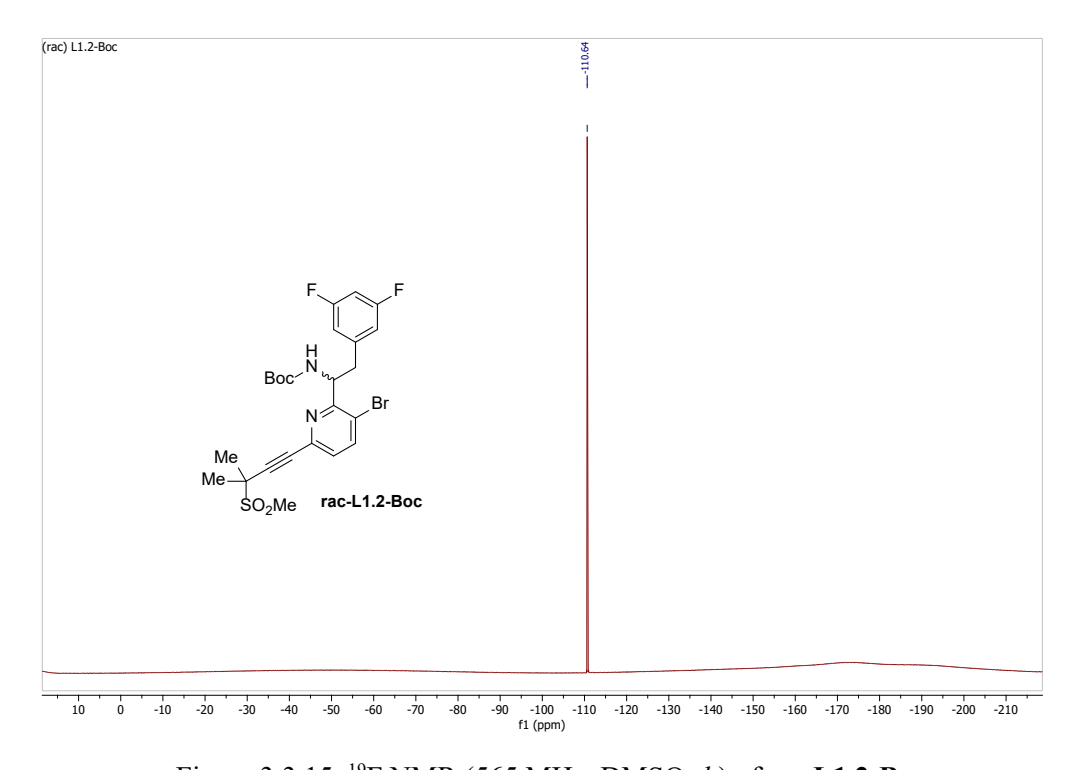


Figure 3.3.15. ¹⁹F NMR (565 MHz, DMSO-*d*₆) of rac-**L1.2-Boc.**

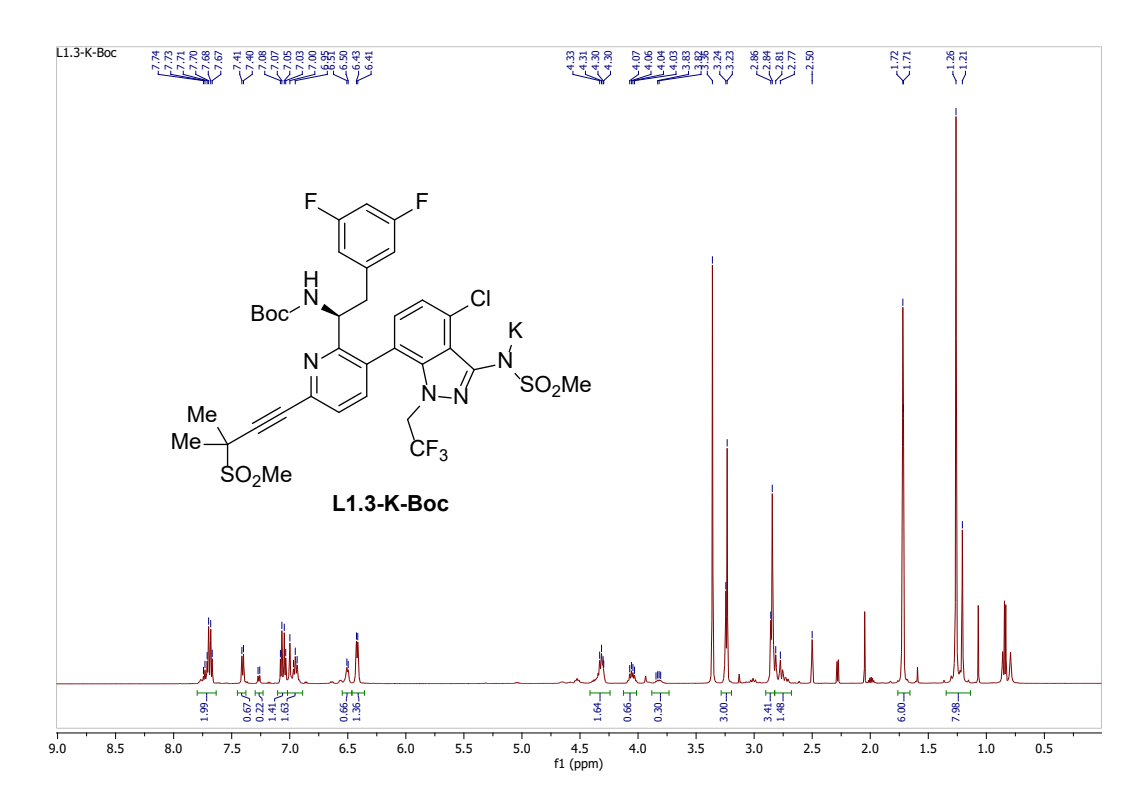


Figure 3.3.16. ¹H NMR (600 MHz, DMSO-*d*₆) of **L1.3-K-Boc**.

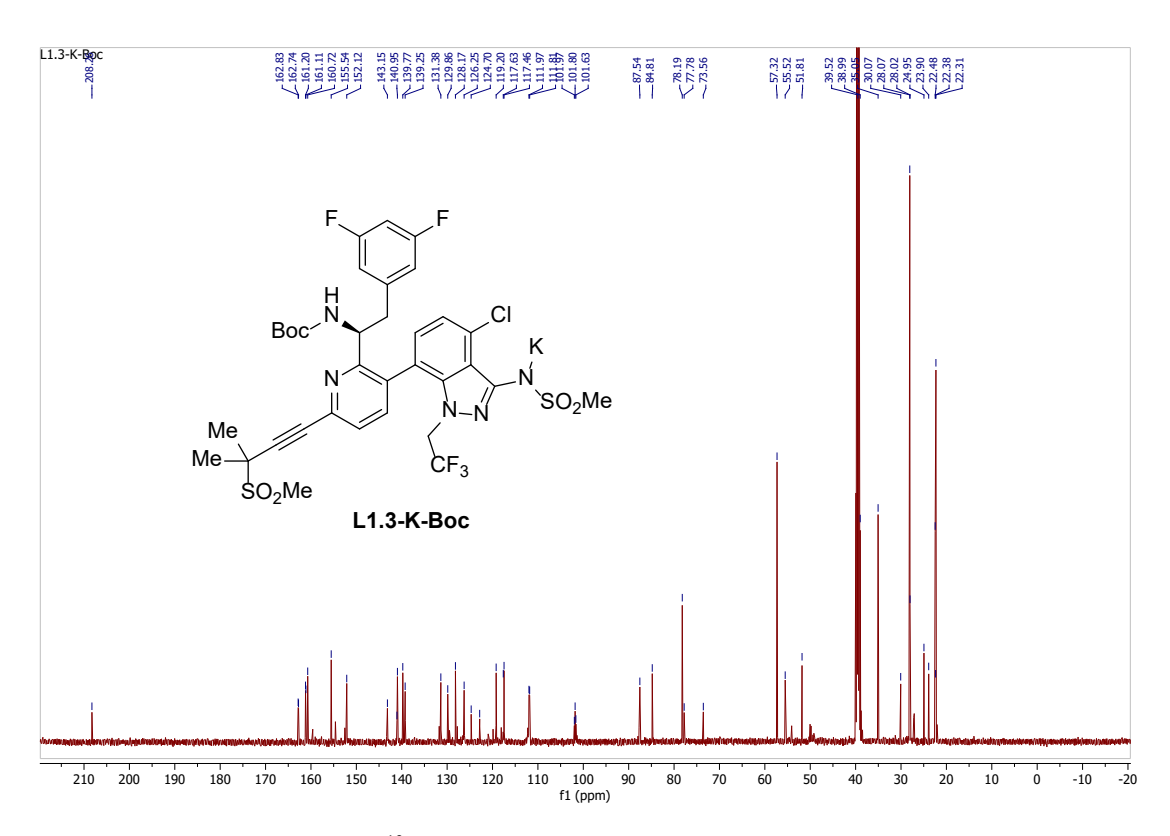


Figure 3.3.17. ¹³C NMR (600 MHz, DMSO-*d*₆) of **L1.3-K-Boc.**

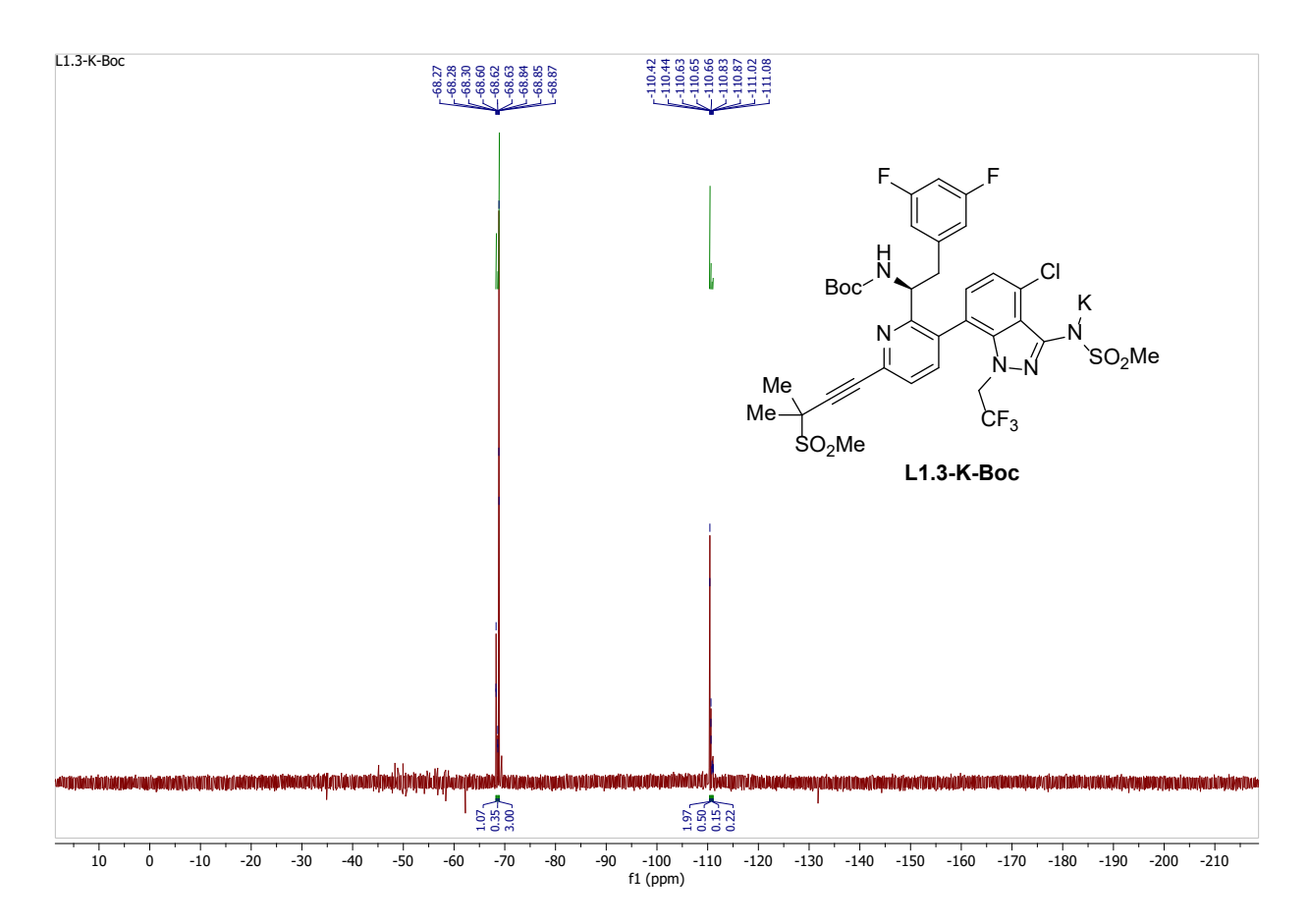


Figure 3.3.18. ¹⁹F NMR (565 MHz, DMSO-*d*₆) of **L1.3-K-Boc.**

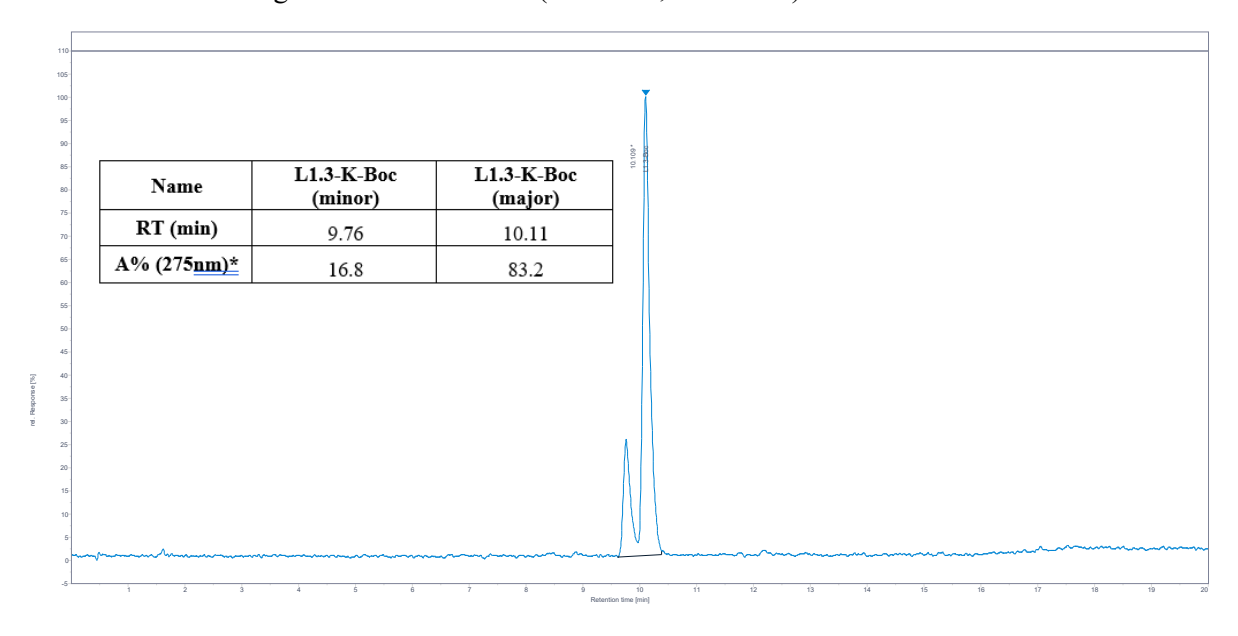


Figure 3.3.19. HPLC spectrum of L1.3-K-Boc and atropoisomeric ratio based on A% (275 nm).

GFN-002-S1-B1-15.95 (LC-DAD Wt% and Area % Analysis)

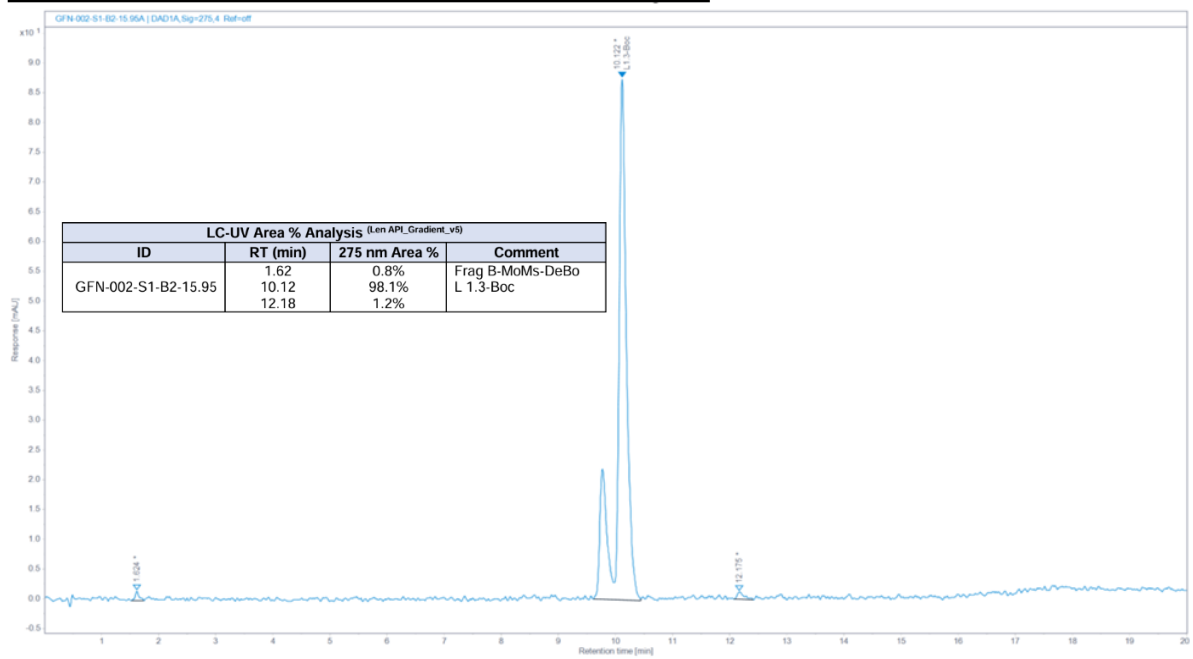
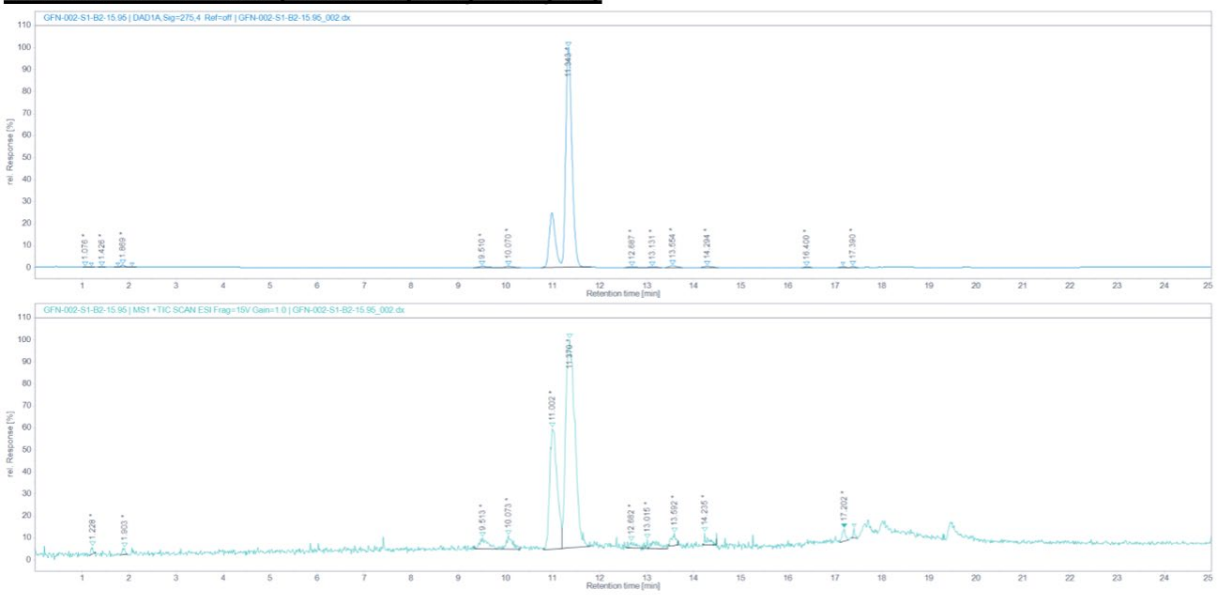


Figure 3.3.20. LC-UV area% analysis of L1.3-K-Boc (275 nm).

GFN-002-S1-B1-15.95 (LC-MS Impurity Analysis)



Impurity Analysis by LC-MS (LCMS A_LenAPI_MS)					
ID	RT (min)	275 nm Area %	m/z	Comment	
	1.08	0.01%	No Ionization		
	1.20	0.01%	308 (ESI+)		
	1.43	0.02%	No Ionization		
GFN-002-	1.77	0.03%	No Ionization		
S1-B2	1.87	0.44%	328 (M+H)	Frag B-MoMs-Debo	
15.95	2.07	0.01%	279 (ESI+)		
	9.51	0.42%	623 (M+H)	L1.2-Boc-DiFd	
	10.07	0.40%	770 (ESI+); 714 (M+H-Boc)		
	11.34	96.85%	804 (M+H)	L1.3-Boc	

Impurity Analysis by LC-MS (LCMS A_LenAPI_MS)					
ID	RT (min)	275 nm Area %	m/z	Comment	
	12.69	0.23%	1075 (ESI+)	Contains 2-3 Cl atoms	
	13.13	0.18%	1095 (ESI+)	Contains 1 Cl atom	
	13.55	0.66%	1095 (ESI+)	Contains 1 Cl atom	
	14.29	0.37%	1095 (ESI+)	Contains 1 Cl atom	
	16.40	0.10%	No Ionization		
	17.18	0.13%	725 (ESI+); 668 (M+H-Boc)	Contains 1 Cl atom	
	17.39	0.12%	995 (ESI+)	Contains 2 Cl atoms	

Figure 3.3.21. Impurity analysis of **L1.3-K-Boc** by LC-MS.

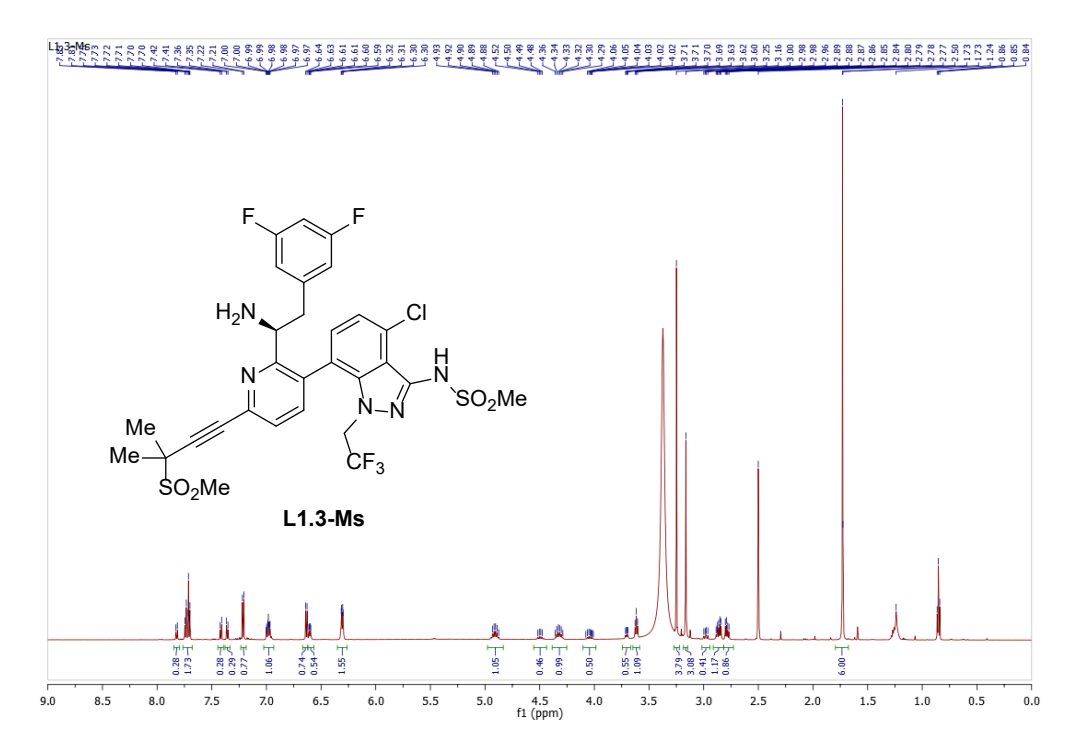


Figure 3.3.22. ¹H NMR (600 MHz, DMSO-*d*₆) of **L1.3-Ms**.

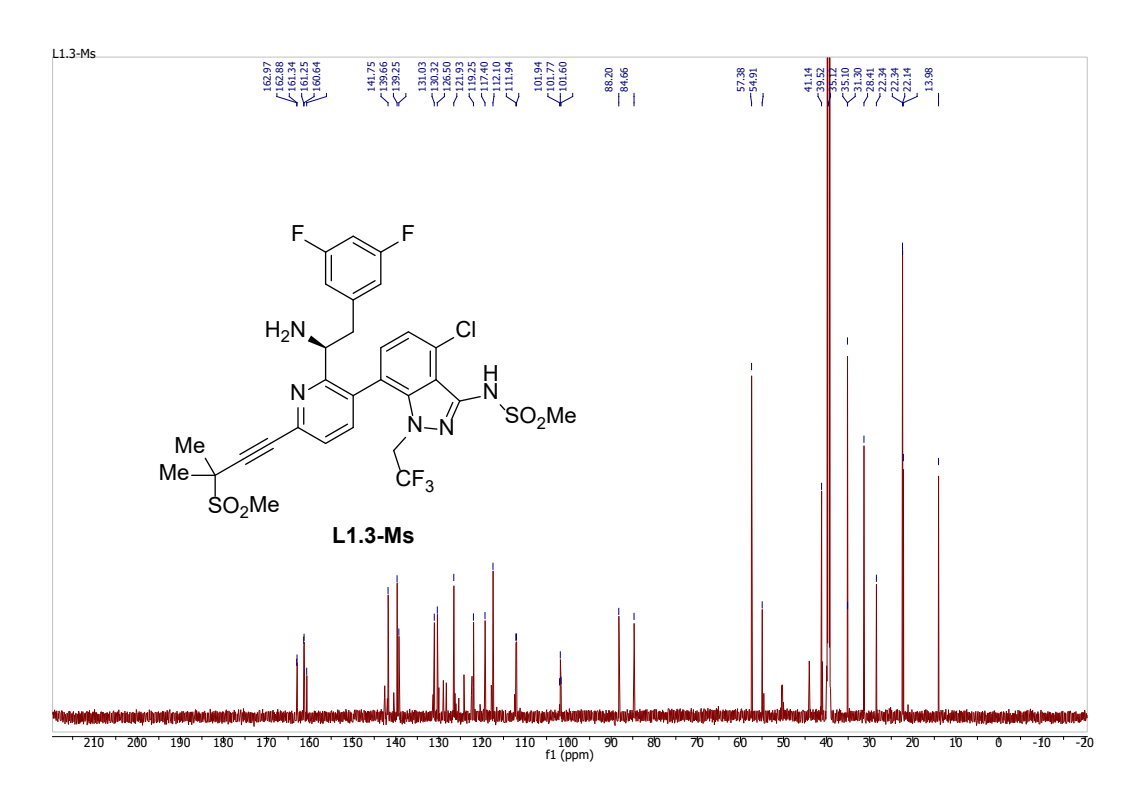


Figure 3.3.23. 13 C NMR (600 MHz, DMSO- d_6) of **L1.3-Ms.**

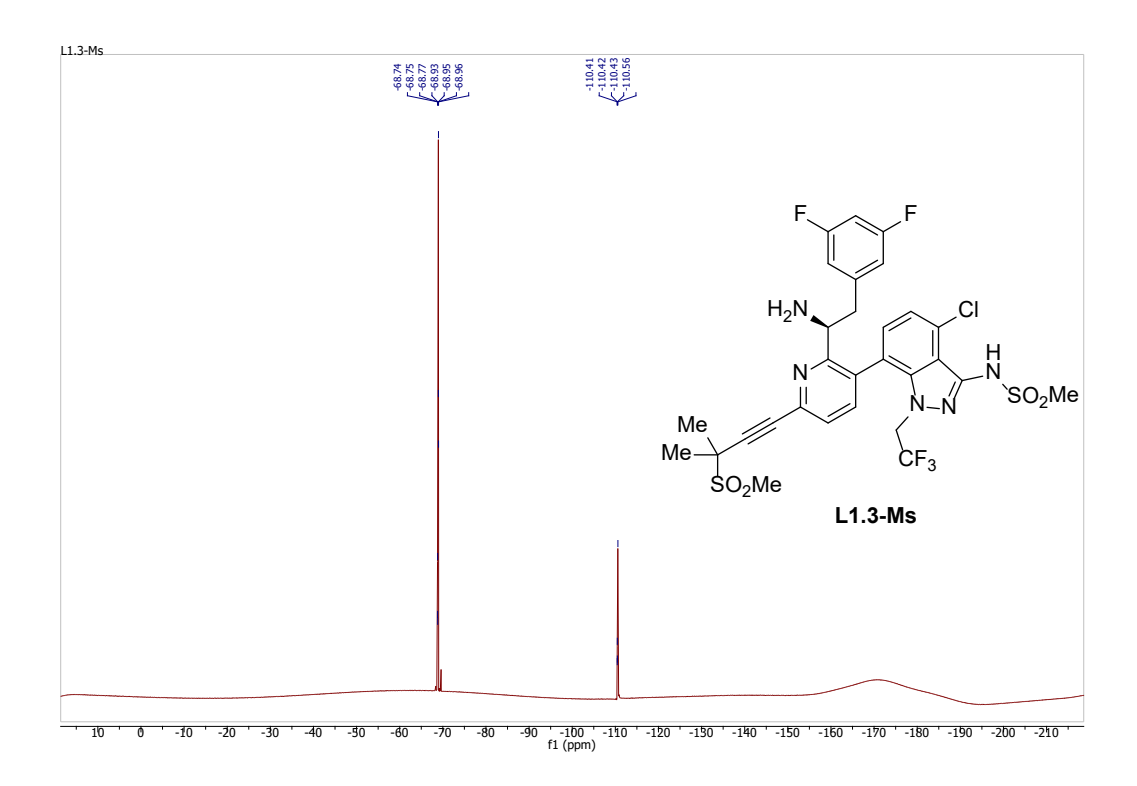


Figure 3.3.24. ¹⁹F NMR (565 MHz, DMSO-*d*₆) of **L1.3-Ms**.

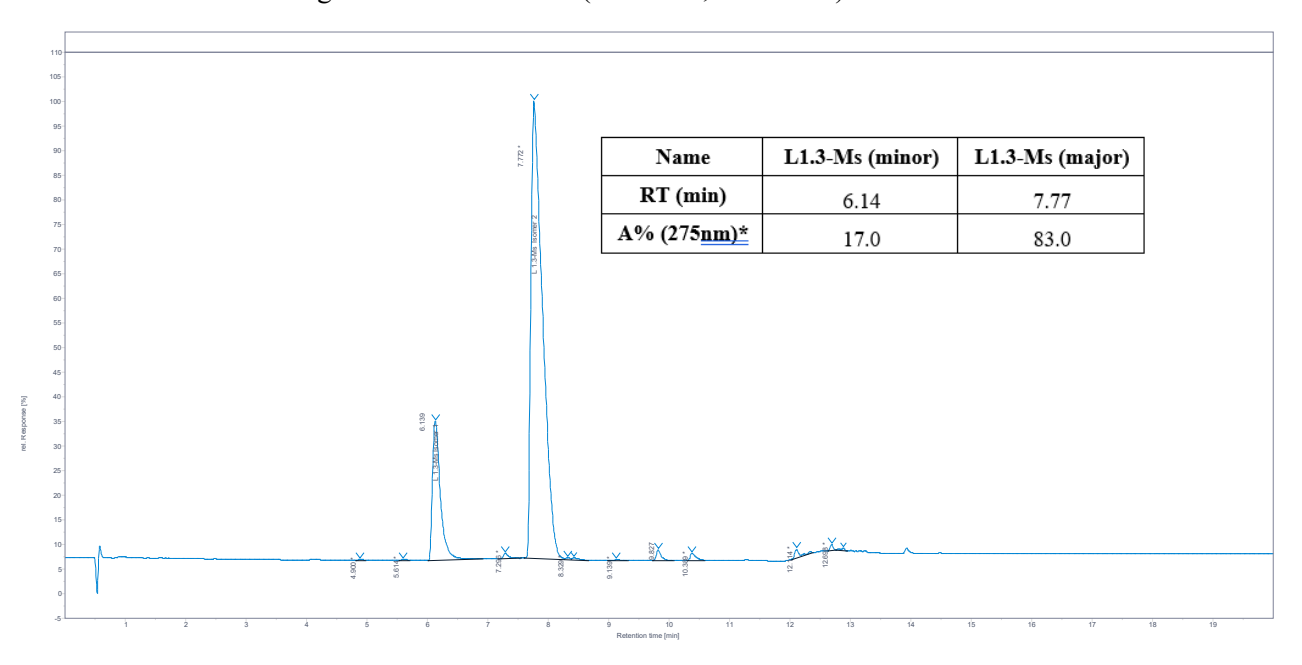
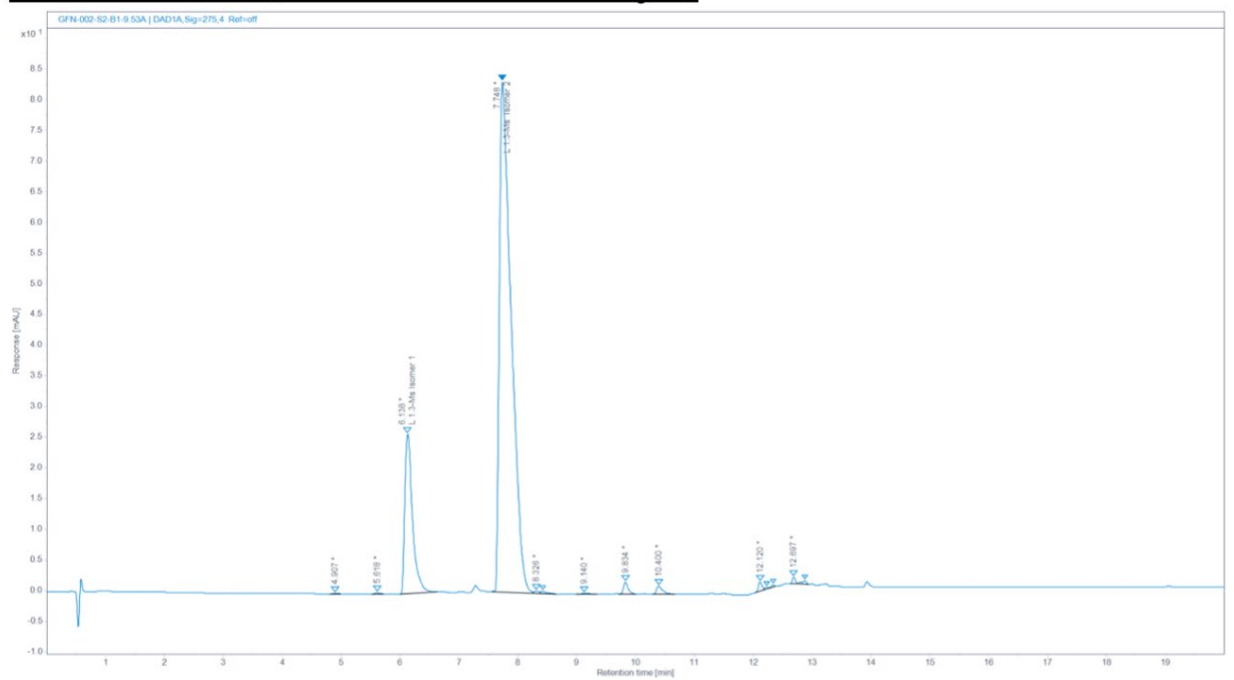


Figure 3.3.25. HPLC spectrum of L1.3-Ms and atropoisomeric ratio based on A% (275 nm).

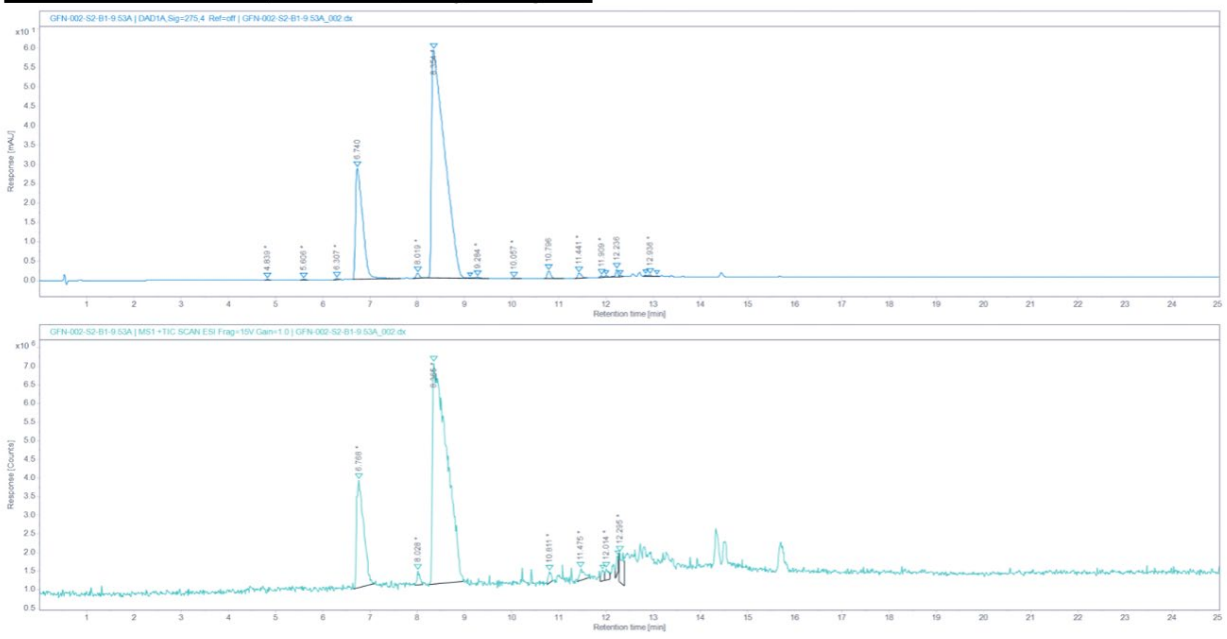
GFN-002-S2-B1-9.53 (LC-UV Wt% and Area % Analysis)



LC-UV Area % Analysis (LCUV_L13Ms)				
ID	RT (min)	275 nm Area %	Comment	
	4.91	0.04%		
	5.62	0.1%		
	6.14	16.5%	L 1.3-Ms Isomer 1	
	7.75	80.5%	L 1.3-Ms Isomer 2	
	8.33	0.1%		
	8.43	0.2%		
GFN-002-S2-B1-9.53	9.14	0.1%		
GFN-002-32-61-9.53	9.83	0.7%		
	10.4	0.7%		
	12.12	0.5%		
	12.24	0.1%		
	12.34	0.1%		
	12.7	0.2%		
	12.89	0.2%		

Figure 3.3.26. LC-UV (275 nm) A% analysis of **L1.3-Ms**.

GFN-002-S2-B1-9.53 (LC-MS Impurity Analysis)



LC-MS Impurity Analysis (LCMS A_LenAPI_MS)					
ID	RT (min)	275 nm Area %	m/z	Comment	
	4.84	0.03%	No Ionization		
	5.61	0.04%	No Ionization		
	6.31	0.1%	No Ionization		
	6.74	20.3%	704 (M+H)	L 1.3-Ms Minor Isomer	
	8.02	0.4%	670 (ESI+)		
	8.35	76.6%	704 (M+H)	L 1.3-Ms Major Isomer	
	9.13	0.2%	No Ionization		
	9.28	0.2%	No Ionization		
GFN-002-S2-B1-	10.06	0.1%	No Ionization		
9.53	10.80	0.8%	995 (ESI+)	Contains 2 Cl atoms	
9.55	11.44	0.6%	995 (ESI+)	Contains 2 Cl atoms	
		Co-elutes	624 (ESI+)	Contains 2 Cl atoms	
	11.91	0.1%	732 (ESI+)		
	12.01	0.1%	No Ionization		
	12.24	0.4%	732 (ESI+)		
	12.31	0.1%	No Ionization		
	12.84	0.1%	No Ionization		
	12.94	0.1%	No Ionization		
	13.09	0.04%	No Ionization		

Figure 3.3.27. Impurity analysis of **L1.3-Ms** by LC-MS.

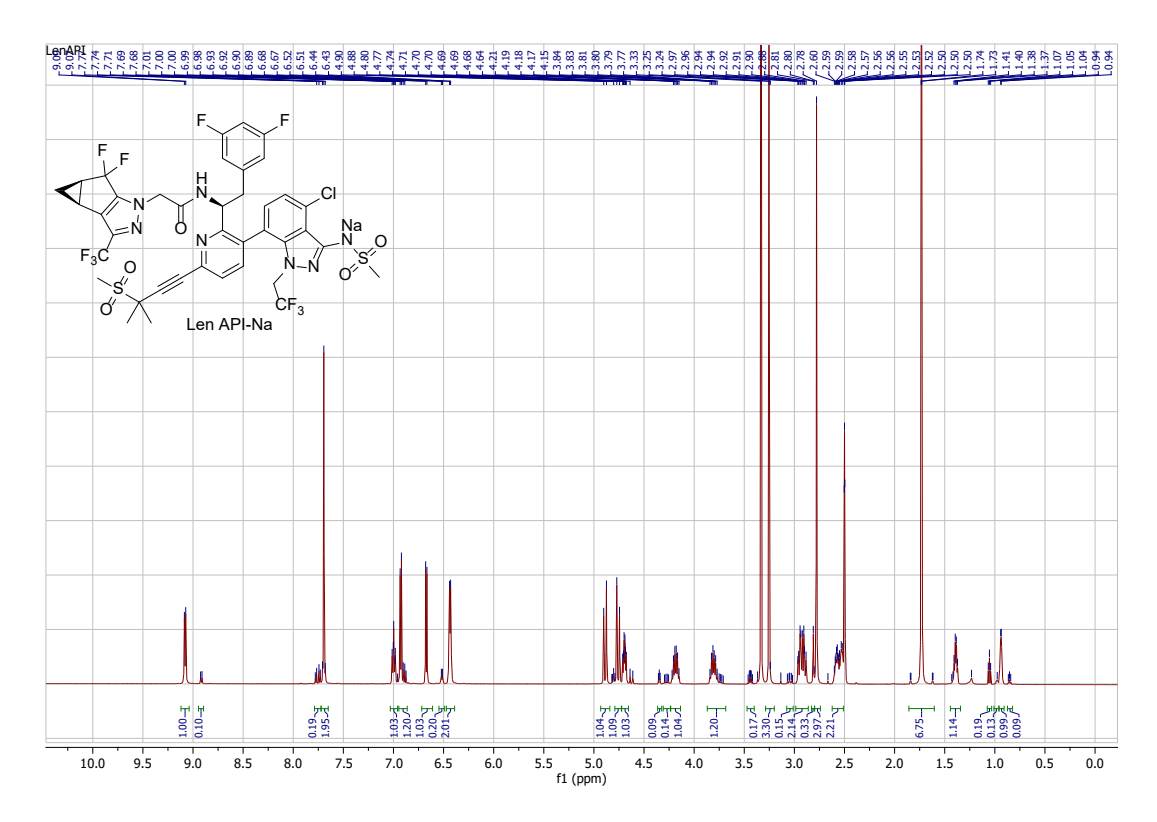


Figure 3.3.28. 1 H NMR (600 MHz, DMSO- d_6) of **Len-API**.

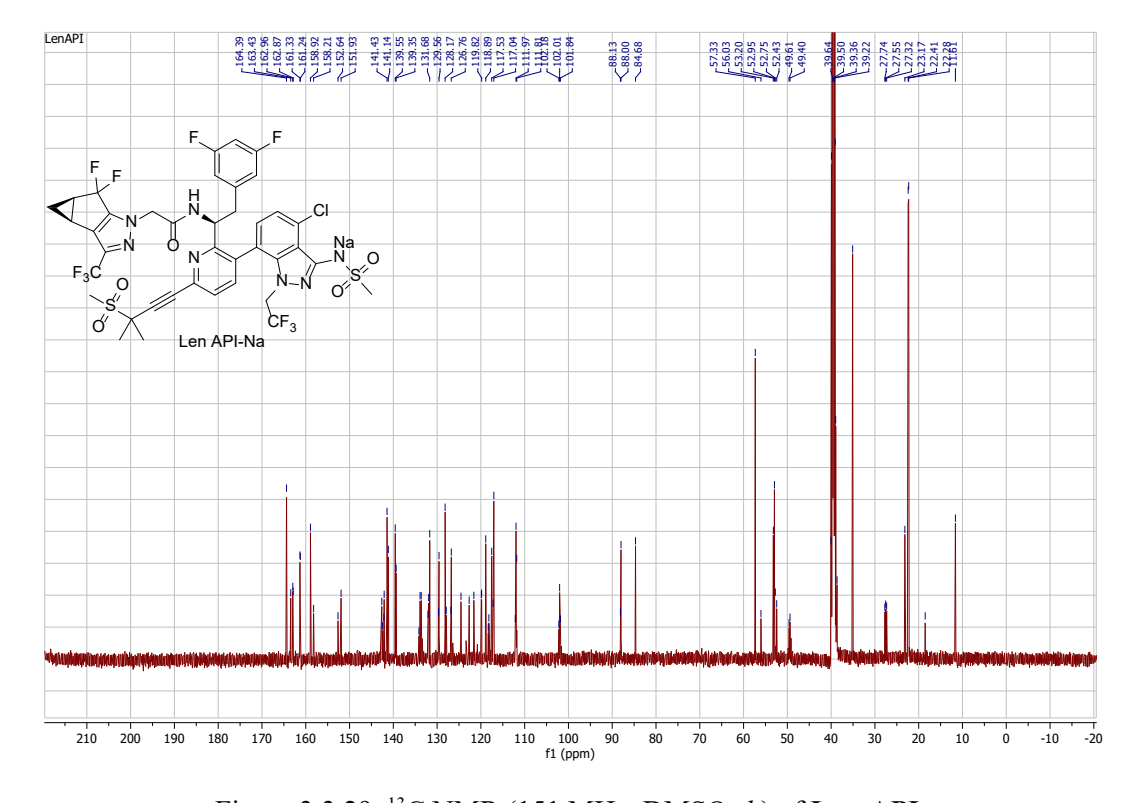


Figure 3.3.29. 13 C NMR (151 MHz, DMSO- d_6) of Len-API.

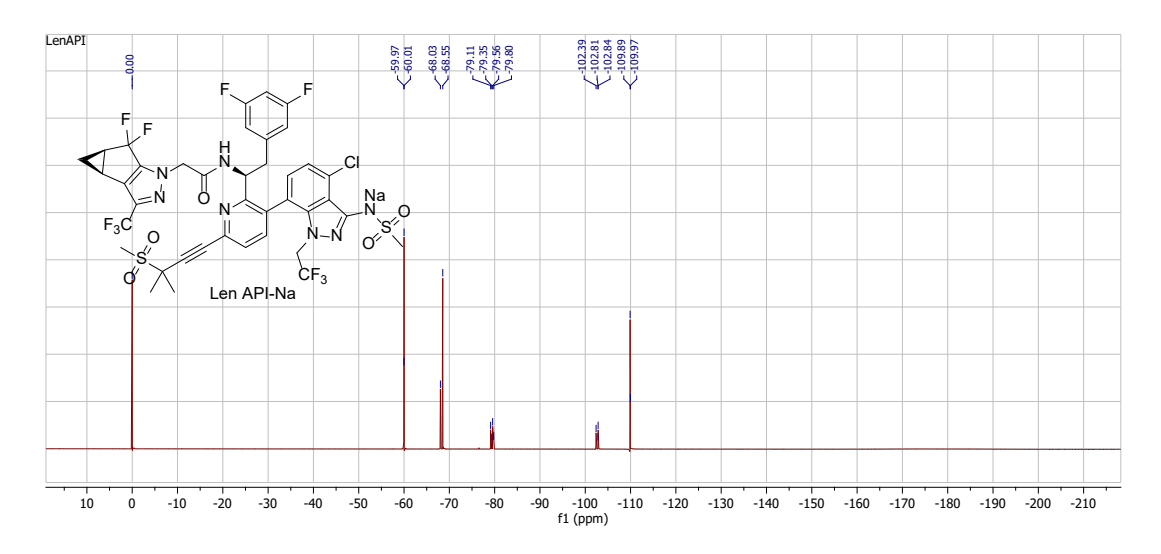


Figure 3.3.30. ¹⁹F NMR (565 MHz, DMSO-*d*₆) of **Len-API**.

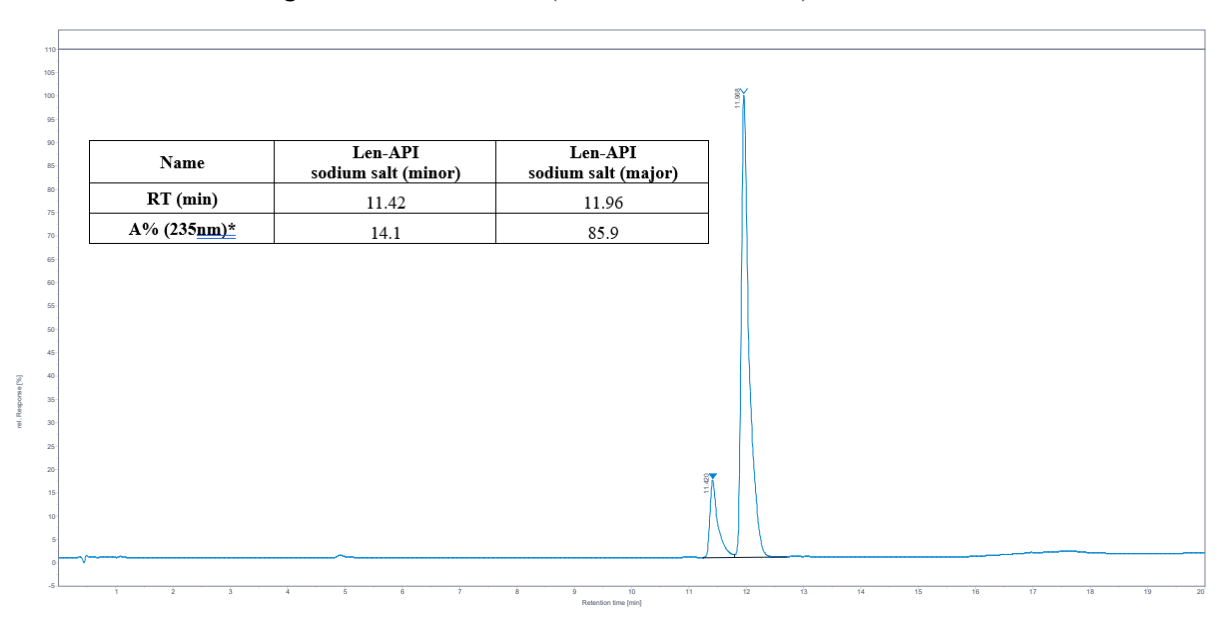
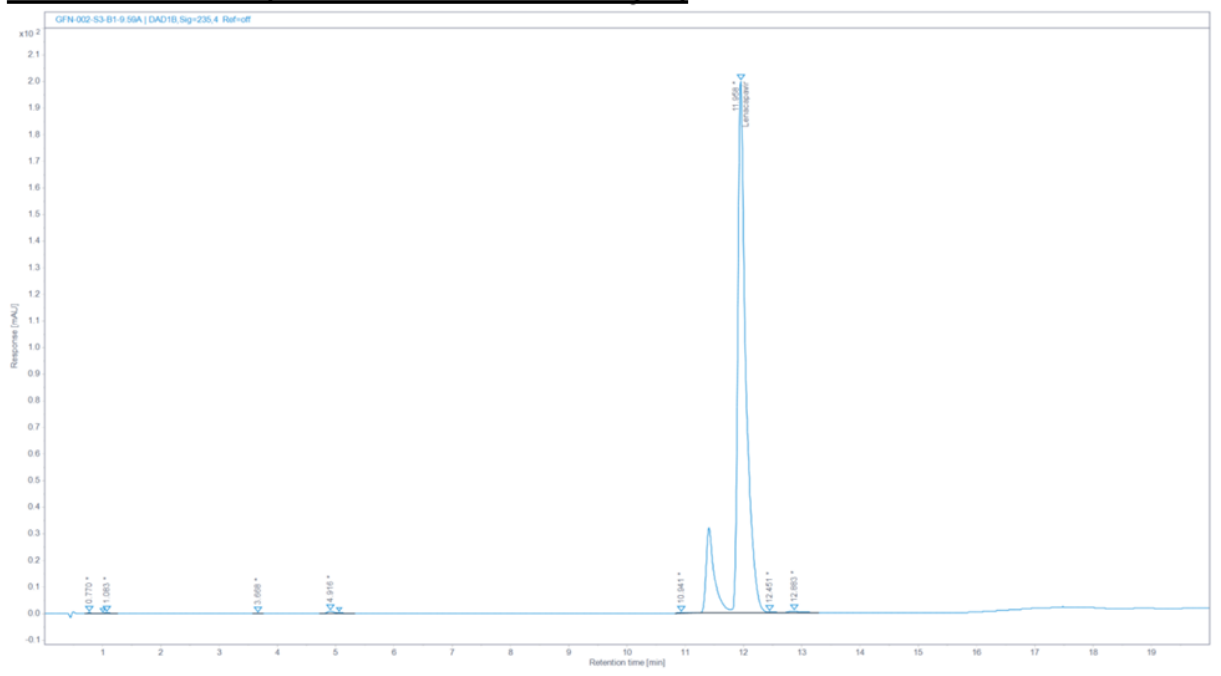


Figure 3.3.31. HPLC spectrum of **Len-API (sodium salt)** and atropoisomeric ratio based on A% (235 nm).

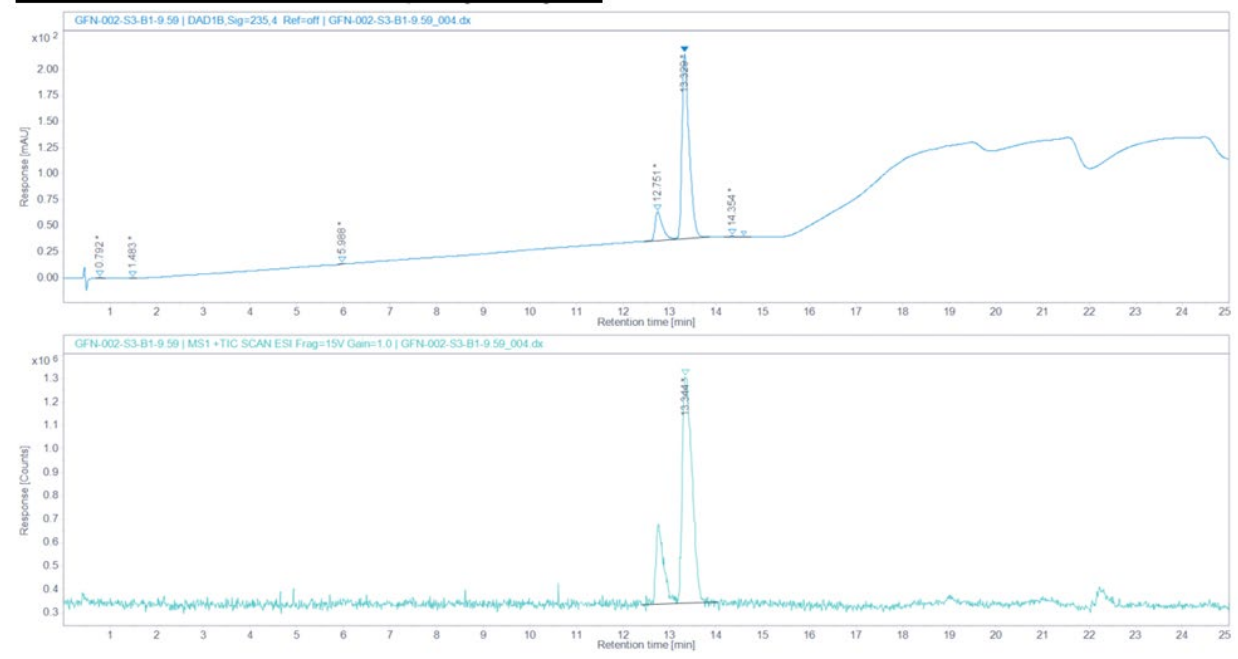
GFN-002-S3-B0-9.59 (LC-UV Wt% and Area % Analysis)



LC-UV Area % Analysis (LCUV_Len API_Gradient)				
ID	RT (min)	275nm Area %	Comment	
	0.77	0.1%	L 1.3-Ms Isomer	
	1.01	0.01%		
	1.08	0.1%	L 1.3-Ms Isomer	
	3.67	0.02%		
GFN-002-S3-B1-9.59	4.92	0.4%		
GFN-002-53-B1-9.59	5.06	0.2%	L1.3-Ms-Ac Isomer	
	10.94	0.1%		
	11.96	98.8%	Len API	
	12.45	0.1%		
	12.88	0.4%		

Figure 3.3.32. LC-UV (235 nm) A% analysis of Len-API.

GFN-002-S3-B0-9.59 (LC-MS Impurity Analysis)



Impurity Analysis by LC-MS (LCMS A_LenAPI_MS)					
ID	RT (min)	235 nm Area %	m/z	Comment	
GFN-002-S3- B1-9.59	0.79	0.2%	No Ionization		
	1.48	0.1%	No Ionization		
	5.99	0.2%	No Ionization		
	12.75	13.7%	968 (M+H)	Len API Isomer	
	13.33	85.6%	968 (M+H)	Len API Isomer	
	14.35	0.3%	No Ionization		
	14.6	0.1%	No Ionization		

Figure 3.3.33. Impurity analysis of **L1.3-Ms** by LC-MS.

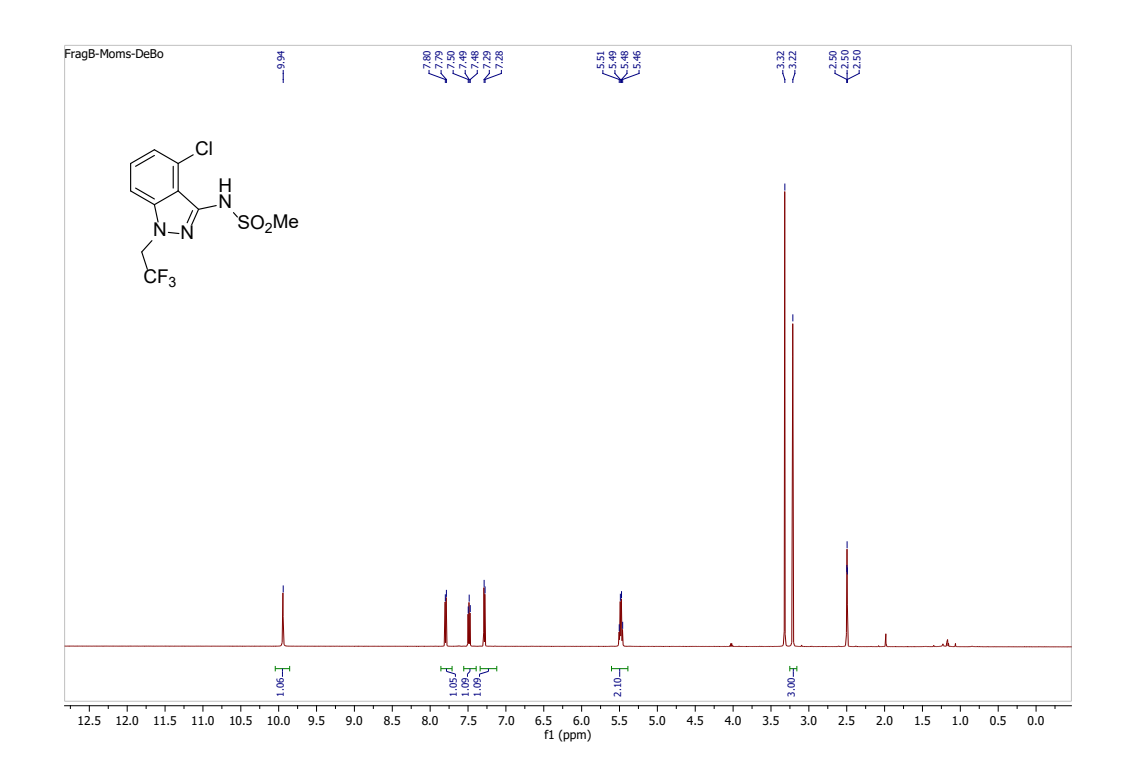


Figure 3.3.34. ¹HNMR (600MHz, DMSO-d₆) of Frag B-DiMs-DeBo.

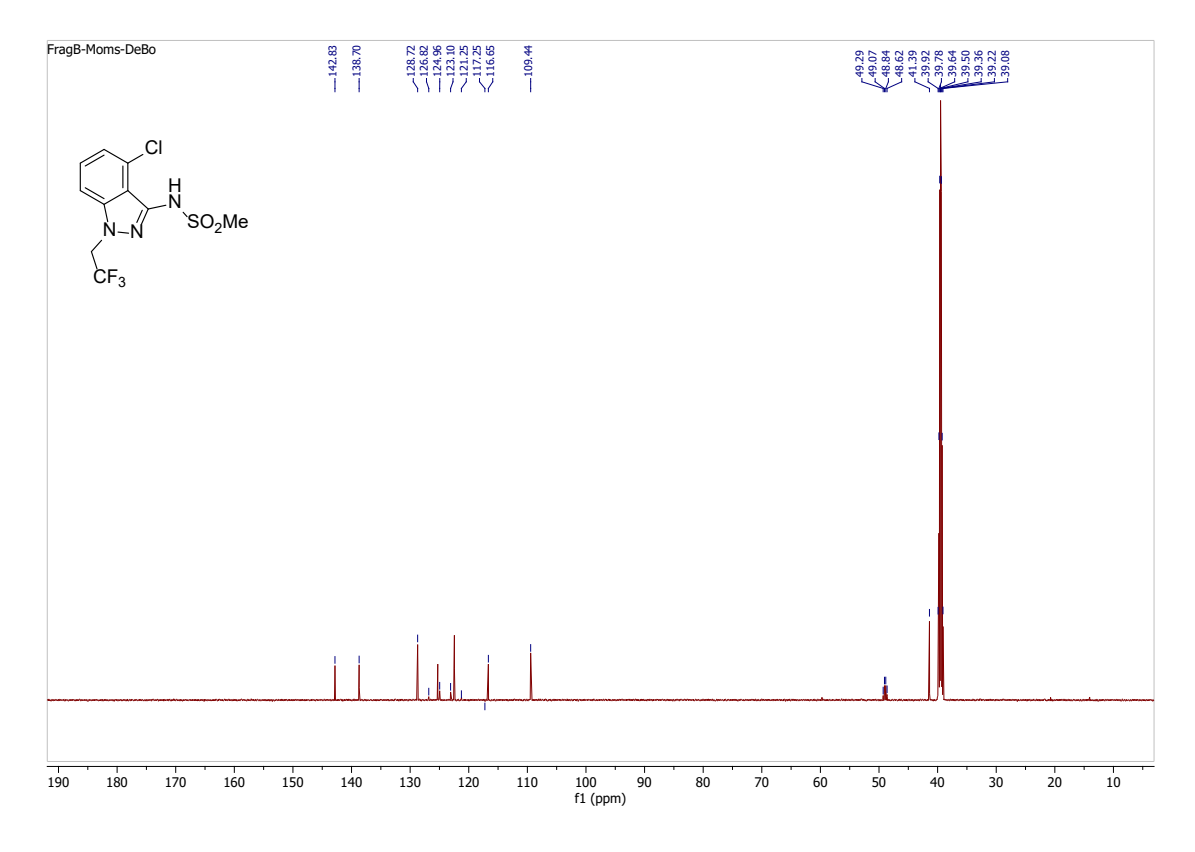


Figure 3.3.35. ¹³CNMR (151MHz, DMSO-d₆) of Frag B-DiMs-DeBo.

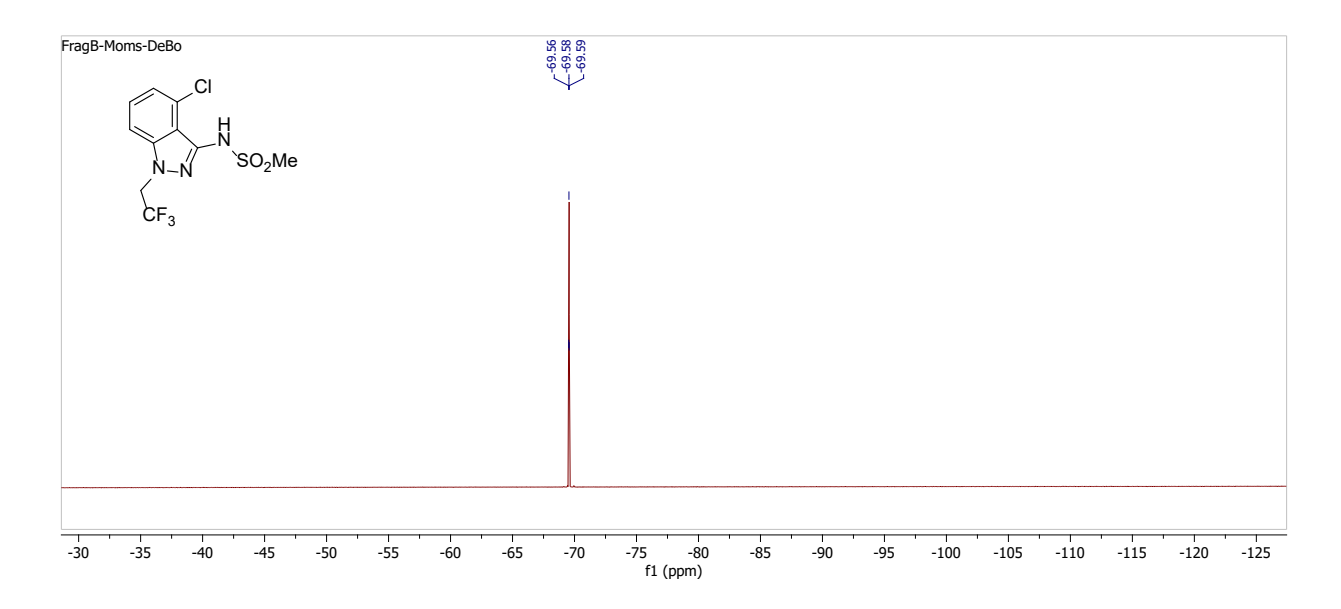


Figure 3.3.36. ¹⁹F (565MHz, DMSO-d₆) of **Frag B-DiMs-DeBo**.

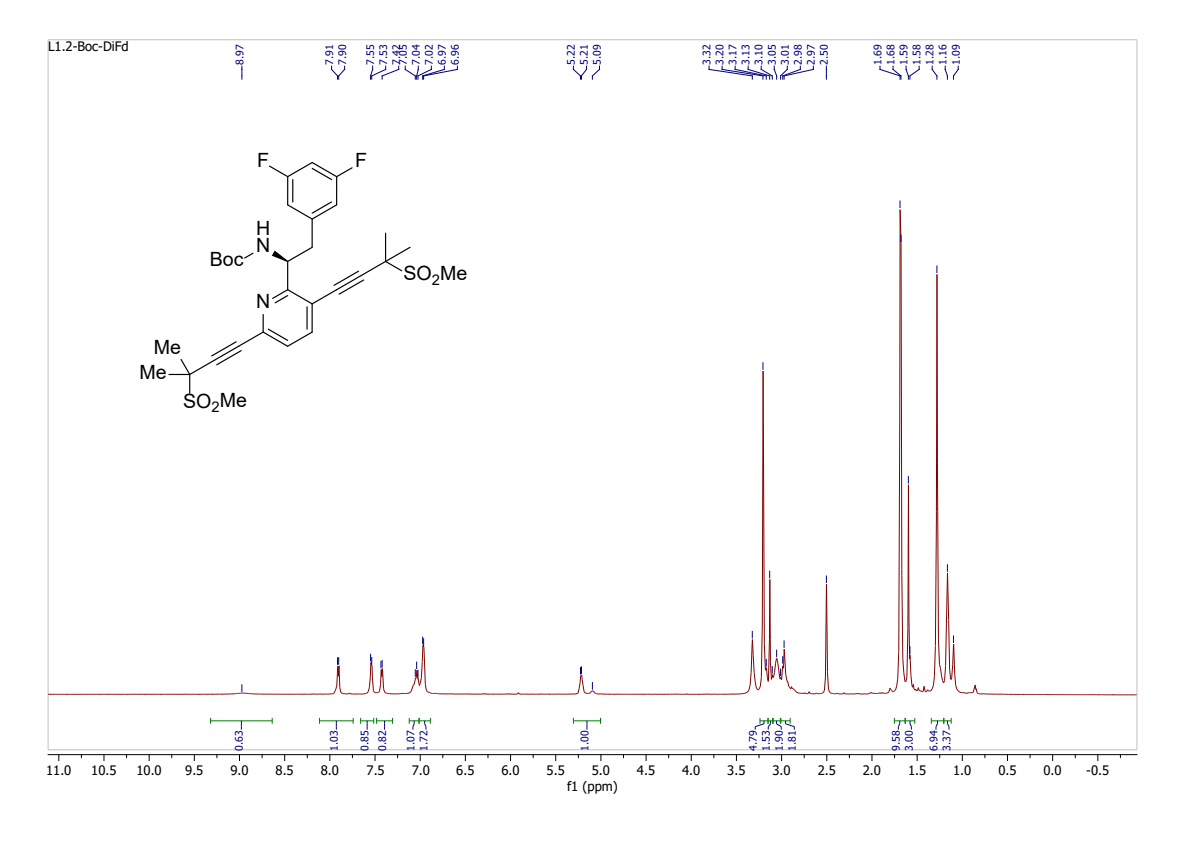


Figure 3.3.37. ¹H (600MHz, DMSO-d₆) of L1.2-Boc-DiFd.

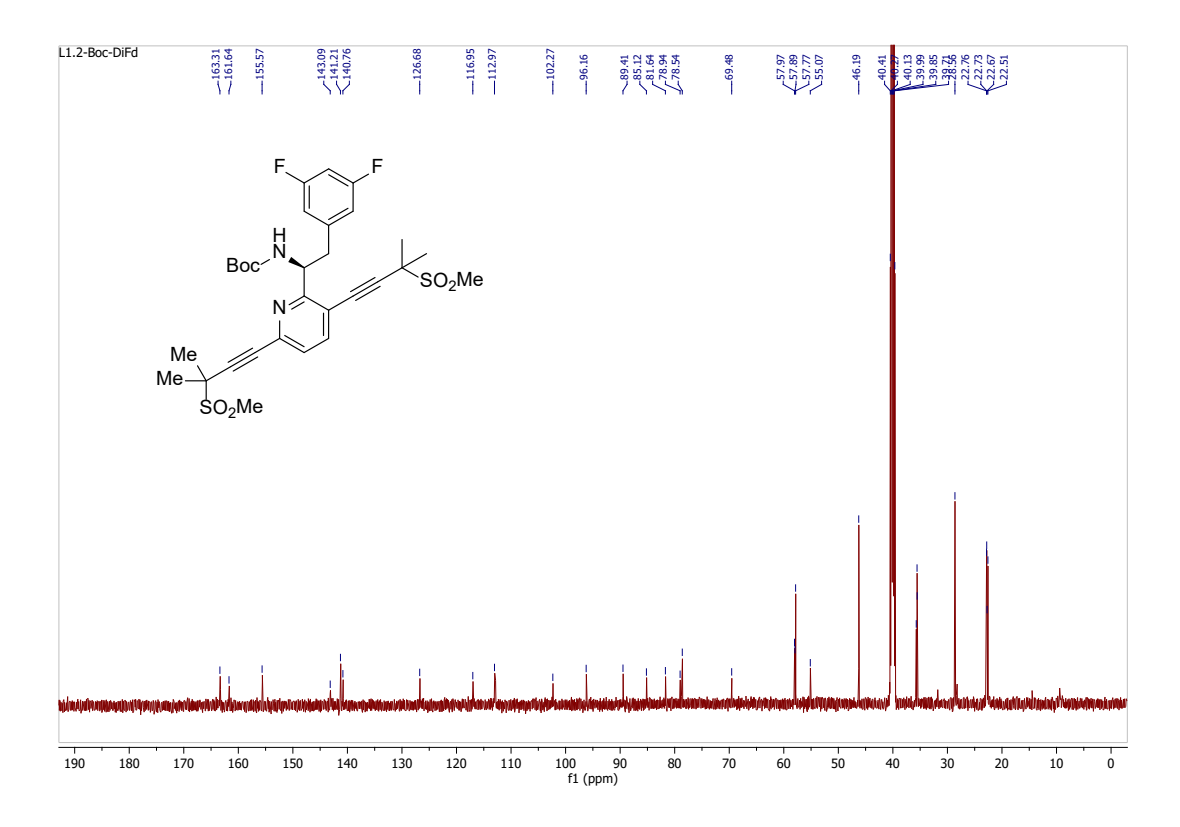


Figure 3.3.38. ¹³C (151MHz, DMSO-d₆) of L1.2-Boc-DiFd.

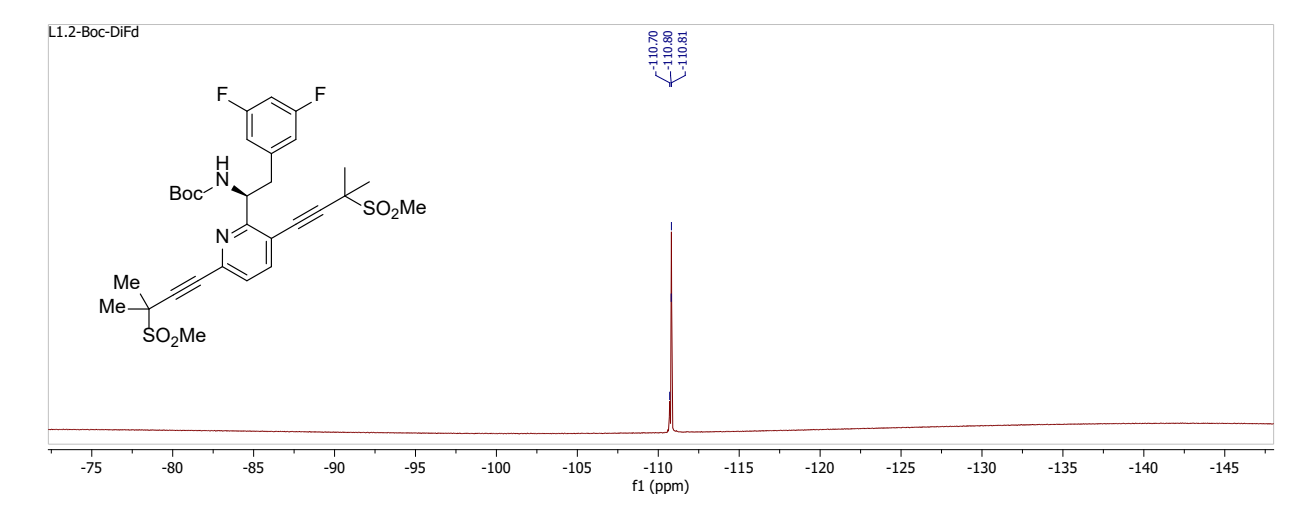


Figure 3.3.39. ¹⁹F (565MHz, DMSO-d₆) of L1.2-Boc-DiFd.

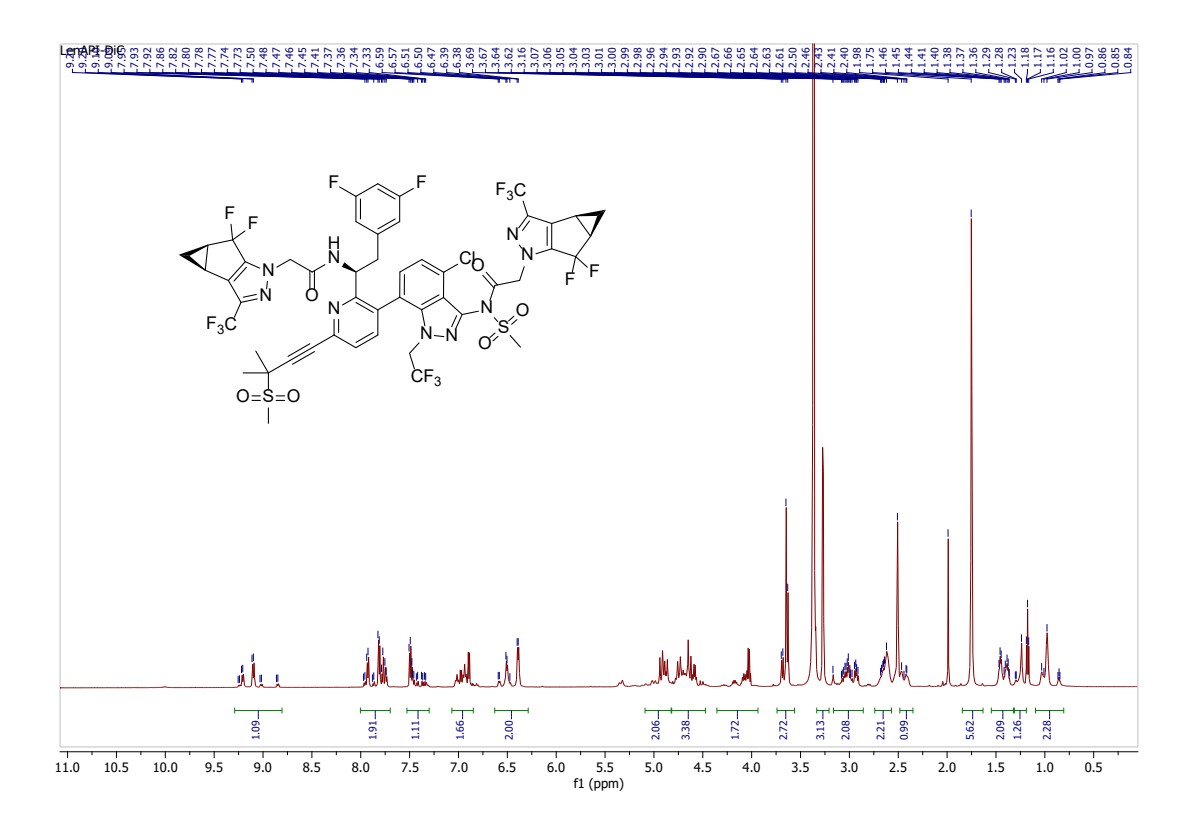


Figure 3.3.40. ¹H NMR (600MHz, DMSO-d₆) of Len API-DiC.

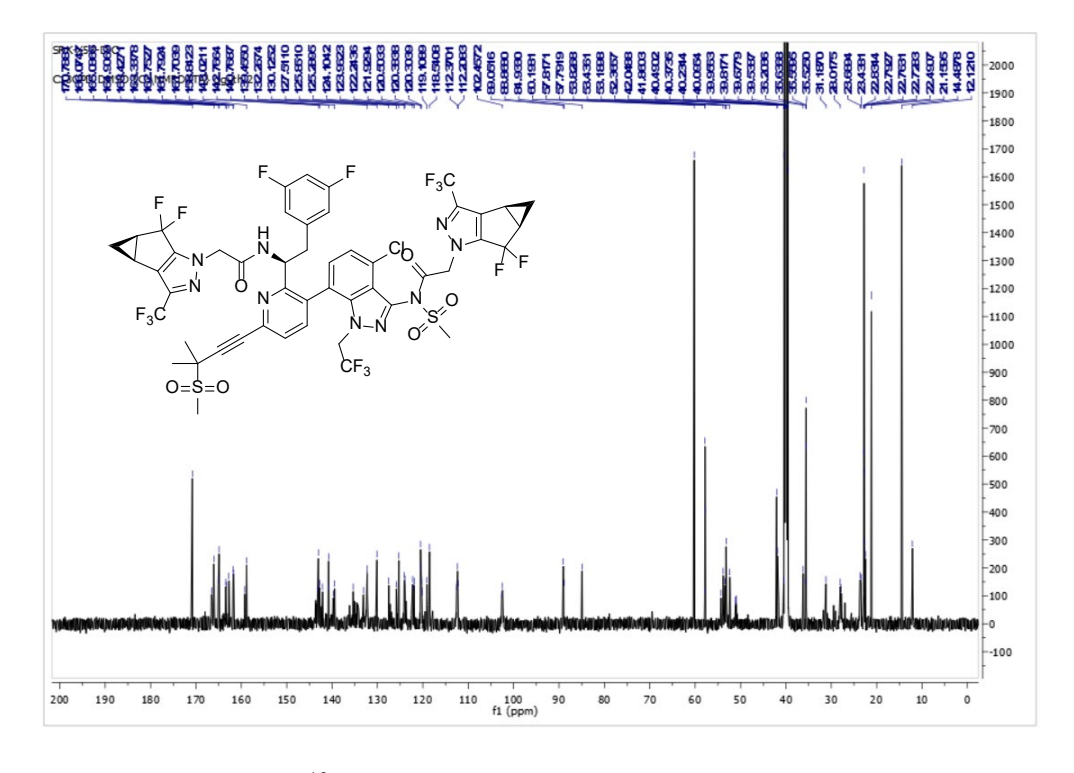


Figure 3.3.41. ¹³C NMR (151MHz, DMSO-d₆) of Len API-DiC.

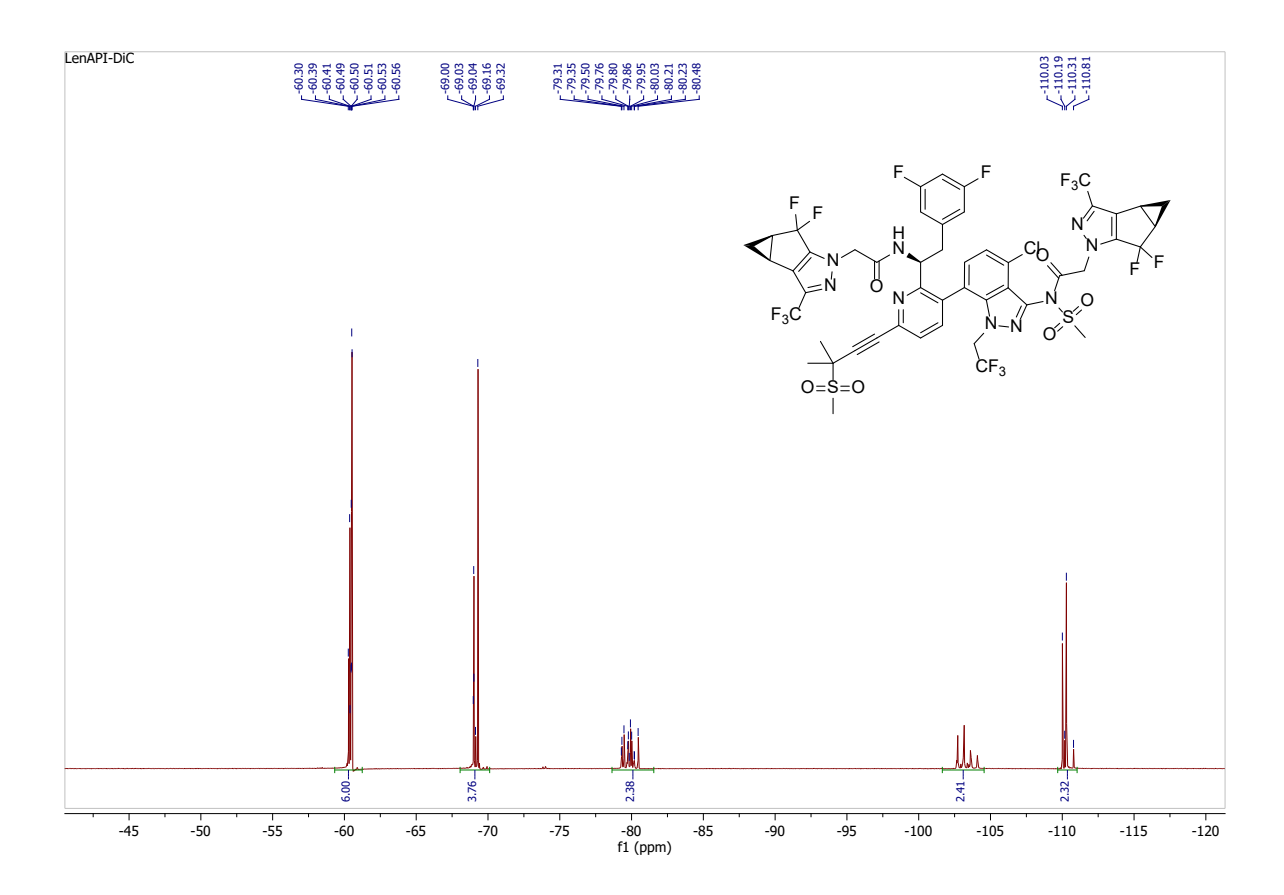


Figure 3.3.42. ¹⁹F NMR (565MHz, DMSO-d₆) of Len-API-DiC.

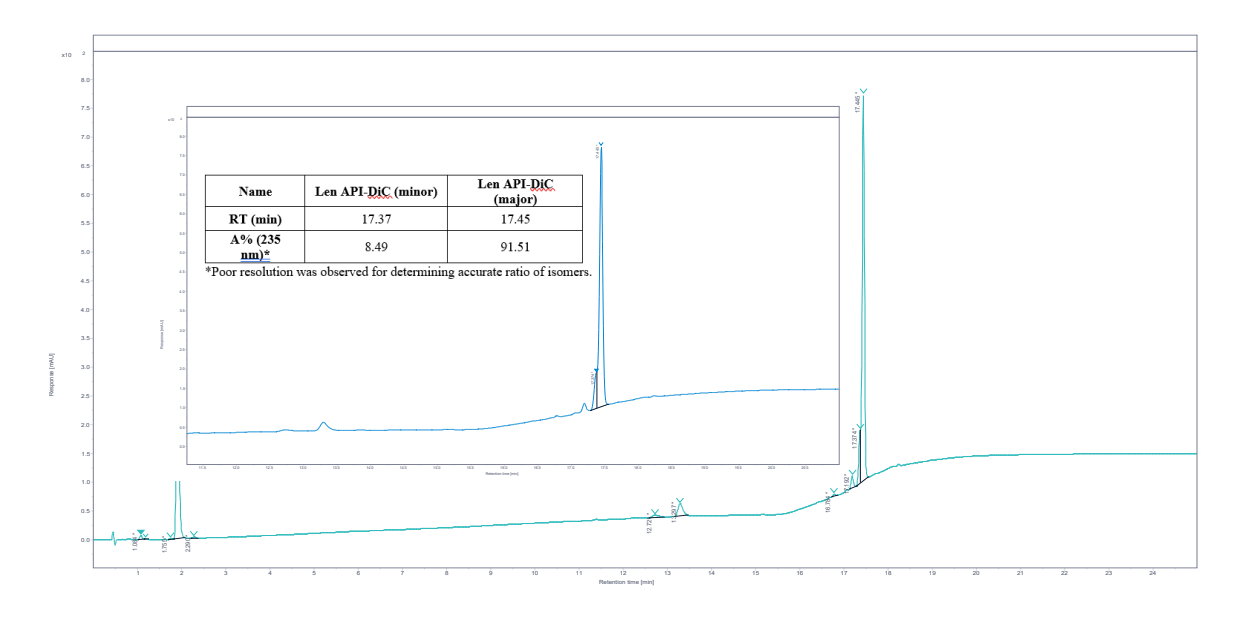


Figure 3.3.43. HPLC spectrum of **Len-API-DiC** and atropoisomeric ratio based on A% (235 nm).

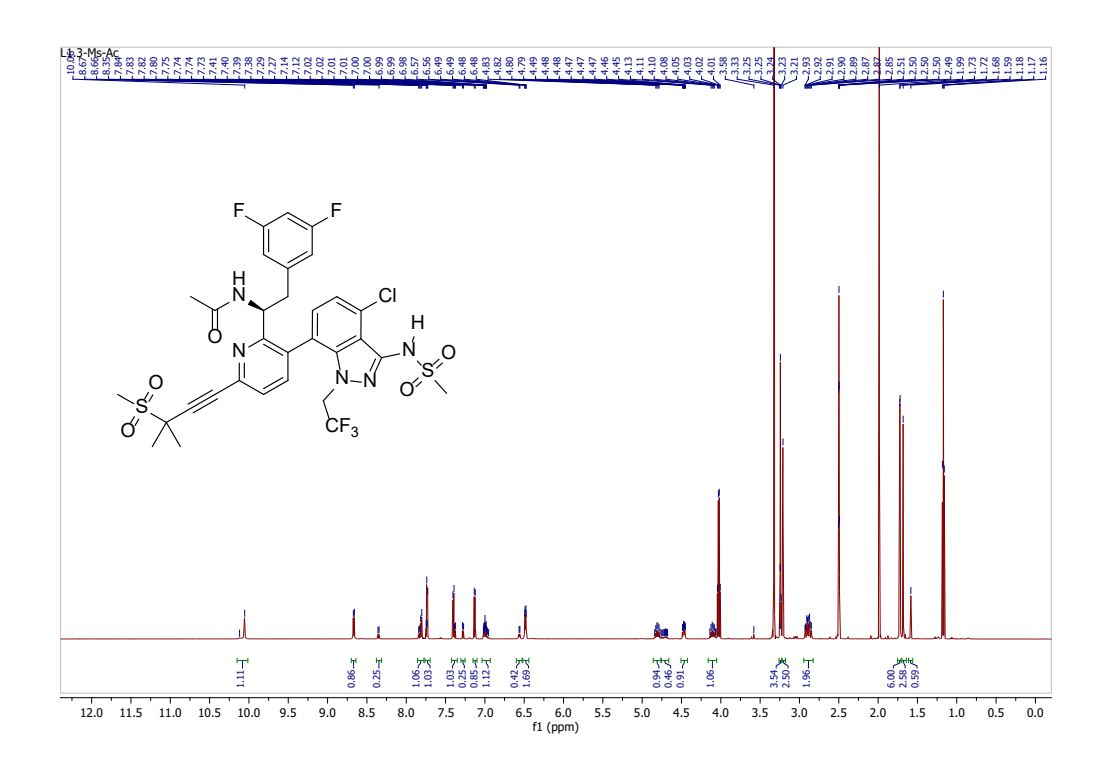


Figure 3.3.44. ¹H NMR (600 MHz, DMSO- d_6) of L1.3-Ms-Ac.

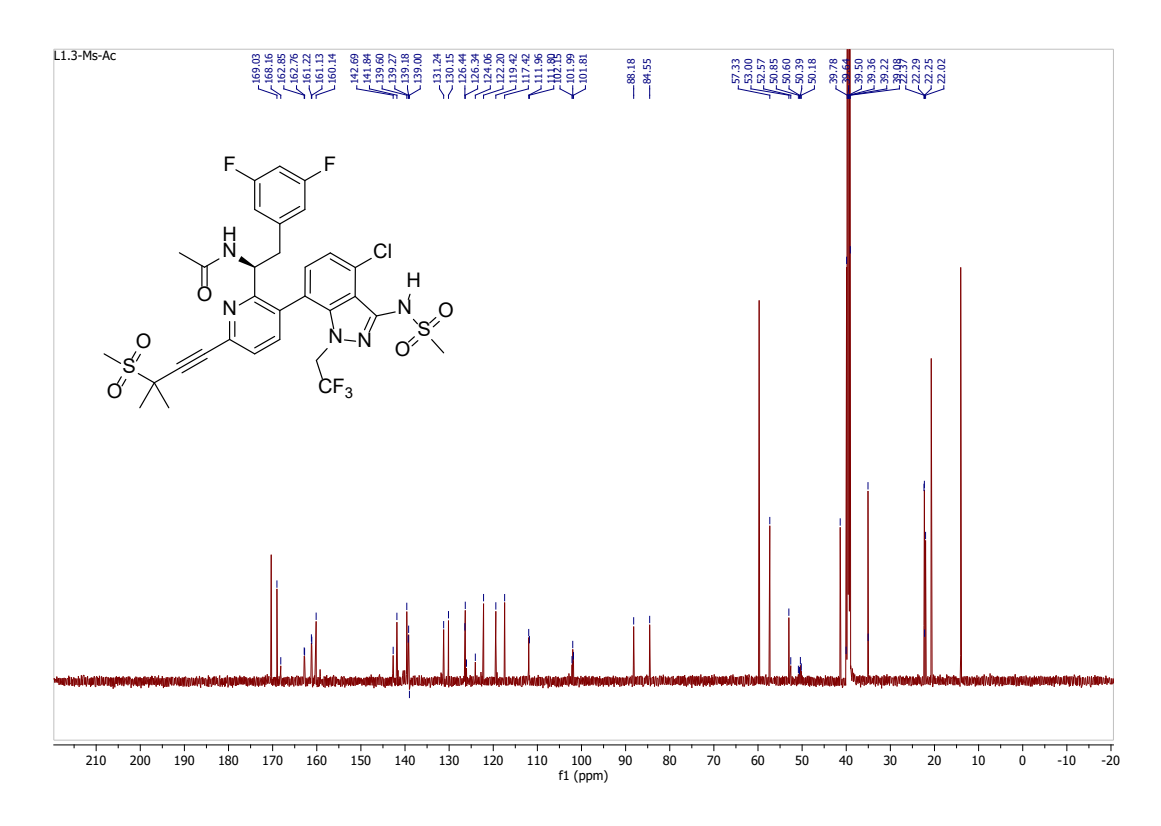


Figure 3.3.45. 13 C NMR (151 MHz, DMSO- d_6) of **L1.3-Ms-Ac.**

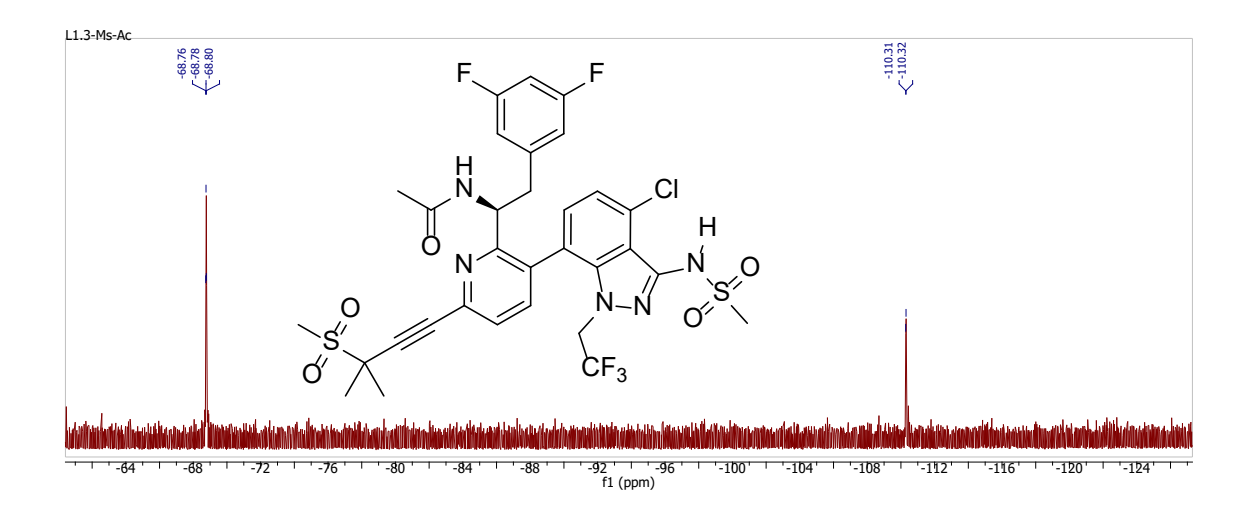


Figure 3.3.46. 19 F NMR (565 MHz, DMSO- d_6) of **L1.3-Ms-Ac.**

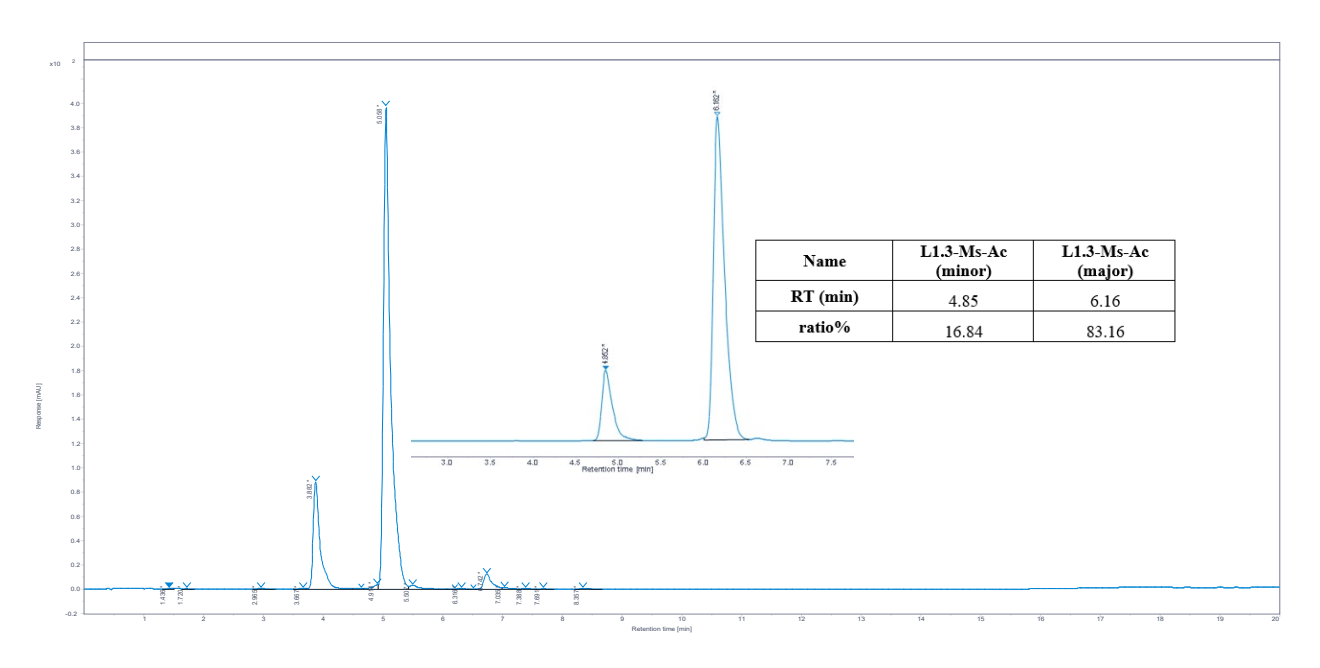


Figure 3.3.47. HPLC spectrum of L1.3-Ms-Ac and atropoisomeric ratio based on A% (275 nm).

4 Acknowledgements

This work was supported with funding from the Gates Foundation. M4ALL would like to express our gratitude to Dr. Trevor Laird, Dr. John Dillon, and Dr. Mark Krook for their helpful technical guidance throughout this project, as well as Dr. John Walker and Mr. Scott Rosenblum for the ongoing collaboration and support of the M4ALL mission. The authors thank Dr. Saeed

Ahmad and his team for their boundless efforts in TE analysis. We also would like to thank Dr. B. Frank Gupton, Dr. Douglas Klumpp, Dr. G. Michael Laidlaw, and Michael Osberg for their input on this work.

5 References

- (1) Homepage. https://www.unaids.org/en/Homepage (accessed 2024-04-12).
- (2) The United States President's Emergency Plan for AIDS Relief United States Department of State %. United States Department of State. https://www.state.gov/pepfar/ (accessed 2024-04-08).
- (3) Anderer, S. WHO Recommends Lenacapavir for HIV Prevention in New Guidelines. *JAMA* **2025**. https://doi.org/10.1001/jama.2025.10988.
- (4) Segal-Maurer Sorana; DeJesus Edwin; Stellbrink Hans-Jurgen; Castagna Antonella; Richmond Gary J.; Sinclair Gary I.; Siripassorn Krittaecho; Ruane Peter J.; Berhe Mezgebe; Wang Hui; Margot Nicolas A.; Dvory-Sobol Hadas; Hyland Robert H.; Brainard Diana M.; Rhee Martin S.; Baeten Jared M.; Molina Jean-Michel. Capsid Inhibition with Lenacapavir in Multidrug-Resistant HIV-1 Infection. *N. Engl. J. Med.* **2022**, *386* (19), 1793–1803. https://doi.org/10.1056/NEJMoa2115542.
- (5) Dvory-Sobol, H.; Shaik, N.; Callebaut, C.; Rhee, M. S. Lenacapavir: A First-in-Class HIV-1 Capsid Inhibitor. *Curr. Opin. HIV AIDS* **2022**, *17* (1), 15–21. https://doi.org/10.1097/COH.0000000000000713.
- (6) Sun, L.; Zhang, X.; Xu, S.; Huang, T.; Song, S.; Cherukupalli, S.; Zhan, P.; Liu, X. An Insight on Medicinal Aspects of Novel HIV-1 Capsid Protein Inhibitors. *Eur. J. Med. Chem.* **2021**, *217*, 113380. https://doi.org/10.1016/j.ejmech.2021.113380.
- (7) McFadden, W. M.; Snyder, A. A.; Kirby, K. A.; Tedbury, P. R.; Raj, M.; Wang, Z.; Sarafianos, S. G. Rotten to the Core: Antivirals Targeting the HIV-1 Capsid Core. *Retrovirology* **2021**, *18* (1), 41. https://doi.org/10.1186/s12977-021-00583-z.
- (8) Zhang, J.-Y.; Wang, Y.-T.; Sun, L.; Wang, S.-Q.; Chen, Z.-S. Synthesis and Clinical Application of New Drugs Approved by FDA in 2022. *Mol. Biomed.* **2023**, *4* (1), 26. https://doi.org/10.1186/s43556-023-00138-y.
- (9) Anderer, S. FDA Approves First Twice-Yearly PrEP for Long-Acting HIV Prevention. *JAMA* **2025**. https://doi.org/10.1001/jama.2025.10325.
- (10) Iacobucci, G. "Hard to Justify" \$28 000 Price Tag for Breakthrough HIV Prevention Treatment, Says UN Agency. **2025**. https://doi.org/10.1136/bmj.r1284.
- (11) Hill, A.; Levi, J.; Fairhead, C.; Pilkington, V.; Wang, J.; Johnson, M.; Layne, J.; Roberts, D.; Fortunak, J. Lenacapavir to Prevent HIV Infection: Current Prices versus Estimated Costs of Production. *J. Antimicrob. Chemother.* **2024**, dkae305. https://doi.org/10.1093/jac/dkae305.
- (12) Cousins, S. Lenacapavir Approved for HIV but Draws Ire over Cost. *The Lancet* **2025**, *405* (10497), 2269. https://doi.org/10.1016/S0140-6736(25)01322-4.
- (13) Based on personal communication with John Walker, Joseph Marian Fortunak and team determined that, with modest process improvements and increased demand, the projected cost of generic lenacapavir could range from \$35 to \$46 per person-year for a committed volume of two million treatments. As demand expands to five to ten million treatment-years, the cost is expected to decline to approximately \$25 per person-year.

- (14) Gilead Signs Royalty-Free Voluntary Licensing Agreements with Six Generic Manufacturers to Increase Access to Lenacapavir for HIV Prevention in High-Incidence, Resource-Limited Countries. https://www.gilead.com/news/news-details/2024/gilead-signs-royalty-free-voluntary-licensing-agreements-with-six-generic-manufacturers-to-increase-access-to-lenacapavir-for-hiv-prevention-in-high-incidence-resource-limited-countries (accessed 2025-07-31).
- (15) Bauer, L. E.; Gorman, E. M.; Mulato, A. S.; Rhee, M. S.; Rowe, C. W.; Sellers, S. P.; Stefanidis, D.; Tse, W. C.; Yant, S. R.; Chiu, A. Capsid Inhibitors for the Treatment of Hiv. WO2020018459A1, January 23, 2020. https://patents.google.com/patent/WO2020018459A1/en?oq=WO%C2%A02020018459 (accessed 2021-02-17).
- (16) Allan, K. M.; Batten, A. L.; Brizgys, G.; Dhar, S.; Doxsee, I. J.; Goldberg, A.; Heumann, L. V.; Huang, Z.; Kadunce, N. T.; Kazerani, S.; Lew, W.; Ngo, V. X.; O'keefe, B. M.; Rainey, T. J.; Roberts, B. J.; Shi, B.; Steinhuebel, D. P.; Tse, W. C.; Wagner, A. M.; Wang, X.; Wolckenhauer, S. A.; Wong, C. Y.; Zhang, J. R. Methods and Intermediates for Preparing a Therapeutic Compound Useful in the Treatment of Retroviridae Viral Infection. WO2019161280A1, August 22, 2019.
- (17) Bester, S. M.; Wei, G.; Zhao, H.; Adu-Ampratwum, D.; Iqbal, N.; Courouble, V. V.; Francis, A. C.; Annamalai, A. S.; Singh, P. K.; Shkriabai, N.; Van Blerkom, P.; Morrison, J.; Poeschla, E. M.; Engelman, A. N.; Melikyan, G. B.; Griffin, P. R.; Fuchs, J. R.; Asturias, F. J.; Kvaratskhelia, M. Structural and Mechanistic Bases for a Potent HIV-1 Capsid Inhibitor. *Science* **2020**, *370* (6514), 360–364. https://doi.org/10.1126/science.abb4808.
- (18) Du, Z.; Farand, J.; Guney, T.; Kato, D.; Link, J. O.; Mack, J. B. C.; Mun, D. M.; Watkins, W. J.; Zhang, J. R. Therapeutic Compounds for HIV Virus Infection. WO2023102529A1, June 8, 2023.
- (19) Link, J. O.; Rhee, M. S.; Tse, W. C.; Zheng, J.; Somoza, J. R.; Rowe, W.; Begley, R.; Chiu, A.; Mulato, A.; Hansen, D.; Singer, E.; Tsai, L. K.; Bam, R. A.; Chou, C.-H.; Canales, E.; Brizgys, G.; Zhang, J. R.; Li, J.; Graupe, M.; Morganelli, P.; Liu, Q.; Wu, Q.; Halcomb, R. L.; Saito, R. D.; Schroeder, S. D.; Lazerwith, S. E.; Bondy, S.; Jin, D.; Hung, M.; Novikov, N.; Liu, X.; Villaseñor, A. G.; Cannizzaro, C. E.; Hu, E. Y.; Anderson, R. L.; Appleby, T. C.; Lu, B.; Mwangi, J.; Liclican, A.; Niedziela-Majka, A.; Papalia, G. A.; Wong, M. H.; Leavitt, S. A.; Xu, Y.; Koditek, D.; Stepan, G. J.; Yu, H.; Pagratis, N.; Clancy, S.; Ahmadyar, S.; Cai, T. Z.; Sellers, S.; Wolckenhauer, S. A.; Ling, J.; Callebaut, C.; Margot, N.; Ram, R. R.; Liu, Y.-P.; Hyland, R.; Sinclair, G. I.; Ruane, P. J.; Crofoot, G. E.; McDonald, C. K.; Brainard, D. M.; Lad, L.; Swaminathan, S.; Sundquist, W. I.; Sakowicz, R.; Chester, A. E.; Lee, W. E.; Daar, E. S.; Yant, S. R.; Cihlar, T. Clinical Targeting of HIV Capsid Protein with a Long-Acting Small Molecule. Nature 2020, 584 (7822), 614–618. https://doi.org/10.1038/s41586-020-2443-1.
- (20) Wagner, A. M.; Bonderoff, S. A.; Chang, S.; Deignan, J.; Esanu, M. M.; Van Huynh, H.; Niu, T.; Ngo, V.; O'Keefe, B. M.; Phoenix, J.; Rainey, T. J.; Roberts, B. J.; Shen, J.; Stewart, C.; Vandehey, A. L.; Wolckenhauer, S. A.; Wong, C. Y.; Yarmuch, B. H. Synthesis of Lenacapavir Sodium: Active Pharmaceutical Ingredient Process Development and Scale-Up. *Org. Process Res. Dev.* **2024**, *28* (8), 3382–3395. https://doi.org/10.1021/acs.oprd.4c00242.

- (21) Pu, X.; Li, H.; Colacot, T. J. Heck Alkynylation (Copper-Free Sonogashira Coupling) of Aryl and Heteroaryl Chlorides, Using Pd Complexes of t-Bu2(p-NMe2C6H4)P: Understanding the Structure–Activity Relationships and Copper Effects. *J. Org. Chem.* 2013, 78 (2), 568–581. https://doi.org/10.1021/jo302195y.
- (22) M4ALL. PDR for Synthesis of Frag A of Lenacapavir. **2024**. https://medicines4all.vcu.edu/media/medicines4all/assets/documents/Len%20Frag%20A%2 0PDR.pdf.
- (23) PDR for Synthesis of Frag B of Lenacapavir. https://doi.org/chrome-extehttps://medicines4all.vcu.edu/media/medicines4all/assets/documents/Len%252520Frag %252520B%252520PDR.pdf.
- (24) PDR for Synthesis of Frag C of Lenacapavir, 2024. https://medicines4all.vcu.edu/media/medicines4all/assets/documents/Summary%20of%20P rocess%20Development%20Work%20on%20Asymmetric%20Synthesis%20of%20the%20 Frag%20C%20of%20Lenacapavir,%20pp.%201-88.pdf.
- (25) Shinde, A. H.; Sayini, R.; Singh, P.; Burns, J. M.; Ahmad, S.; Laidlaw, G. M.; Gupton, B. F.; Klumpp, D. A.; Jin, L. A New Synthesis of Enantiopure Amine Fragment: An Important Intermediate to the Anti-HIV Drug Lenacapavir. *J. Org. Chem.* **2025**, *90* (1), 471–478. https://doi.org/10.1021/acs.joc.4c02380.
- (26) Asad, N.; Lyons, M.; Muniz Machado Rodrigues, S.; Burns, J. M.; Roper, T. D.; Laidlaw, G. M.; Ahmad, S.; Gupton, B. F.; Klumpp, D.; Jin, L. Practical Synthesis of 7-Bromo-4-Chloro-1H-Indazol-3-Amine: An Important Intermediate to Lenacapavir. *Molecules* **2024**, *29* (12), 2705. https://doi.org/10.3390/molecules29122705.
- (27) Kotovshchikov, Y. N.; Latyshev, G. V.; Lukashev, N. V.; Beletskaya, I. P. Alkynylation of Steroids via Pd-Free Sonogashira Coupling. *Org. Biomol. Chem.* **2015**, *13* (19), 5542–5555. https://doi.org/10.1039/C5OB00559K.
- (28) Mohajer, F.; Mofatehnia, P.; Rangraz, Y.; Heravi, M. M. Pd-Free, Sonogashira Cross-Coupling Reaction. An Update. *J. Organomet. Chem.* **2021**, *936*, 121712. https://doi.org/10.1016/j.jorganchem.2021.121712.
- (29) Mohajer, F.; Heravi, M. M.; Zadsirjan, V.; Poormohammad, N. Copper-Free Sonogashira Cross-Coupling Reactions: An Overview. *RSC Adv.* **2021**, *11* (12), 6885–6925. https://doi.org/10.1039/D0RA10575A.
- (30) Biffis, A.; Centomo, P.; Del Zotto, A.; Zecca, M. Pd Metal Catalysts for Cross-Couplings and Related Reactions in the 21st Century: A Critical Review. *Chem. Rev.* **2018**, *118* (4), 2249–2295. https://doi.org/10.1021/acs.chemrev.7b00443.
- (31) Kader, D. A.; Sidiq, M. K.; Taher, S. G.; Aziz, D. M. Recent Advances in Palladium-Catalyzed Suzuki-Miyaura Cross-Coupling Reactions: Exploration of Catalytic Systems, Reaction Parameters, and Ligand Influences: A Review. *J. Organomet. Chem.* **2025**, *1030*, 123569. https://doi.org/10.1016/j.jorganchem.2025.123569.
- (32) Martin, R.; Buchwald, S. L. Palladium-Catalyzed Suzuki-Miyaura Cross-Coupling Reactions Employing Dialkylbiaryl Phosphine Ligands. *Acc. Chem. Res.* **2008**, *41* (11), 1461–1473. https://doi.org/10.1021/ar800036s.
- (33) Sergeev, A. G.; Zapf, A.; Spannenberg, A.; Beller, M. Synthesis and Crystal Structure of Palladium(0) and Arylpalladium(II) Bromide Complexes of CataCXium A. *Organometallics* **2008**, *27* (2), 297–300. https://doi.org/10.1021/om700889b.
- (34) Tang, W.; Patel, N. D.; Xu, G.; Xu, X.; Savoie, J.; Ma, S.; Hao, M.-H.; Keshipeddy, S.; Capacci, A. G.; Wei, X.; Zhang, Y.; Gao, J. J.; Li, W.; Rodriguez, S.; Lu, B. Z.; Yee, N. K.;

- Senanayake, C. H. Efficient Chiral Monophosphorus Ligands for Asymmetric Suzuki–Miyaura Coupling Reactions. *Org. Lett.* **2012**, *14* (9), 2258–2261. https://doi.org/10.1021/ol300659d.
- (35) Kraft, A. The Determination of the pKa of Multiprotic, Weak Acids by Analyzing Potentiometric Acid-Base Titration Data with Difference Plots. *J. Chem. Educ.* **2003**, *80* (5), 554. https://doi.org/10.1021/ed080p554.
- (36) Economidou, M.; Mistry, N.; Wheelhouse, K. M. P.; Lindsay, D. M. Palladium Extraction Following Metal-Catalyzed Reactions: Recent Advances and Applications in the Pharmaceutical Industry. *Org. Process Res. Dev.* **2023**, *27* (9), 1585–1615. https://doi.org/10.1021/acs.oprd.3c00210.
- (37) ICH HARMONISED GUIDELINE GUIDELINE FOR ELEMENTAL IMPURITIES Q3D(R2), 2022. https://database.ich.org/sites/default/files/Q3D-R2 Guideline Step4 2022 0308.pdf.
- (38) Elmekawy, A. Simultaneous Determination of Residual Palladium and Thiol Homogeneous Scavenger N-Acetylcysteine in Active Pharmaceutical Ingredients Using Inductive Coupled Plasma-Mass Spectrometry. *Org. Process Res. Dev.* **2021**, *25* (6), 1352–1359. https://doi.org/10.1021/acs.oprd.0c00542.
- (39) Ren, H.; Strulson, C. A.; Humphrey, G.; Xiang, R.; Li, G.; Gauthier, D. R.; Maloney, K. M. Potassium Isopropyl Xanthate (PIX): An Ultra-Efficient Palladium Scavenger. *Green Chem.* **2017**, *19* (17), 4002–4006. https://doi.org/10.1039/C7GC01765K.
- (40) SiliCycle. Metal Scavenging with SiliaMetS®. https://www.velocityscientific.com.au/images/pdf/Silicycle/Catalogues/Catalogue_Sections/SiliaMetS%20Metal%20ScavengersV.pdf.
- (41) Bullock, K. M.; Mitchell, M. B.; Toczko, J. F. Optimization and Scale-Up of a Suzuki-Miyaura Coupling Reaction: Development of an Efficient Palladium Removal Technique. *Org. Process Res. Dev.* **2008**, *12* (5), 896–899. https://doi.org/10.1021/op800064y.
- (42) Yang, Q.; Babij, N. R.; Good, S. Potential Safety Hazards Associated with Pd-Catalyzed Cross-Coupling Reactions. *Org. Process Res. Dev.* **2019**, *23* (12), 2608–2626. https://doi.org/10.1021/acs.oprd.9b00377.
- (43) Liu, X.; Yang, X.; Tan, X. Adiabatic Thermal Runaway and Safety Relief Design for Hexamethylene Diisocyanate Reaction System. *E3S Web Conf.* **2024**, *573*, 02024. https://doi.org/10.1051/e3sconf/202457302024.
- (44) Significance of Impurity Profiling in the Pharmaceutical Industry. Global Pharma Tek. https://www.globalpharmatek.com/blog/impurities-and-their-importance-of-profiling-in-the-pharma-industry/ (accessed 2025-08-24).
- (45) Chaughule, R. Advances in Impurity Profiling of Pharmaceutical Formulations. *Biomed. J. Sci. Tech. Res.* **2024**, *60* (1), 52185–52191. https://doi.org/10.26717/BJSTR.2024.60.009393.
- (46) Tapkir, N.; Soni, F.; Sahu, A. K.; Jadav, T.; Tekade, R. K.; Sengupta, P. A Comprehensive Review on Assessment and Key Control Strategies for Impurities in Drug Development with a Special Emphasis on Post-Marketing Surveillance. *J. Pharm. Innov.* **2022**, *17* (4), 1510–1529. https://doi.org/10.1007/s12247-021-09607-9.
- (47) ICH HARMONISED TRIPARTITE GUIDELINE IMPURITIES IN NEW DRUG SUBSTANCES Q3A(R2), 2006. https://database.ich.org/sites/default/files/Q3A%28R2%29%20Guideline.pdf.

- (48) Kwiatkowski, C. F.; Andrews, D. Q.; Birnbaum, L. S.; Bruton, T. A.; DeWitt, J. C.; Knappe, D. R. U.; Maffini, M. V.; Miller, M. F.; Pelch, K. E.; Reade, A.; Soehl, A.; Trier, X.; Venier, M.; Wagner, C. C.; Wang, Z.; Blum, A. Scientific Basis for Managing PFAS as a Chemical Class. *Environ. Sci. Technol. Lett.* **2020**, *7* (8), 532–543. https://doi.org/10.1021/acs.estlett.0c00255.
- (49) Guariglia, D.; Kindschuh, J.; Brooks, E.; Cavender, B. *Federal PFAS Regulation: A Changing Landscape in 2024 and Beyond*. https://www.bamsl.org/?pg=StLouisLawyerBlog&blAction=showEntry&blogEntry=12149 5 (accessed 2025-08-24).
- (50) Navigating the PFAS Challenge in Pharma | Pharmaceutical Engineering. https://ispe.org/pharmaceutical-engineering/ispeak/navigating-pfas-challenge-pharma (accessed 2025-08-24).
- (51) *PFAS in Pharmaceuticals: An Evolving Regulatory Landscape*. Separation Science. https://www.sepscience.com/pfas-in-pharmaceuticals-an-evolving-regulatory-landscape-7945 (accessed 2025-08-24).
- (52) BOC Deprotection Wordpress. https://reagents.acsgcipr.org/reagent-guides/bocdeprotection/ (accessed 2025-08-24).
- (53) Nunes De Souza, A.; Sakkani, N.; Guthrie, D.; Sahani, R. L.; Saathoff, J. M.; Hochstetler, S. R.; Burns, J. M.; Ahmad, S.; Laidlaw, G. M.; Gupton, B. F.; Klumpp, D. A.; Jin, L. Development of a Scalable Synthetic Route to (1R,5R)-2,2-Dimethoxybicyclo[3.1.0]Hexan-3-One: An Important Intermediate in the Synthesis of Lenacapavir. *Org. Process Res. Dev.* 2025, 29 (3), 846–855. https://doi.org/10.1021/acs.oprd.4c00527.
- (54) Nash, R. A.; Wachter, A. H. Pharmaceutical Process Validation: An International (Drugs and the Pharmaceutical Sciences Book 129) 3rd Edition; CRC Press, 2003.